Master of Philosophy (Engineering)

The University of Adelaide

School of Electrical & Electronic Engineering

Flexible Transmission Lines and Asymmetrically Counter-Poised Monopoles

Author:
Deshan Govender

Supervisor:
Prof. Christophe Fumeaux

January 18, 2022

Thesis Declaration

I certify that this work contains no material which has been accepted for the award of any other degree or diploma in my name, in any university or other tertiary institution and, to the best of my knowledge and belief, contains no material previously published or written by another person, except where due reference has been made in the text. In addition, I certify that no part of this work will, in the future, be used in a submission in my name, for any other degree or diploma in any university or other tertiary institution without the prior approval of the University of Adelaide and where applicable, any partner institution responsible for the joint-award of this degree. The author acknowledges that copyright of published works contained within the thesis resides with the copyright holder(s) of those works. I also give permission for the digital version of my thesis to be made available on the web, via the University's digital research repository, the Library Search and also through web search engines, unless permission has been granted by the University to restrict access for a period of time. I acknowledge the support I have received for my research through the provision of an Australian Government Research Training Program Scholarship.

Acknowledgements

It is impossible to acknowledge the full debt I owe to so many over the years.

To my friends and colleagues at the Defence Science & Technology Group. Wayne Martinsen, Joseph Magarelli, Leonard Hall, Adrian Caldow & Jon Arnold. I have benefited tremendously from the hours of technical discussions and white board sessions, where we have traversed through all manner of technical matter, and in the pursuit of truth, left no stone unturned! I have always appreciated the willingness of Wayne & Joseph to study a problem in detail. They have been able investigators and good friends and to each I am grateful. I am thankful to Jon and Adrian who had seen the potential in this work & created the provision for my part-time study.

My friends, colleagues, and particularly Professor David Reilly, within Microsoft Quantum & the University of Sydney, who have taken an active interest in my part-time study. Your curiosity & perspectives have helped me develop a deeper physical understanding of my own work. Indeed my technical creativity has expanded as a result & I am continually fascinated as we work at the quantum-classical interface.

Foremost, I have benefited incredibly from the support of my supervisor Professor Christophe Fumeaux, whose fingerprints are found throughout this thesis. Through a great many changes in my life, he has made time to pour over this work, remained consistent, offered encouragement and helped make this a better work. I am profoundly grateful.

I am thankful to Dr. Shengjian Chen who assisted in the fabrication and measurement of the antennas whilst I worked remotely. I am appreciative of his diligence, attention to detail, and for the calibre of output produced.

My Mum and Dad who have never refused me a book, or a textbook, who have a deep sense in the power of the written word and it's ability to shape a mind. Your wisdom on this point will remain with me always.

My wife, Jillian, who continues to faithfully support and walk alongside me, through innumerable hours of modelling, writing and refining. Thank you.

Abstract

In the pursuit of miniaturised antennas and flexible transmission lines, several techniques have been explored in the open literature to address physical aspects of size, weight, flexibility and electrical reconfigurability, all whilst sustaining a reasonable degree of electrical operation. In the first part of this thesis, these themes are further explored with transmission lines, through the experimentation of transmission lines that use standard, readily available materials of a conformal nature, that would appreciably suit our context of operation. Two distinct types of transmission lines are designed, simulated, investigated and reported on. In the second half of this thesis, we explore asymmetrical antenna design in relation to antenna miniaturisation, aiming at creating a design method for this type of antennas.

The first transmission line examined in the first part of the thesis, is what we now refer to as a Wire-Over-Ground-Plane transmission line. Structurally, this is standard gauge wire, placed over a polyimide sheet beneath which exists ground plane. A model of this transmission line is created and thereafter numerically simulated. A rough prototype of this design was created to validate operation. Thereafter, proposed is the design with realistic simulations of a branch-line coupler and modified Marchand balun, using this technology.

The second transmission line created, is a stripline transmission line constructed primarily from fleece and a conductive textile. Once more, this structure is numerically simulated to validate operation prior to construction. Thereafter a number of samples are created to explore the physical robustness of the connection, through the application of mechanical stress and strain of varied transmission line constructions.

In the second part of the thesis three antennas were created taking an asymmetrical approach to antenna realisation. The first Counter-Poised monopole antenna is experimentally realised by replacing one of the dipole arms with a coil of equivalent inductance. Decent performance here led to a second antenna design that builds on the first asymmetrical design, implementing a planar integrated balun into the feed-structure and developing a planar counter-poise fabricated on a circuit board. The third antenna design, builds further on the second design by adding a frequency reconfigurability feature through the addition of active circuit elements to the counter-poise. As we worked from developing the experimental antenna to realising the frequency reconfigurable variant, we have sought to understand the principle of operation and establish a design method which has allowed for the development of an advanced reconfigurable variant. The counter-poise is the fulcrum of all three asymmetrical antennas designed here, so a thorough grasp on its design and operation is required to ensure adequate antenna operation.

In summation, this thesis develops ideas and realisations of flexible transmission lines using standard off-the-shelf components as well as conductive textiles and clothing. Further, asymmetrical antenna design techniques are explored leading to antenna miniaturisation. Thereafter, design methods are developed to aid in planar fixed-frequency implementation, whereupon a more advanced frequency reconfigurable variant is created.

Contents

Chapter 1

Motivation, Context & Literature Review

1.1 Introduction

The overarching aim of this research is to help drive and facilitate improved operational conditions and outcomes for soldiers in a modern-day battle-space. Typically, the modern soldier carries several electronics systems and sensors that host antennas for wireless operation. The research focus of this work is to target the research and development of antennas, which radiate effectively off the soldier whilst also improving the size, weight and power constraints of the antennas and systems carrying these antennas. These are constraints that may inhibit the mobility of systems, units, or soldiers in operation, therefore any potential antenna solution must seek to address these constraints. Here, we shall seek to demonstrate the importance of effective antenna operation as it relates to size, weight, and power factors. Thereafter, areas of focused research shall be suggested and explored to address shortcomings and offer improvements to the user.

1.2 Context of Operation

From a system perspective, design and development of an efficient antenna structure is crucial to the reduction of power consumption within the system. Energy stored within the batteries of a radio must be used with the upmost care and provide electrical energy capability for extended duration whilst units are out on operation. For example, if the antenna is placed against a body, the resonant frequency of the antenna will likely shift and a significant amount of radiation will be absorbed by the body. In order to overcome the associated drop in antenna gain and maintain an adequate level of connectivity, more power would be required from the Radio Frequency (RF) amplifier and hence a greater draw on current from the power supply would be required. In turn, there would be a requirement on the soldier, to carry a larger power supply or failing that, deal with the consequences of reduced communication or sensor coverage from supporting units.

An antenna, that is designed inefficiently, places a high cost on this total system energy resource. Additionally, the antenna must also be miniature in nature, and as seamlessly integrated as possible, while avoiding interference with the operator and providing an adequate amount of gain, directivity and efficiency.

From the cartoon in Figure 1.1 [1], one may observe the various elements that a soldier, or multiple soldiers in operation, would ostensibly be required to interact with wirelessly. There are airborne elements - aircraft, unmanned-aerial-vehicles, satellites, as well as land-based elements, - tanks, humvees and troop carriers. In order for the soldier to operate with this combination of air and land based assets, the soldier requires a communication system with an antenna radiation pattern capable of hemispherical operation, thereby encompassing the elements of operation within the radiating aperture of the antenna.

Further, from the strategic perspective of a commander, a tactical communication system in the field equips the commander with “eyes and ears”, and helps providing situational awareness in the battle-space [2]. An outage, or "blank-spot", in communications or sensory systems

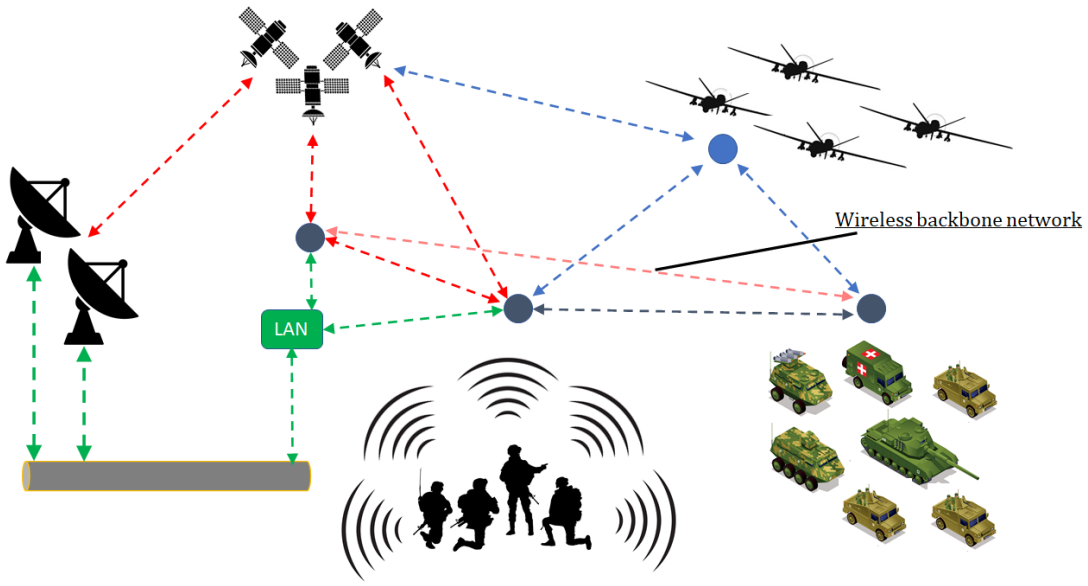

Figure 1.1: A cartoon depicting the various elements within a given battle-space to which a soldier may require connectivity. [1]

would place the command at a significant disadvantage to the adversary, an outcome that is unacceptable. Thus, as one can see from the example illustrated above, the antenna is a critical component in providing access to the battle-space, and is key not only to the successful operation of the system but to the success of the mission as well.

1.3 Design Requirements

The context of operation carries with it constraints that the total antenna system must adhere to as well. Figure 1.2 is a basic diagram of a RF transmission System. The electrical elements at the centre of this discussion are the "Feed-Network", responsible for providing energy from the radio system to the antenna itself. Given the context of operation discussed previously, the requirements of the feed structure and the antenna are detailed below.

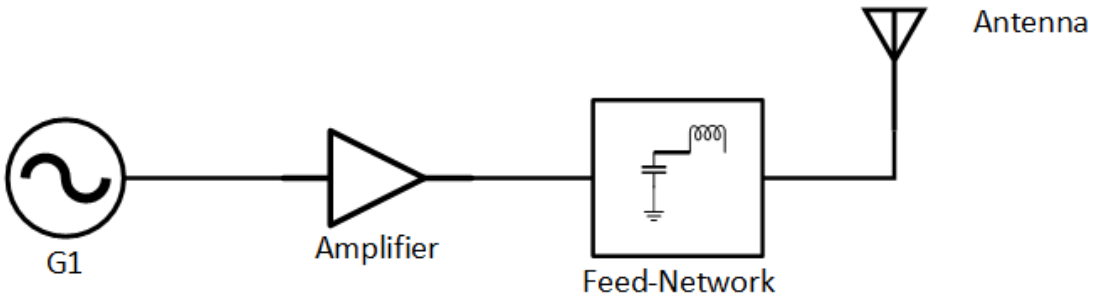

Figure 1.2: Basic RF Transmission System.

The essential requirements of the feed structure are that it must be:

1. Low loss.
2. Small, relative to the size of the antenna.
3. Robust, flexible, conformal, resistant to deformation.
4. Present a balanced input to the antenna.

The essential requirements of the antenna are that it must:

1. Radiate efficiently.
2. Maintain a form factor as small as possible without compromising on radiation performance.
3. Ideally, provide omni-directional coverage, to allow for connectivity to various elements in the theatre of operation.

1.4 Fundamental Antenna Theory and Overlapping Requirements

In order to address the above requirements, and the interactions between the feed-structure and antenna, it is necessary to delve deeper and provide some basic antenna theory and background on the electrical efficiency of an antenna.

The radiation efficiency of an antenna is governed by the following equation:

$$\epsilon_R = \frac{P_{RAD}}{P_{INP}} \tag{1.1}$$

ϵ_R - Radiation Efficiency

P_{RAD} - Power Radiated

P_{INP} - Power Accepted by the Antenna

It can be seen that the radiation efficiency of the antenna, is a ratio of the power radiated to the power accepted into the antenna. Hence, by improving overall antenna efficiency, we can achieve overall power efficiency of the system by reducing the power lost within the antenna and the associated feed. Further the total efficiency of the antenna is governed by the following mathematical relationship:

$$\epsilon_T = M_T * \epsilon_R \tag{1.2}$$

ϵ_T - Total Antenna Efficiency

M_T - Mismatch Efficiency

The above relationship, 1.2, reveals that the total antenna efficiency depends not only on the radiation efficiency but on the mismatach efficiency of the antenna as well. More specifically, the mismatch efficiency takes into account the impedance mismatch loss between the antenna and the RF Transmitter (Tx) or Receiver (Rx), that it is connected to.

The following equation, describes the reflection coefficient, Γ, between two systems of various impedance. In the case of the antenna and the feed structure, Γ is a critical measure of the amplitude reflected back from the antenna due to any mismatch with the feed structure. To preserve energy and avoid unnecessary loss, the characteristic impedance ($Z0$) of the line should be close to the load impedance (ZL).

$$\Gamma = \frac{ZL - Z0}{ZL + Z0} \tag{1.3}$$

ZL - Load Impedance

$Z0$ - Characteristic Impedance

Γ - Reflection Coefficient

Once Γ is known, the mismatch loss (ML) can thereafter be found using the equation below and following related to the mismatch efficiency.

$$ML = -10 * \log(1 - \mid \Gamma \mid^2) \text{ dB} \tag{1.4}$$

ML - Mismatch Loss (dB)

With respect to antenna miniaturisation, there is a limit on how far the antenna may be miniaturised before it is ineffective as a source of radiation. This limit is widely known in antenna literature as the Chu-Harrington Limit [3][4]. The theorem effectively states that as the total volume of the antenna is reduced, the radiation resistance of the antenna shall be reduced as well. The radiation resistance of an antenna can be defined as an equivalent resistance that models the power dissipated, when electromagnetic energy radiates from the antenna element. Further the Chu-Harrington limit, makes known that as the volume of the antenna decreases, the Q factor increases, hence the bandwidth decreases.

$$Q \geq \frac{1}{k^3 a^3} + \frac{1}{ka} \tag{1.5}$$

k - Wave Number

a - Radius of the sphere within which the antenna is enclosed

$$k = \frac{2\pi}{\lambda}$$

λ - Wavelength

The preceding discussions on antenna efficiency and miniaturisation make known the electrical limitations on the design and development of the intended antenna. Figure 1.3 is a Venn diagram capturing the overlapping requirements and aids in providing guidance and direction to the intended research. It is placed here to help one visualise the themes that pull or push the antenna development in a given direction. For example, the use of flexible dielectric may allow for the build of a more conformal antenna structure, however losses associated with the use of a particular dielectric may reduce the efficiency of the antenna structure. A successful design should meet the overall design objective to achieve a miniature, flexible and relatively cost-effective antenna, capable of behavior conducive to use in a theatre of operation. An additional

desirable characteristic is that of frequency agility. In that, if the antenna itself becomes detuned due to interference from the surrounding environment, the ability to electrically reconfigure itself to maintain a high degree of efficiency is certainly appreciated. Alternatively, should the user request a different frequency of operation, within the electrically achievable bounds of the antenna, this would add a degree of flexibility to the user's context, a valuable trait of the antenna.

It must be stated that the research performed aims to inform the technological underpinnings of future antenna development, targeted at platforms in the battle-space. The research is not directed at addressing a specific application. Instead the use-case presented is designed to motivate the targeted development and design of antenna structures that are underpinned by size, weight, cost and power constraints.

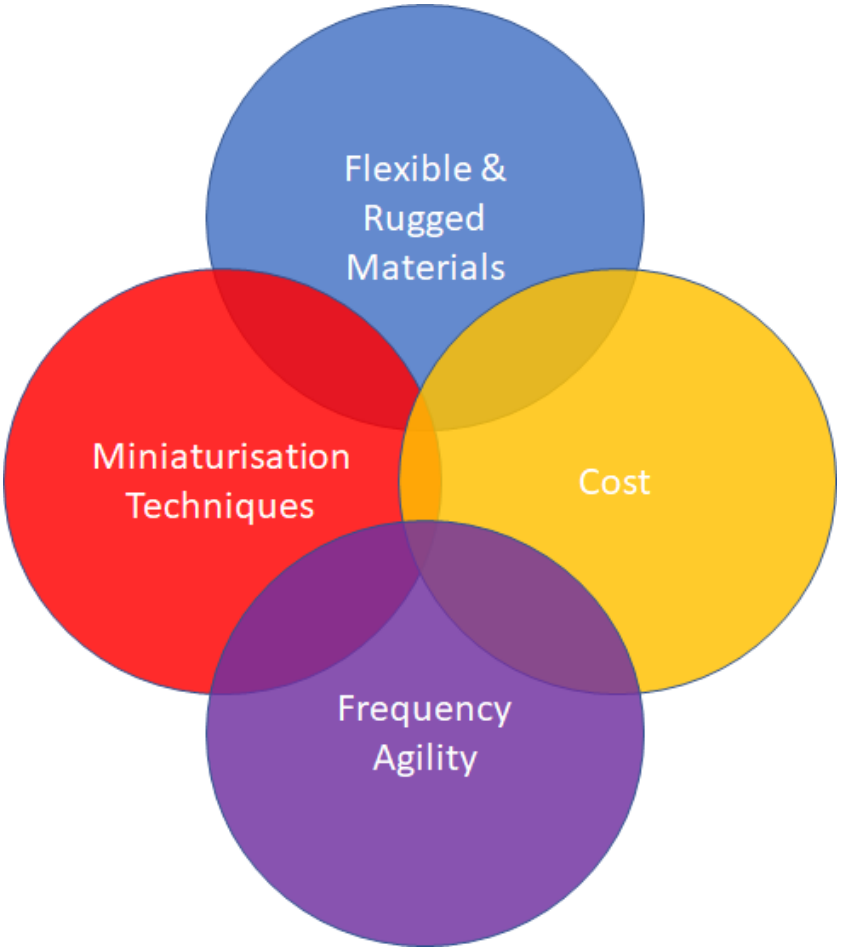

Figure 1.3: Overlapping Antenna Design Requirements

1.5 Basic Antenna Operation

In order to present the path forward in the proceeding chapters, it is necessary to describe the basic operation of an antenna and thereafter describe the changes to the antenna structure that will be made in the intended area of exploration and research.

In order to try and understand how an antenna operates, it is worthwhile exploring the general behaviour of an antenna, as described in Figure 1.4. Here a general description is made to a wave propagating along a two wire transmission line [5]. From the entry point of the two wire transmission line, one may observe the electric-field propagating between the conductors of the transmission line, as a guided wave. Thereafter, the conductors of the transmission line have been bent open, and as such the waveguide is now exposed to free-space and from Figure 1.4, one may observe a field appearing between the conductors and subsequently propagating into free space from the bent arms of the transmission line. In this configuration the open arms form a dipole and serve as the active radiators. An antenna can be considered as a special case of the above operation, with its design aiming for the structure to resonate and radiate efficiently at a given frequency. The antenna allows for the transformation of a guided electromagnetic wave propagating within a waveguide, coaxial cable or any other transmission line to an electromagnetic wave propagating in free space.

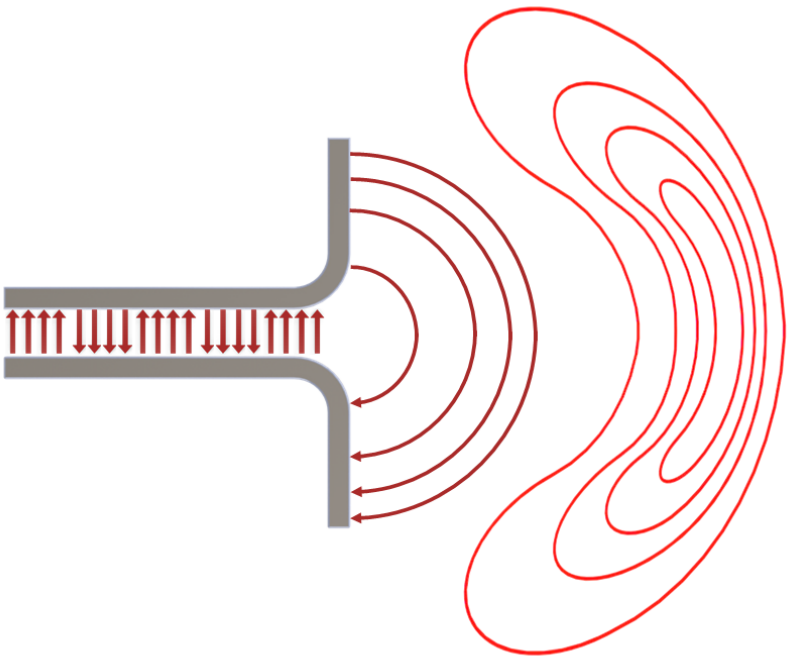

Figure 1.4: Basic Antenna Theory of Operation, adapted from [6]

To try and understand the conditions for antenna resonance, one must consider the currents and voltages on the bent open edges of the two wire transmission line, or the dipole arms to understand the nature of the resonant behaviour. When the physical dimension along the antenna arms is set to $\lambda/2$, as described in Figure 1.5 [7], one may observe that the currents

along each arm are in phase. Correspondingly, along the length of each opposing arm the net potential becomes more negative or positive as one travels along the particular arm. The nature of the in-phase currents along the arm and the differential voltages on the arms, sets up the field conditions for a standing wave to form along the dipole, thereby giving rise to a radiated electromagnetic wave.

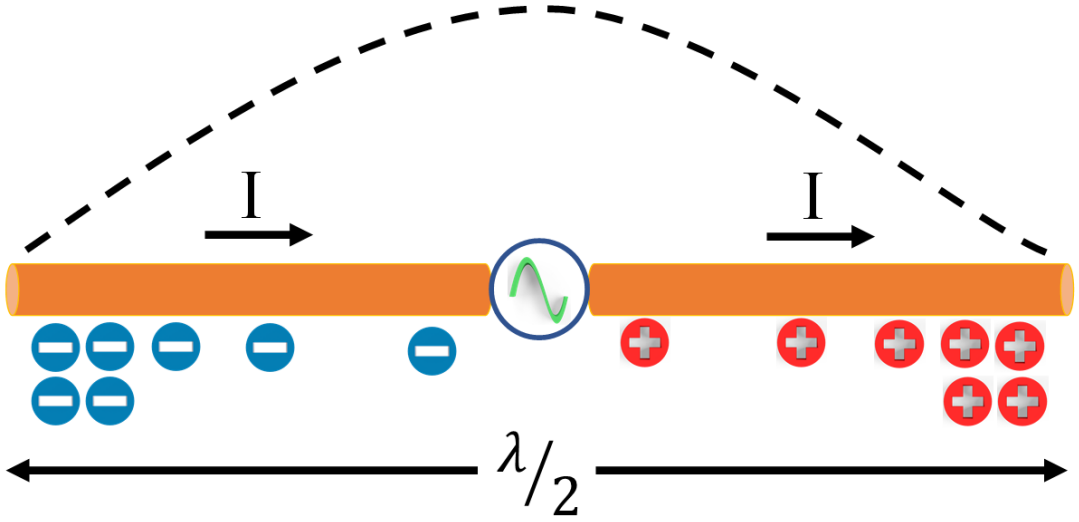

Figure 1.5: Standing Wave Pattern [7]

Now within the operational context, it is of great value to operators in the field to possess an antenna which generates an omni-directional radiation pattern, with close to uniform spread of the radiation. The classical dipole does exactly this, with its typical radiation pattern presented in Figure 1.6. Further the demands of a rugged and constantly changing operational setting, require a robust antenna structure with the ability to vary electrical response to maintain a desired level of electrical operation. It is here that the research questions, with respect to antenna miniaturisation, flexibility, reconfigurability and cost are presented:

1. Is it possible to counterpoise or reduce the size of one of the arms considerably and thereafter still maintain a reasonable degree of antenna operation?
2. If asymmetry is introduced into the manipulated dipole structure, how does the radiation pattern of the antenna change?
3. Will the antenna structure lend itself to flexible implementation?
4. Is it possible to construct a modified antenna and associated feed structure using existing fabrication technology to reduce cost, improve quality and reliability?
5. In a situation where the environment varies and effects antenna electrical operation, can the antenna be electrically reconfigured to perform optimally?

A possible advantage of pursuing the asymmetrical dipole line of thought is as follows: Asymmetrical antenna structures, such as the basic monopole exist. A drawback of this family of monopole based structures, is that they require a ground-plane with sufficient lateral extent to operate. The principle of operation here, is that an image or reflected wave off the ground-plane,

constructively interferes with the incident wave in phase giving rise to radiation [6], as described by the illustration of monopole image theory in Figure 1.7. In contrast, the dipole uses "itself" as the counterpoise, requiring no additional ground-plane structure. If one were able to replace one of the arm's, with a more miniature equivalent component that still allowed for reasonable antenna operation, such a manipulation would prove advantageous. In this asymmetrically modified case, the manipulated dipole would more closely resemble a counterpoised monopole, without a ground plane of required lateral extent. Within the context of antennas mounted on soldiers, ground planes of sufficient lateral extent may not exist, hence an antenna solution without this dependency would prove valuable.

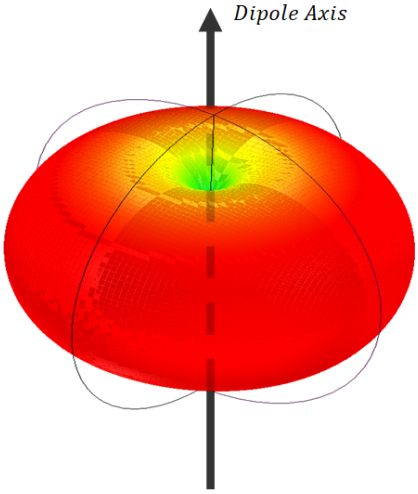

Figure 1.6: Omni-directional dipole radiation pattern.

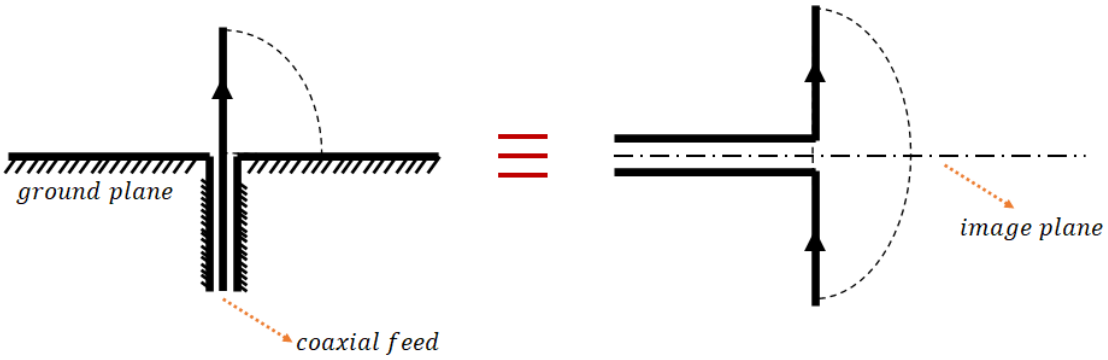

Figure 1.7: Basic monopole antenna and reflected image. Adapted from [6]

If the experimental structure operates adequately, a means of fabricating the antenna to withstand environmental effects must be considered. This antenna should be practically and repeatably realised, optimally in planar form to make use of existing PCB manufacturing processes. Additionally, the exploration of flexible materials to build the antenna or supporting feed structures is beneficial to the soldiers context.

To further the antenna performance and benefit to the user, an electrically reconfigurable antenna adds a valuable degree of flexibility. Specifically, should the potential of a counterpoise lend itself to electrical manipulation, this is an aspect of the design that should certainly be explored.

Cost reduction should be achieved through the use of commercial-off-the-shelf (COTS) materials and make use of routine, readily accessible fabrication processes. Emphasis in the design and development stages should be placed on using readily available components, in comparison to the development of bespoke or exotic materials to construct the antenna. The development phases should target the use of readily accessible fabrication technologies or equipment, such as PCB manufacturing processes, to facilitate antenna construction where possible.

1.6 Literature Review

1.6.1 Asymmetric Antenna Structures

Prior to embarking on any radical asymmetrical changes to the dipole, it is worthwhile investigating changes that have been applied to planar dipole structures to reduce their size. Focus has been placed on planar structures since these types of structures lend themselves to existing PCB fabrication techniques. Hence such structures lend themselves to be conveniently manufactured and are subject to higher degrees of quality control [8]. Figure 1.8 (a) and (b) are illustrative of crossed-dipole antenna structures [9]. In these references, the authors examined the dipole arms, and thereafter presented examples of possible changes to the dipole structure for reduction of their arm length. From Figure 1.8(a), one may observe that in "Number 2", a meander is introduced to each arm of the dipole. This addition has the effect of reducing the total length of the dipole. The mechanism via which it achieves this antenna shortening is through an inductively loaded meander and capacitive-coupling between adjacent turns of the meander. In "Number 3", the addition of arrows at the end of the dipole have been used to reduce overall antenna length. The downside to using these techniques is a reduction in overall efficiency and the introduction of additional modes due to parasitic effects of the geometry. In the reflection coefficient frequency response shown in Figure 1.8(b), one may observe that as the antenna structure continues to be manipulated, additional modes are added to the frequency response between 1.2 and 1.4 GHz.

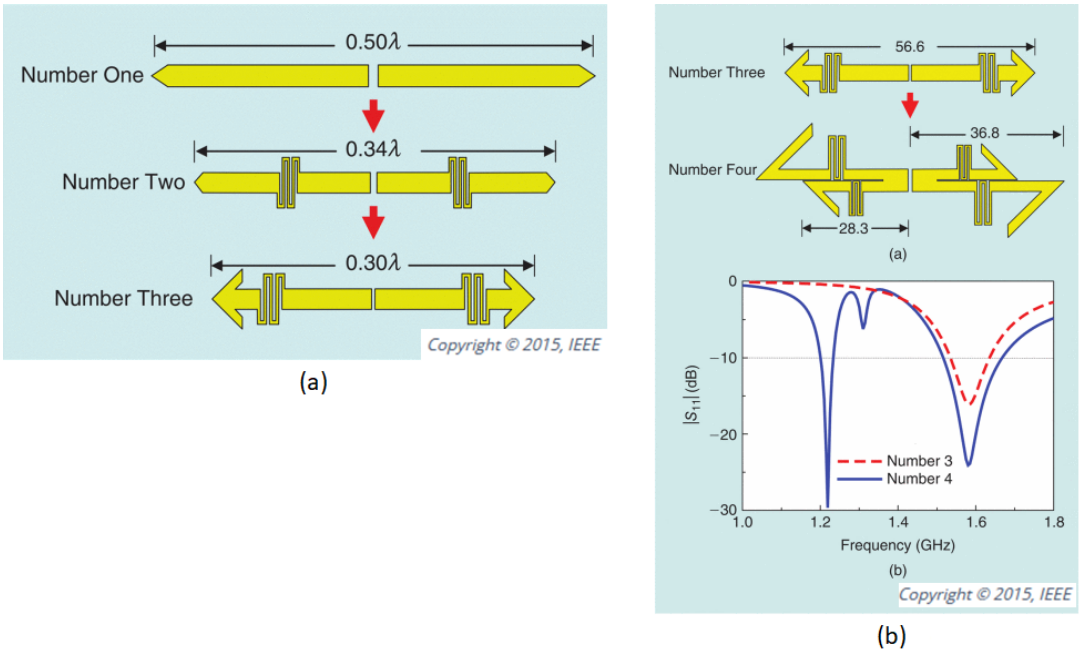

Figure 1.8: (a) Dipole structure reduction [9] (b) Dipole structure reduction leading to asymmetry in arms [9]

These modes may not be disruptive to the total system behaviour or surrounding components along the signal chain, however care must be taken to isolate the unwanted frequency behaviour from the antenna by use of appropriate filtering, circulator or similar [10]. Further one may observe from Figure 1.8(b), drawing "Number 4", asymmetry in the design. The electrical

response of the antenna at the frequency of interest, 1.6 GHz, presents with a match of less than -20 dB, indicating that it is more closely matched now to the characteristic impedance of the system. Given that the well-known impedance of a half-wave dipole is 72 +j42.5 Ohms [11], the match closer to the characteristic impedance of the system may result in a reduction of total system efficiency. Additionally notice must be taken to the slight increase in bandwidth in comparison to drawing "Number 3" in Figure 1.8(a). This feature of increased bandwidth may be of use in applications that require larger amounts of available spectrum.

Another asymmetrical example is shown in Figure 1.9, from Kolitsidas et al., [12], presented is an asymmetrically opposed dipole. The changes to the dipole were made through the application of a genetic algorithm, programmed to enhance the overall bandwidth of the dipole. An initial solution was presented to the algorithm using the dipole form of (i) from Figure 1.9. Optimization of the physical structure was performed through an iterative approach using the algorithm, with a figure of merit generated to rewarding larger bandwidths. The outcome from this optimization, from Kolitsidas et al., showed an improvement in overall available antenna bandwidth.

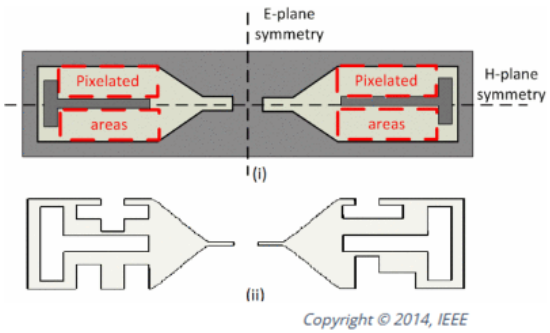

Figure 1.9: Asymmetrical Dipole Antenna applied through optimization [12]

The next example of an of an asymmetrically constructed dipole is from Tsai et al.[13], Figure 1.10. Presented is a dipole constructed using the top and bottom conducting planes of a double-sided printed circuit board. The antenna is fed from a 50 Ohm microstrip [5] transmission line. Considering the antenna feed, it is not apparently obvious how the balun in this application has been implemented. However, since the approach makes use of the top and bottom planes on the PCB, it is assumed that the differential currents between the planes are exploited to provide a balanced feed to the antenna. In this case one may notice that the two opposing radiating elements are vastly different in shape from each other. The design intent of the author here, is to generate a dual-band antenna. To this end, a cut-out along "W4" is introduced to provide additional degrees of freedom in the manipulation of the antenna dimensions, to converge on a response suitable for their application.

Figure 1.11 [13], presents the reflection coefficient of this dual-band dipole. One may observe that multiple frequency resonances are generated by this structure. A point of note here is that the authors used a parametric trial-and-error approach of designing an antenna in this fashion. It may be said that significant numerical computation may be required in the design space, prior to converging on an acceptable result.

The surface currents at 2.4 GHz on this dual band dipole are displayed in Figure 1.12, showing the energy from the feed exciting the asymmetrical dipole. One may observe the capacitively excited currents on the bottom section of the PCB as highlighted by the light green and yellow region on the surface. In contrast, the top layer with the cut-out is fed by energy from the trace above and travels across the ground-plane discontinuity to excite the radiating conductor on the

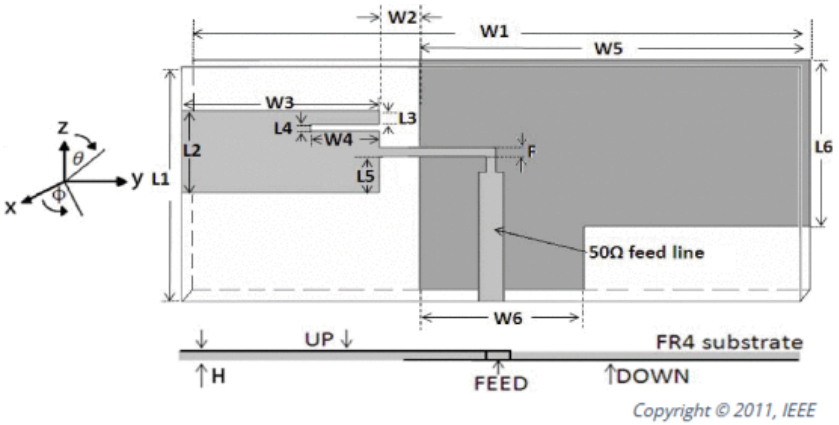

Figure 1.10: Asymmetrical dual band dipole antenna structure [13]

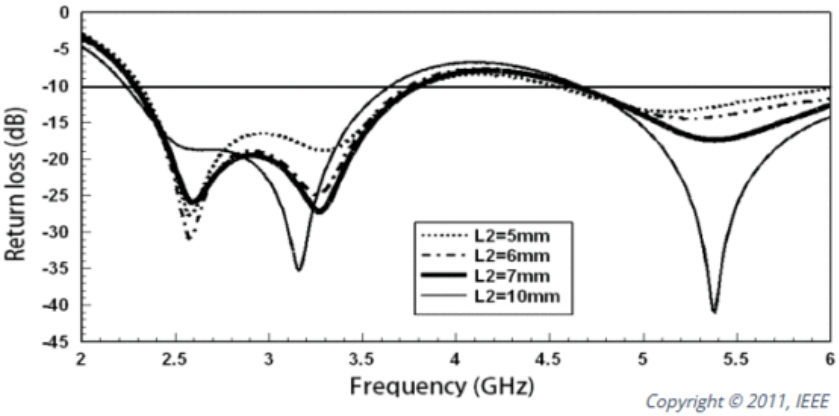

Figure 1.11: Frequency Response of dual band dipole antenna [13]

top layer. Indeed, this is quite an interesting means of feeding an antenna without an explicit balun in place.

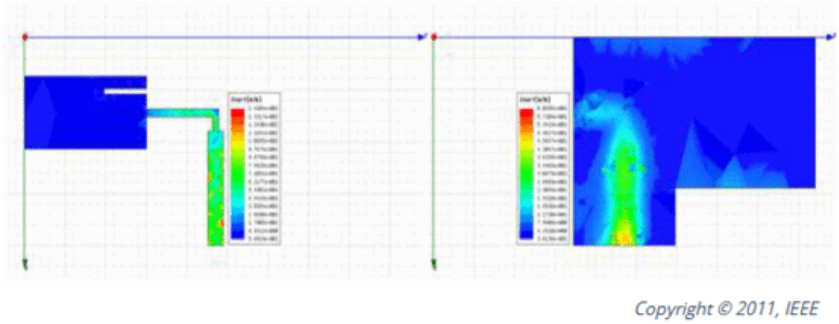

Figure 1.12: Surface currents of dual band dipole antenna [13]

1.6.2 Flexible Antenna Structures

Given that the design intent here is to create flexible, planar conformal structures, an aspect of the research has been dedicated towards designing, constructing, and exploring the limitations of such implementations. Of particular interest to the work program is the behaviour of fabric based conductors [14][15] and flexible thin-films such as polyimide [16]. In the following, examples of antennas that have been designed and tested using these techniques and materials are presented.

The first of these examples from is built on a flexible polymer, in this case sticky-tape, upon which a thin conductive layer is deposited. It is an ultra-wideband planar antenna with a coplanar waveguide (CPW) feed. Further the authors of [17], have flexed the antenna and measured its responses in bent shapes accordingly.

It is of interest to understand the geometry of the structure which leads to the generation of the ultra-wideband characteristic of the antenna. We notice from Figure 1.13, that the antenna is fed from an unbalanced CPW feed. Thereafter the wave propagates to the antenna, with a minor gap between the tapered antenna section and the sections where the CPW grounds are reduced on either side of the primary transmission line. These techniques may be useful to the research here in an attempt to excite higher order modes and extending the operation bandwidth of the antennas. RF connectivity to the antenna is provided by a 50 Ohm SMA connector which has been soldered to the conductive film (PEDOT) deposited onto the sticky tape. This is informative, in that the antenna itself is capable of surviving significant thermal shock during the soldering process [18].

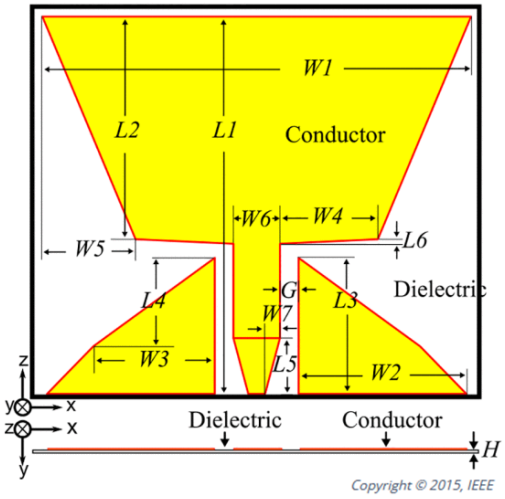

Figure 1.13: Polymer ultra-wideband antenna structure [17]

Focusing on the deformation of the structure, from Figure 1.14 [17], the electrical testing of the UWB antennas is subjecting to bending across a large range. It can be seen from the reflection coefficient shown in Figure 1.15 [17], that in the case where the antenna is bent by 90° in either direction, the frequency responses remain quite similar and variation is minimal from the planar case, in particular exhibiting similar lower frequency antenna operation. In the cases where the antenna experiences 180° folding, the frequency behaviour across the band is significantly altered. In these extreme cases it may be said that the overlapping of the antenna unto itself, alters the antenna's near-field, in comparison to a flat configuration. This illustrates that antennas of this nature are subject to significant electrical variation as the antenna itself

experiences physical deformation.

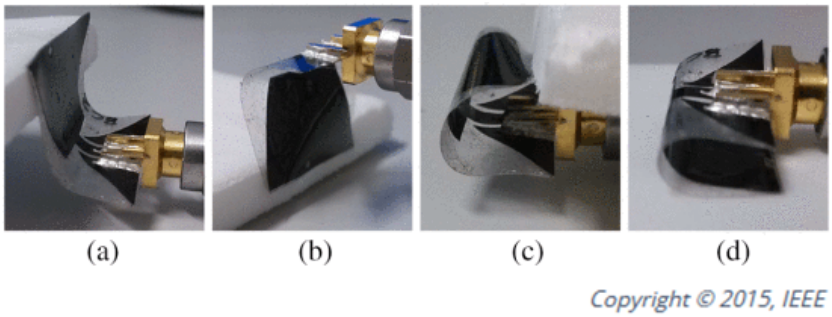

Figure 1.14: Polymer ultra-wideband antenna undergoing stress testing [17]

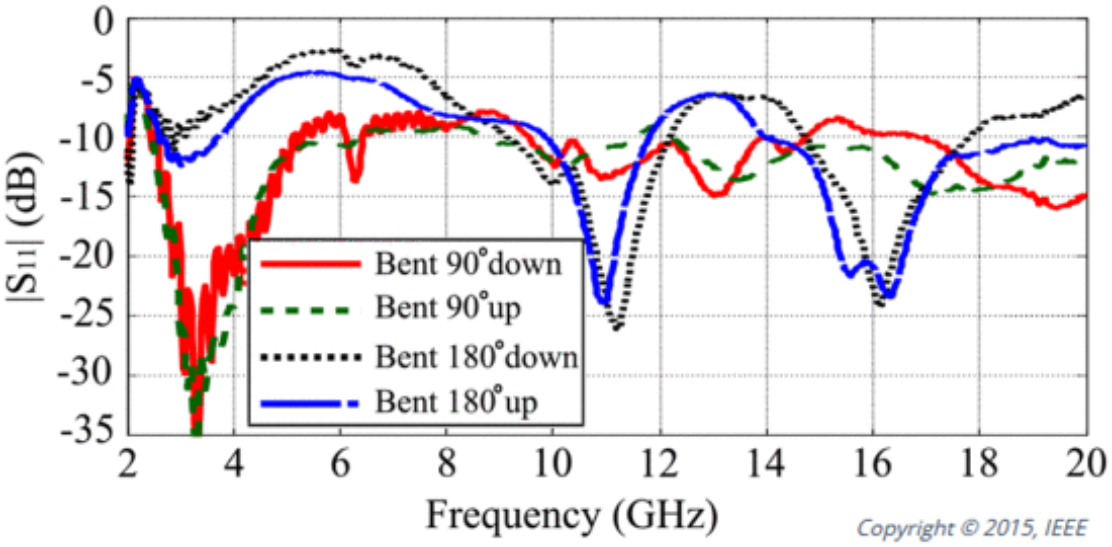

Figure 1.15: Frequency Response during applied stress test [17]

The final aspect of this literature review concerns itself with the development of transmission lines, antennas, and related mechanisms to establish reliable operation for flexible devices, using conductive fabrics or threads. Examples of this type of antenna may now be found in the open literature [19][20][21][22].

The research completed by Kiourti et al. [19], demonstrates a wearable class of antenna, with particular emphasis around on-body communications and medical applications. Demonstrated is the ability to seamlessly integrate antennas into clothing and blending antennas into logos to make these antennas less obtrusive. Further demonstrated is the integration of these antennas with polymer ceramic composites to realise stretchable substrates. The antenna structures are realised through embroidery techniques, with fabrication accuracies of 0.1 mm using this process. The pattern may be electronically programmed using a computerised embroidery machine, making for repeatable and accurate processing of a given design. A process such as this may present as useful to applications that are of focus for the present research here, given the requirement of flexible

transmission lines and antennas. The devices presented demonstrate reasonable performance and a good degree of success for their given applications.

In [21], the authors present a comparison of fabric and embroidered dipole antennas [21]. Of particular interest, are the findings around the losses with respect to use of either technique in realizing a conductor for the antenna. The article includes comparisons made between a conductive Ripstop nylon fabric, and two other conductor implementations using an embroidery machine to stitch the antenna's pattern. Importantly, the stitch efficiency of the embroidery machine is shown to have an impact on the total gain of the antenna. The simulations around sheet-resistivity show that as the thickness of the sheet increases, so does the antenna efficiency. The thread density used by the embroidery machine to realise the design also had an impact on antenna efficiency. To more efficiently use the conductive thread, the authors have suggested increasing the density in regions where concentrated RF currents exist along the antenna. The findings in that work are relevant to the direction of the work performed herein. In particular, one of the aims of the research is to realise flexible antenna structures, potentially using conductive threads or fabrics, whilst also reducing cost through the efficient usage of materials, as in the case of the embroidery machine with efficient stitch parameters.

Antenna structures capable of operation in rugged conditions is a further aspect of interest in the present thesis. In [23], the authors demonstrated the usage of snap-on buttons as mechanisms to mechanically affix the antenna together as well as provide RF connectivity. Implementation is quite interesting in the sense that the antenna configuration may be varied by simply removing the snap-on buttons and affixing a new resonant radiator element. This makes for quite versatile antenna use, depending on application, without duplication of further resources, hence reducing the cost of potential deployments. This was done by maintaining the same substrate and ground plane, whilst changing the top-layer of the antenna. Results indicated efficient operation of the antenna, in both linear, LHCP and RHCP implementations, with demonstrated antenna operation of up to 8 GHz. A characterization of the antenna under certain bending conditions was performed as well, with little variation in frequency response. Rais et al., [24] presented a "Review of wearable antenna". The themes presented in this review are similar to the aforementioned examples from other groups. The authors, reviewed flexible implementation and fabrication of a number of conventional antennas, such as monopoles, PIFA's and patch antennas. These antennas were fabricated using a number of methods, namely conductive thread to stitch the antenna, conductive spray as a flexible conductor, and copper tape. Of particular interest in the fabrication of these antennas [25] is the use of conductive spray in an attempt to create a more flexible antenna. Similarly, inkjet printing processes have been deployed to printing antennas using conductive ink [26][27][28]. In the examples referenced, the substrates used for printing were paper [26][27] and textiles [28]. The conductive textile [28] demonstrated an antenna efficiency of 57%. Further demonstrated was the frequency response under deformation, such as wrapping the antenna around a cylinder. The variation in frequency response was shown to be minimal during the performed bending tests. This testing regime is informative, in that, if warranted, the antennas or associated RF structures under test may be placed under similar stress whilst conducting electrical characterisation.

1.6.3 Frequency Reconfigurable Antennas

The concept of frequency-reconfigurable antennas aims at maintaining the same physical shape of the antenna whilst adjusting, or reconfiguring, the antenna electrically to perform across desired frequency bands. There are numerous examples in the literature [29][30][31] [32][33][34][35], demonstrating various techniques to achieve frequency reconfigurability. Christodoulou et al. categorized these various methods of achieving frequency agility namely as electrical, optical,

physical or altering the material properties of the antenna. The target of this research, if realisable with the investigated antenna structures, shall be to achieve this frequency variation using electrical components, potentially varactors, FET's or PIN-diodes given the resources available at hand. Within the context of electrically re-configurable antennas, these devices allow for frequency reconfigurability of the antenna by altering or redistributing the surface currents on the antenna itself [30], thereby allowing for variation in the resonant frequency of the antenna and manipulating the electromagnetic fields in the immediate vicinity of the antenna. Reconfiguration is typically used to adjust 3 distinct antenna properties, namely radiation pattern, frequency agility and polarization. In addition to the implementation of a re-configurable design, the negative effects such as parasitic loss through the varactor or diode, must be considered.

An excellent example of switches used to reconfigure the impedance and radiation properties of a patch antenna is demonstrated by Yang et al. [36]. By creating two orthogonal slots in the feed of the antenna and placing a switch on either slot, the polarization of the antenna could be varied between RHCP and LHCP, without need to change the physical position of the feed probe. In a physically constrained environment, such as such as a Deep Space application, where keeping total equipment weight down is paramount, an implementation such as this is very useful in that there is a reduction in the number of antenna elements required to support various operation modalities. Within the application area targetted in the current thesis for instance, if one were able to reduce weight without additional physical fixtures and was able to control frequency variation electrically, this would indeed be a valuable system attribute.

An implementation of reconfigurable antenna was presented in [32] whereby varactors were used to alter both resonant frequency and polarization of an antenna. The varactors were placed between quarter-wavelength stubs and a patch antenna. Variation was achieved by tuning the voltage across the varactors to manipulate the antenna impedance. A 40% fractional bandwidth was achieved whilst also allowing use of linear and circular antenna polarization. Of note in the previously described examples is the judicious selection of bias components required to implement the tuning effects. It is noted that the DC supply voltage to the 12 varactors is fitted with both large resistors and inductors. These components were selected for their high impedances to reduce the propagation of RF currents back up into the DC supply lines, which if left untreated would make the task of accurately varying the impedance increasingly difficult. For the variable antenna designed and constructed in this work a similar implementation in the bias network will be required.

1.7 Conclusion

The areas of antenna research surveyed within this literature review have been primarily motivated by the operational context within which the antenna is designed to operate. Specifically, the antenna characteristics desired are miniaturisation, flexibility, and frequency reconfigurability.

Firstly, with respect to miniaturisation, a specific aspect of the research is to conduct exploration of asymmetric antenna operation. Very few examples were found in the open literature [12][13]. The general monopole antenna provides an example of elegant asymmetry, in that the monopole is counterpoised to a ground-plane, which mirrors the image currents of the monopole stub. Of the miniaturised dipole structures that were found, the structures were, in most cases, manipulated in a symmetrical fashion with shrinkage of the antenna achieved by manipulating the dimensions of both dipole arms. The general monopole antenna provides an example of elegant asymmetry, in that the monopole is counterpoised to a ground-plane, which mirrors the image currents of the monopole stub. Of the miniaturised dipole structures that were found,

the structures were, in most cases, manipulated in a symmetrical fashion with shrinkage of the antenna achieved by manipulating the dimensions of both dipole arms. Normally these manipulations were introduced by way of additive inductive [37] or capacitive [38][39] reactance, in the form or meanders and arrows on the antennas. Radical asymmetrical manipulations of dipole structures were found to be quite rare in the literature. The antenna miniaturisation work conducted within the present thesis shall focus on asymmetrically opposing the dipole, through replacement of a dipole arm with an equivalent reactive loading.

Secondly, the use of flexible materials and planar implementations to fabricate an antenna and transmission lines is an area that requires exploration. Reflecting on the environment within which the antenna must operate there are demands placed on the antenna with respect to the antenna function and operation in harsh environmental conditions. There are several examples now in the literature of successfully demonstrated flexible antenna structures[19][20][22][17] [28]. The structures analysed were realised from conductive fabrics, threads, tapes, and conductive inks. Of interest was the antenna efficiency generated with use of the implemented material system. Flexible performance of these structures was also characterised through bending, wrapping and structural deformation. These findings yield information that may help inform potential trade-offs, in mechanical versus electrical performance and will help guide the design decisions of the structures studied during this thesis. These authors have further provided experimental results to validate their findings. Certainly, the work conducted by these authors will serve to provide direction to fabrication of the antenna and associated feed structures in this thesis.

Thirdly, the antenna must not only be capable of withstanding treatment within harsh environments but in the presence of environmental effects and variable operating conditions possess capability to tune across frequency to improve operation. Frequency reconfigurability is an important attribute of the antenna within this context. The work performed by several authors in this space, shall inform and help guide the addition of reconfigurable attributes to the antenna. Specifically, electrical configurability will be explored through the application of electrical components to the antenna itself to modify the frequency response.

After examination of the terrain covered during this literature review, there are distinct openings in the literature surveyed. For one, radically altering a dipole asymmetrically with a reactive counterpoise is an aspect under-explored. This is an area of interest to the research here, and experimentation will be conducted in this area. Development of flexible transmission lines, of low cost and with ease of realisation, is a complimentary area of research and focus shall be placed on in this area as well. Should the structure of the antenna further lend itself to frequency reconfigurability, via use of microwave circuit components, an implementation of this design would be explored too. Of note, is that this is an enormous body of work, however the characteristics identified here are of tremendous value where size, weight, power, and form factor are of concern. The body of work analysed has been instructive in providing clarity and direction to drive forward the direction of research.

In terms of thesis structure, the first design idea, presented and explored in Chapter 2, is that of a novel flexible transmission line, developed with off-the-shelf components, possessing material characteristics that allow for flexible, conformal articulation of the transmission line. Once a simple line is designed, further ideas of device designs are presented and explored using this technology. The third chapter presents a transmission line design and fabrication geared towards wearable applications. Here further analysis is conducted with respect to the physical robustness of the structure, and constraints associated with variations in the fabrication of the transmission line. The fourth chapter, puts forward a design, fabrication and results for an asymmetrical antenna. This experimental design forms a basis of which the subsequent antennas, in Chapter 5 & 6, are developed. Chapter 5 builds further of the design presented in Chapter 4, by developing a design method for the antenna and presents a planar implementation of the antenna. Chapter

6, introduces the feature of frequency reconfigurability into the design through the introduction of active circuit elements, which aid to shift the resonant frequency of the antenna. It is intended that the exploration of these transmission lines and antennas overlap with overarching antenna design goals of building structures which are flexible, robust, miniature, frequency agile and can be fabricated at low cost to our users.

Bibliography

[1] Jean-Jacques DeLisle. Bringing cognition to tactical networks. *https://www.mwrf.com/systems/bringing-cognition-tactical-networks*, 2013.

[2] Michael Ryan and Michael Frater. A tactical communication system for future land warfare. *Land Warfare Studies Centre*, 2000.

[3] Lan Jen Chu. Physical limitations of omni-directional antennas. *Journal of applied physics*, 19(12):1163–1175, 1948.

[4] Roger F Harrington. Effect of antenna size on gain, bandwidth, and efficiency. *J. Res. Nat. Bur. Stand*, 64(1):1–12, 1960.

[5] David M Pozar. Microwave Engineering. *Fourth Editions, University of Massachusetts at Amherst, John Wiley & Sons, Inc*, 2012.

[6] Christopher Coleman. *An Introduction to Radio Frequency Engineering.* Cambridge University Press, Cambridge, 2004.

[7] Willian J Highton. How does an antenna work? *https://chemandy.com/technical-articles/antenna/.*

[8] Steven McIntyre. 7 Simple Technology Driven PCB Quality Control Methods, PCB Assembly Resources. *https://www.syscomtechusa.com/simple-technology-driven-pcb-quality-control-methods/.*

[9] Son Xuat Ta, Ikmo Park, and Richard W Ziolkowski. Crossed dipole antennas: A review. *IEEE Antennas and Propagation Magazine*, 57(5):107–122, 2015.

[10] Reinhold Ludwig and Pavel Bretchko. RF circuit design, 2000.

[11] Constantine A Balanis. *Antenna theory: analysis and design.* John wiley & sons, 2016.

[12] Christos I Kolitsidas, B Lars G Jonsson, P Persson, and A Stjerman. Exploiting asymmetry in a capacitively loaded strongly coupled dipole array. In *2014 Loughborough Antennas and Propagation Conference (LAPC)*, pages 723–726. IEEE, 2014.

[13] Churng-Jou Tsai, Wei-Chih Chen, Chia-Hsun Lin, Jinn-Kwei Guo, and Chun-Lin Lu. An asymmetry printed WLAN/WiMax dipole antenna. In *2011 Fifth International Conference on Genetic and Evolutionary Computing*, pages 135–138. IEEE, 2011.

[14] Leah Buechley and Michael Eisenberg. Fabric PCBs, electronic sequins, and socket buttons: techniques for e-textile craft. *Personal and Ubiquitous Computing*, 13(2):133–150, 2009.

[15] Xiaoming Tao. *Wearable electronics and photonics.* Elsevier, 2005.

[16] Claudius Feger. *Advances in polyimide: science and technology.* CRC Press, 1993.

[17] Shengjian Jammy Chen, Thomas Kaufmann, Roderick Shepherd, Benjamin Chivers, Bo Weng, Anthony Vassallo, Andrew Minett, and Christophe Fumeaux. A compact, highly efficient and flexible polymer ultra-wideband antenna. *IEEE Antennas and Wireless Propagation Letters*, 14:1207–1210, 2015.

[18] Zequn Mei, Helen A Holder, and Hubert A Vander Plas. Low-temperature solders. *Hewlett Packard Journal*, 47:91–98, 1996.

[19] Asimina Kiourti and John L Volakis. Wearable antennas using electronic textiles for rf communications and medical monitoring. In *2016 10th European Conference on antennas and propagation (EuCAP)*, pages 1–2. IEEE, 2016.

[20] Thomas Kaufmann and Christophe Fumeaux. Wearable textile half-mode substrate-integrated cavity antenna using embroidered vias. *IEEE Antennas and Wireless Propagation Letters*, 12:805–808, 2013.

[21] Thomas Kaufmann, Ilse-Marie Fumeaux, and Christophe Fumeaux. Comparison of fabric and embroidered dipole antennas. In *2013 7th European Conference on Antennas and Propagation (EuCAP)*, pages 3252–3255. IEEE, 2013.

[22] Shengjian Jammy Chen, Thomas Kaufmann, Damith Chinthana Ranasinghe, and Christophe Fumeaux. A modular textile antenna design using snap-on buttons for wearable applications. *IEEE Transactions on Antennas and Propagation*, 64(3):894–903, 2016.

[23] Shengjian Jammy Chen, Damith Chinthana Ranasinghe, and Christophe Fumeaux. Snap-on buttons as detachable shorting vias for wearable textile antennas. In *2016 International Conference on Electromagnetics in Advanced Applications (ICEAA)*, pages 521–524. IEEE, 2016.

[24] NHM Rais, Ping Jack Soh, Farek Malek, Shahad Ahmad, NBM Hashim, and PS Hall. A review of wearable antenna. In *2009 Loughborough Antennas & Propagation Conference*, pages 225–228. IEEE, 2009.

[25] Jaime G Santas, Akram Alomainy, and Yang Hao. Textile antennas for on-body communications: Techniques and properties. 2007.

[26] William G Whittow, Alford Chauraya, JC Vardaxoglou, Yi Li, Russel Torah, Kai Yang, Steve Beeby, and John Tudor. Inkjet-printed microstrip patch antennas realized on textile for wearable applications. *IEEE Antennas and Wireless Propagation Letters*, 13:71–74, 2014.

[27] Li Yang, Amin Rida, Rushi Vyas, and Manos M Tentzeris. RFID tag and RF structures on a paper substrate using inkjet-printing technology. *IEEE transactions on microwave theory and techniques*, 55(12):2894–2901, 2007.

[28] George Shaker, Safieddin Safavi-Naeini, Nagula Sangary, and Manos M Tentzeris. Inkjet printing of ultrawideband (UWB) antennas on paper-based substrates. *IEEE Antennas and Wireless Propagation Letters*, 10:111–114, 2011.

[29] Randy L Haupt and Michael Lanagan. Reconfigurable antennas. *IEEE Antennas and Propagation Magazine*, 55(1):49–61, 2013.

[30] Christos G Christodoulou, Youssef Tawk, Steven A Lane, and Scott R Erwin. Reconfigurable antennas for wireless and space applications. *Proceedings of the IEEE*, 100(7):2250–2261, 2012.

[31] Songnan Yang, Chunna Zhang, Helen K Pan, Aly E Fathy, and Vijay K Nair. Frequency-reconfigurable antennas for multiradio wireless platforms. *IEEE microwave magazine*, 10 (1):66–83, 2009.

[32] Nghia Nguyen-Trong, Leonard Hall, and Christophe Fumeaux. A frequency-and polarization-reconfigurable stub-loaded microstrip patch antenna. *IEEE Transactions on Antennas and Propagation*, 63(11):5235–5240, 2015.

[33] Somarith Sam and Sungjoon Lim. Compact frequency-reconfigurable half-mode substrate-integrated waveguide antenna. *IEEE Antennas and Wireless Propagation Letters*, 12:951–954, 2013.

[34] Jeen-Sheen Row and Jia-Fu Tsai. Frequency-reconfigurable microstrip patch antennas with circular polarization. *IEEE Antennas and Wireless Propagation Letters*, 13:1112–1115, 2014.

[35] CW Jung, M-J Lee, and F De Flaviis. Reconfigurable dual-band antenna with high frequency ratio (1.6: 1) using mems switches. *Electronics Letters*, 44(2):76–78, 2008.

[36] Fan Yang and Yahya Rahmat-Samii. A reconfigurable patch antenna using switchable slots for circular polarization diversity. *IEEE Microwave and Wireless Components Letters*, 12 (3):96–98, 2002.

[37] BA Kramer, C-C Chen, and JL Volakis. Size reduction of a low-profile spiral antenna using inductive and dielectric loading. *IEEE Antennas and Wireless Propagation Letters*, 7:22–25, 2008.

[38] Andrew D Harris and Glen A Myers. An investigation of broadband miniature antennas. Technical report, NAVAL POSTGRADUATE SCHOOL MONTEREY CA, 1968.

[39] Zhenxin Hu, Zhongxiang Shen, Wen Wu, and Jian Lu. Low-profile top-hat monopole yagi antenna for end-fire radiation. *IEEE Transactions on Antennas and Propagation*, 63(7): 2851–2857, 2015.

Chapter 2

Wire-Over-Ground-Plane Transmission Line & Related Structures

2.1 Motivation for the Wire-Over-Ground-Plane Transmission Line

Given the drive towards low cost and flexible conformal materials for antenna development, an aspect of research conducted during this study is the design of novel flexible transmission lines. Initial experimentation with polyimide sheets, standard electrical wire and copper tape led us to believe that the creation of an unbalanced transmission line similar in stack up to a microstrip transmission line may be possible. This experimentation led to the development of Wire-Over-Ground-Plane (WOGP) transmission lines. Further explored in this chapter are ideas relating to the development of more advanced RF structures using this technology. A primary advantage of this form of flexible transmission line, is the utility and comfort it potentially offers to a user. For example, in many applications the optimal antenna placement may be higher up on a user, however the radio transceiver may be attached around waist level for user comfort. A means of attachment from the radio unit to the antenna, which leads to a natural fit, and does not encumber the user during operation is beneficial. The materials used to create this transmission line have mechanical characteristics that adapt or conform to various user setups. Firstly, let us examine the microstrip line setup [1]. One can see that the stack is simple in nature. Essentially one requires a ground plane, a substrate and a signal conductor strip to form an unbalanced transmission line capable of signal transmission. The electromagnetic wave is guided by the signal conductor strip and the ground plane beneath, with a certain amount of loss as the wave propagates through the transmission line. In order to fabricate the microstrip geometry, one requires PCB tooling for patterning of the conductor, which may be reasonably costly and time consuming. Additionally, processing of flexible materials, such as polyimide thin films, of thicknesses typically in the tens of microns, make it a difficult material to work with standard PCB fabrication processes. Hence, the focus of research was driven towards the creation of a transmission line with similar unbalanced behavior to that of a microstrip line, yet manufacturing-wise, the line would be easier and more cost effective to realise with materials available off the shelf.

It had been proposed that, if one could use readily available electrical wire for the signal conductor, polyimide tape or sheet for the substrate and copper tape or metalized textile for the ground plane, a stack up of these materials may lend themselves to a process that does not require PCB tooling for manufacture. A transmission line of this nature would be quite useful for conformal applications given the flexible and robust characteristics of polyimide [2][3][4].

2.2 Design and Simulation of the Transmission Line

Examining Figure 2.1 (a) and (b), one may observe the manner in which the electric and magnetic field vectors travel as the wave propagates down a microstrip transmission line. This is demonstrative of a nearly transverse-electromagnetic (quasi-TEM) mode propagation. The magnetic field line circles the signal conductor as the wave propagates down the line and the electric field extends from the signal conductor ending on the ground plane below. It is important to observe these conditions in relation to the behaviour of the WOGP transmission line which will be examined next.

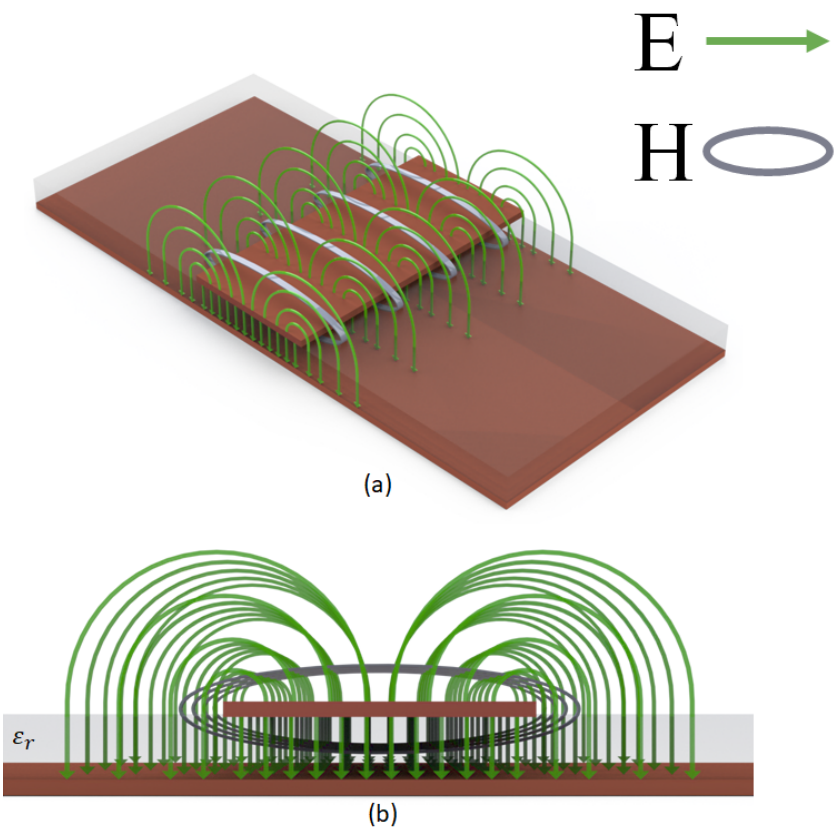

Figure 2.1: (a) 3D Microstrip transmission line illustrating electric and magnetic field behaviour down the line. (b) Illustration of microstrip transmission line stack-up and field lines along this cross-section.

Now let us examine the proposed WOGP structure. Figure 2.2 shows a cross-section of the proposed setup. The setup is quite comparable to that of microstrip in terms of stack with the primary difference being the use of a circular wire for the signal conductor.

$W1$ - Wire Diameter

$H1$ - Substrate Height

$H2$ - Ground Plane Height

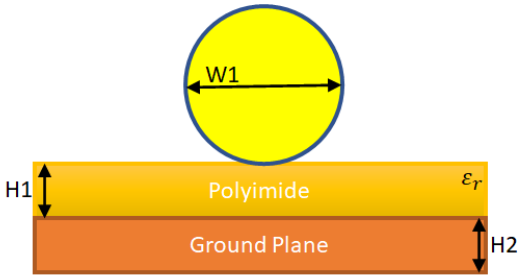

Figure 2.2: WOGP Stackup.

ϵ_R - Relative Permittivity of Polyimide

Wadell [5] does present a transmission line arrangement of this nature, however the analysis performed therein holds to the assumption that $H1/W1 >> W1$. In comparison to the thin-film approach taken in this design, substrate height and wire diameter are similar in magnitude. To explore the behaviour of the WOGP transmission line, a numerical approach using the Finite-Element-Method (FEM) is adopted to evaluate design and performance. Specifically, Ansys HFSS is used throughout this thesis to evaluate the electrical design performance of proposed structures.

To build a practical model, standard off-the-shelf component dimensions were used in the simulation. A copper foil tape thickness of 66 um, and a polyimide substrate thickness of 70 um were applied to the design. The wire diameter was varied parametrically to evaluate the change in characteristic impedance with respect to a changing wire radius. The wire radius was varied from 0.1 mm to 0.4 mm, in 0.05 mm increments. The relative permittivity and loss tangent of the polyimide film are 3.5 and 0.008 respectively.

Examining Figure 2.3, a plot of Z0 as a function of wire radius, it may be seen that a wire radius of 0.1 mm, allows for a transmission line impedance of close to 50 Ohms, a typical characteristic impedance for microwave applications. Since this is the case, further designs considered here shall be made with respect to a 50 Ohm transmission line impedance and will therefore make use of 0.1 mm radius wire conductor with this evaluated stack-up. The closest standard gauge off-the-shelf wire is AWG 32, with a wire radius of 0.101 mm. This wire would be useful in a practical implementation because there is negligible difference in wire radius in comparison to that simulated. This leads us to believe that the transmission line may be built using commercial-off-the-shelf (COTS) standard gauge wire.

Plotted in Figures 2.4 & 2.5, are the attenuation and phase constants of the transmission line modelled with 0.1 mm wire radius. It can be seen that the attenuation of the transmission line increases monotonically with frequency and maintains relatively low loss up to 5 GHz. Similarly the phase constant increases linearly up to 5 GHz and shows no distortion across this bandwidth. These simulated findings indicate that this WOGP structure may be useful for quasi-TEM, guided wave propagation.

Figure 2.6 and 2.7, respectively present the attenuation and reflection coefficient, with respect to a 50 Ohm termination on both ports, for a 50 mm length of transmission line. Simulation indicates a reflection coefficient below -40 dB with a transmission line attenuation of 0.32 dB for this length of line. Granted, these are simulated performance characteristics of the transmission line itself, and as such do not take into interface losses of connectors mounted to the transmission line. Given the low levels of attenuation and reflection coefficient, the WOGP transmission line appears quite a useful structure for guided wave propagation. In the case presented above,

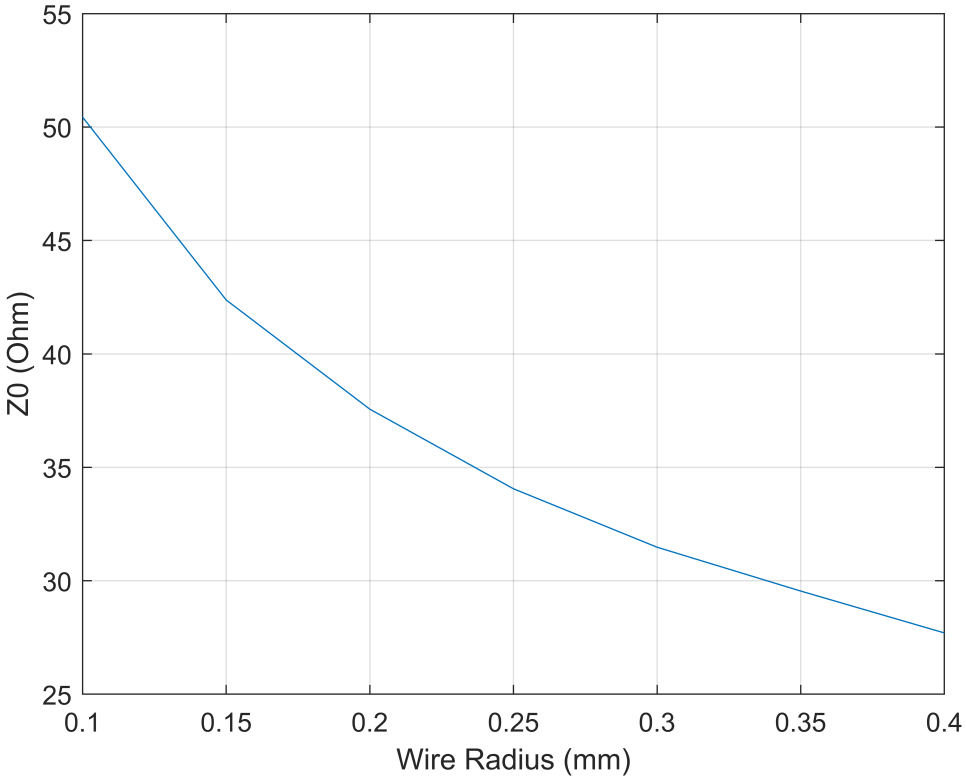

Figure 2.3: Z0 as a function of Wire Radius, at 2.5 GHz.

considering strictly the transmission line itself and no connection mechanism, simulated results indicate that the line itself operates up to at least 5 GHz.

To further try and understand the field behaviour of the WOGP transmission line, a plane was created parallel to the circular cross section of the centre-conductor and the magnetic and electric field plotted in this region. This was done to see how similar the behavior of the WOGP line is compared to that of the microstrip transmission line, presented in Figure 2.1.

From what is deduced from Figure 2.8, the magnetic field vectors in (a) are clearly rotating around the centre conductor and in (b) the electric field vectors transition from the centre conductor, to the ground plane. The nature of these field vectors indicates strong presence of a quasi-TEM mode propagation, allowing the conclusion to be drawn that the microstrip and WOGP transmission line are quite similar in nature and operation.

A prototype structure was constructed to validate operation of the WOGP transmission line. Bare copper wire of 0.1 mm radius was glued to a polyimide substrate, below which a sheet of copper tape was adhered to the back of the substrate. Sheet thicknesses of the polyimide and copper foil tape, are 70 and 66 um respectively. The length of the transmission line alone is 50 mm. A standard edge-mount 50 Ohm SMA connector, suited for 1.6 mm PCB thickness was connected to each end of the transmission line. The copper wire soldered to the inner conductor of the connector and the copper tape soldered to the body of the SMA connector. By no means is this a robust means of connectivity, however it is expected that this transition is an effective

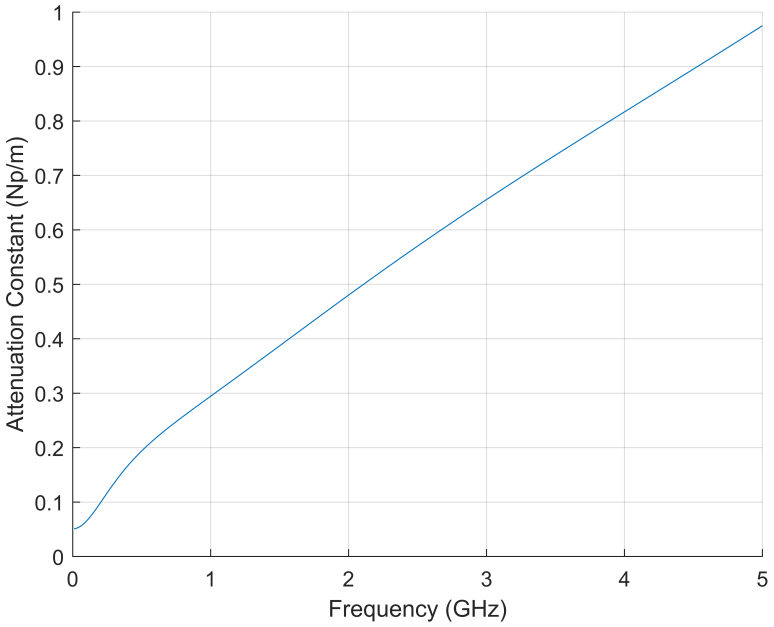

Figure 2.4: Attenuation constant for a WOGP transmission line of 0.1 mm wire radius.

means of exciting the transmission line. The results, Figure 2.9 & 2.10, show input and output reflection at significant better than 2:1 VSWR performance, with a transmission loss of less than 1 dB up to 5 GHz. This loss is higher than the simulated result, however one must take into consideration the loss of the transition, which is appreciable. Indeed, although the physical transition to the line is not robust, it does well to excite the structure. From these results, one may conclude that measured results are respectable and that the WOGP line may be practically useful, especially if a robust means of connectivity to the line is established.

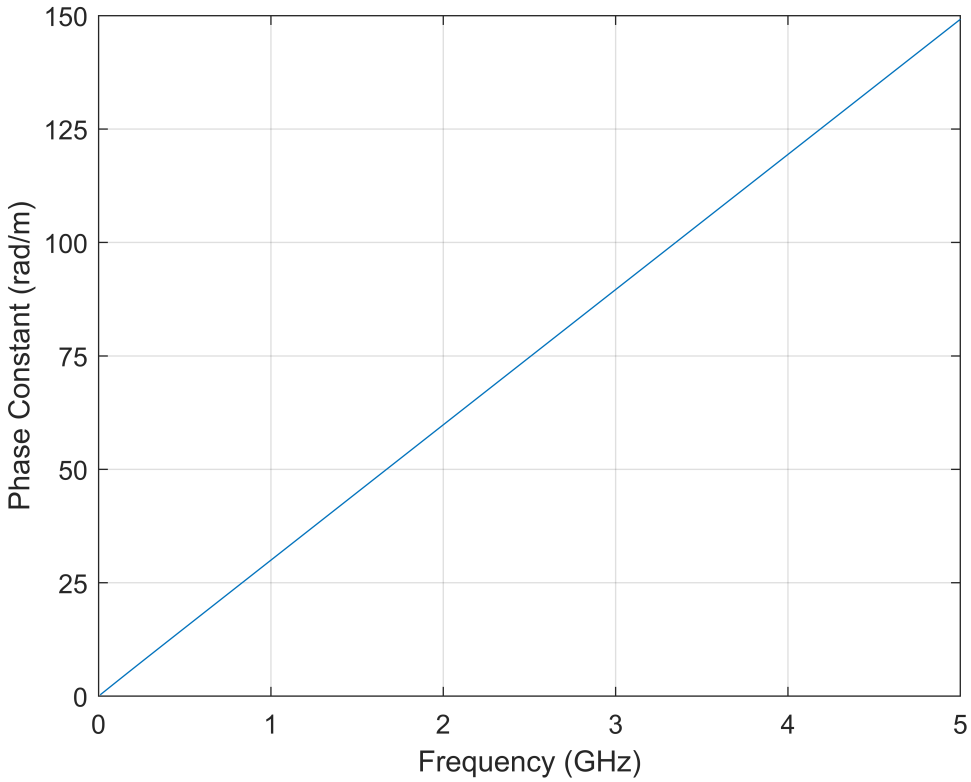

Figure 2.5: Phase constant for a WOGP transmission line of 0.1 mm wire radius.

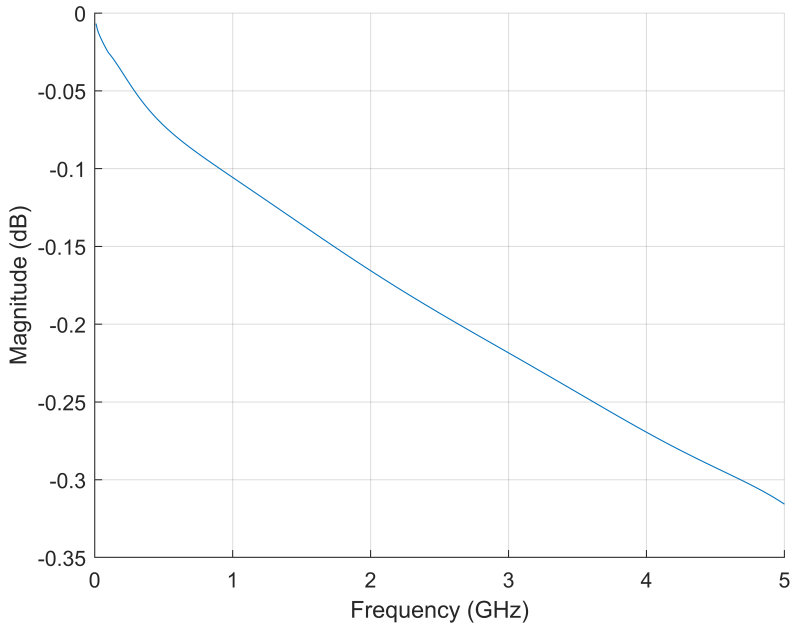

Figure 2.6: Attenuation across frequency for a WOGP transmission line of 0.1 mm wire radius and 50 mm length, with respect to a 50 Ohm port termination.

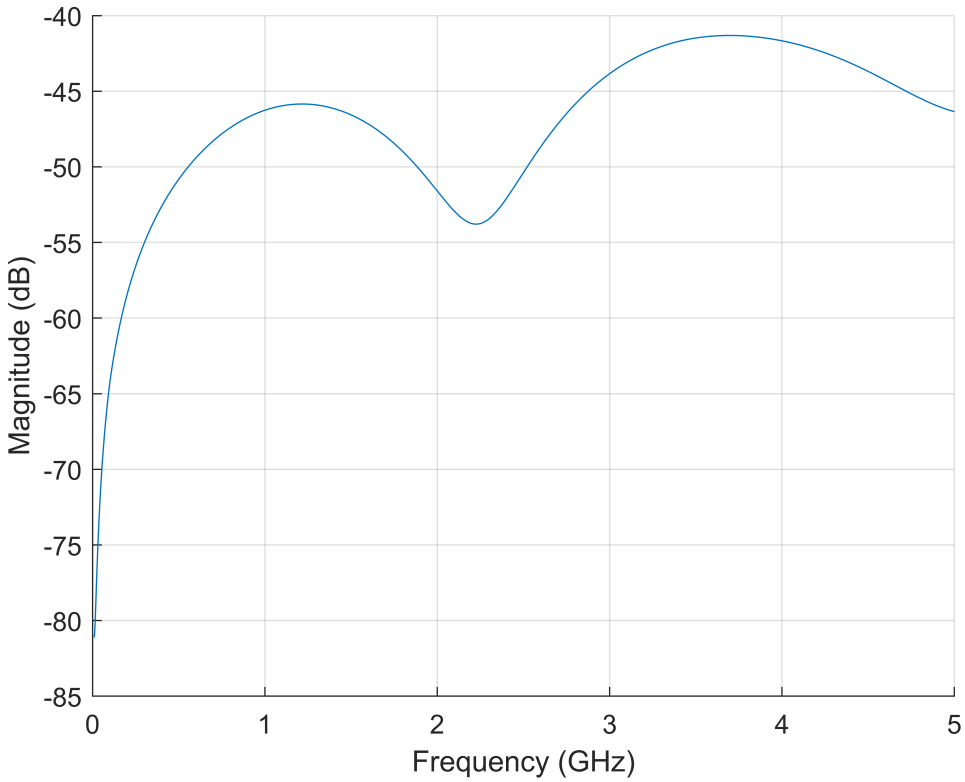

Figure 2.7: Reflection coefficient of a WOGP transmission line of 0.1 mm wire radius, with respect to a 50 Ohm port termination.

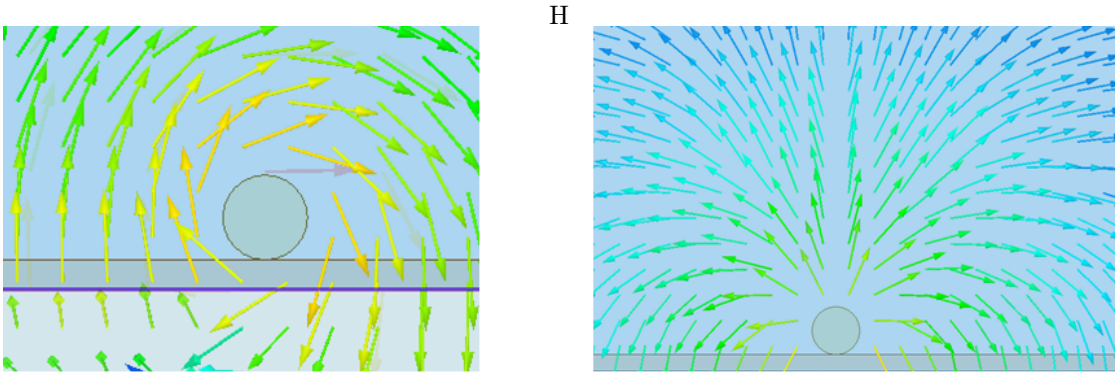

Figure 2.8: (a) Magnetic field circling conductor. (b) Electric field between signal conductor and ground plane.

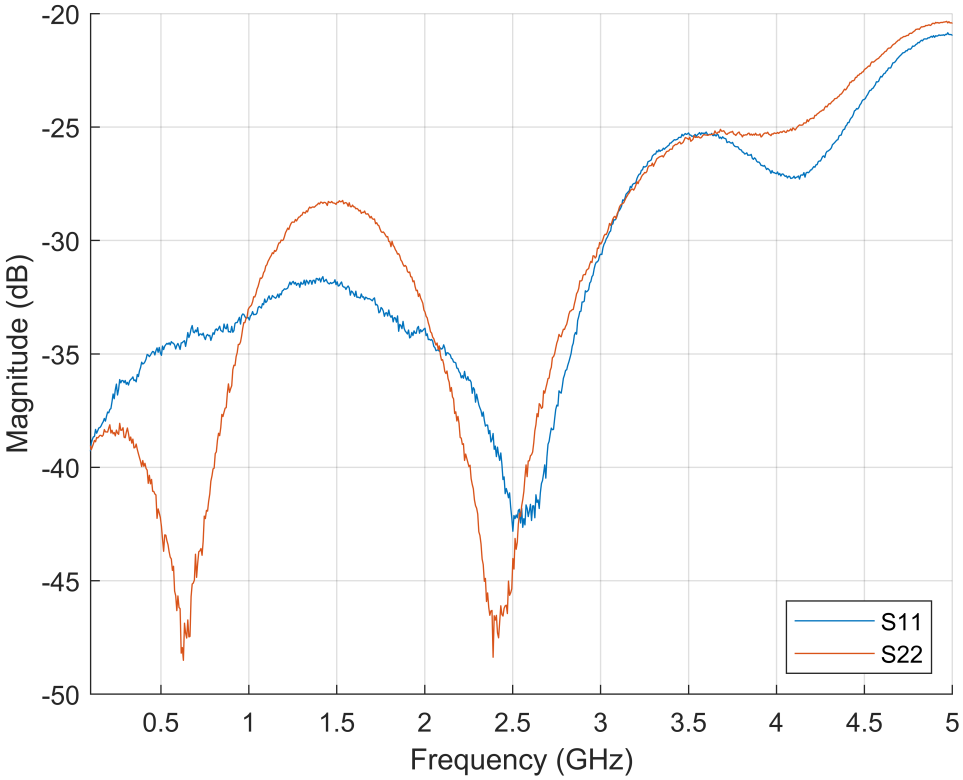

Figure 2.9: Measured input and output reflection coefficient.

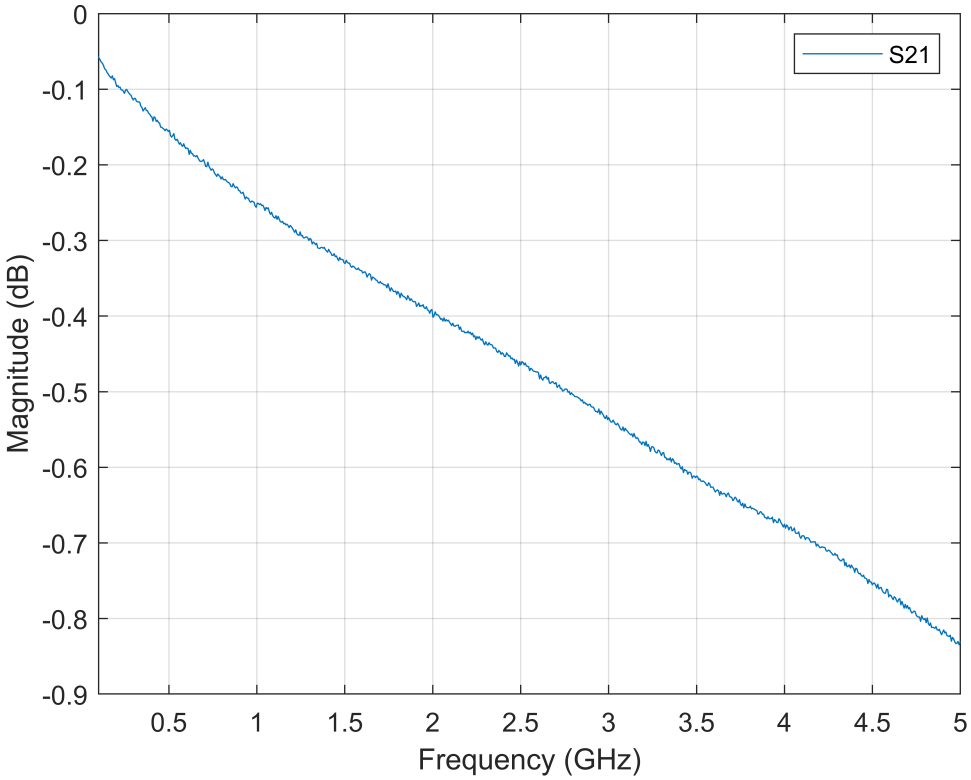

Figure 2.10: Measured forward transmission loss.

2.3 WOGP Implementation of a Branch Line Coupler

Given that the WOGP impedance may be controlled via varying the radius of the centre conductor, for a predetermined substrate height, backed with a conductive sheet on the opposite side, it is logical to assume that phase control may be realised as well, by appropriately adjusting the length of the transmission line.

With control of both amplitude and phase of the WOGP transmission line, the realisation of planar passive structures may be possible by appropriately tuning the line through different sections of the transmission line. Concentration was placed on examining passive structures which produce 90 and 180 degree phase shifts between ports as these may be useful phase shifts to achieve in antenna and balanced amplifier [6] configurations. In order to evaluate if this hypothesis is indeed sensical, the WOGP transmission line implementation was adapted to the Branch-Line-Coupler, presented in Figure 2.11 [1].

The microstrip quadrature branch-line coupler is completely planar in implementation, making it a useful candidate for WOGP implementation. Here the RF wave from Port 1, travels across to Port 2 and 3 with a 3 dB split between the ports. Given the additional quarter-wavelength the wave travels to arrive at Port 3, makes for a 90 degree phase shift between the ports. Given the phase cancellation at Port 4, it ends up isolated from Port 1.

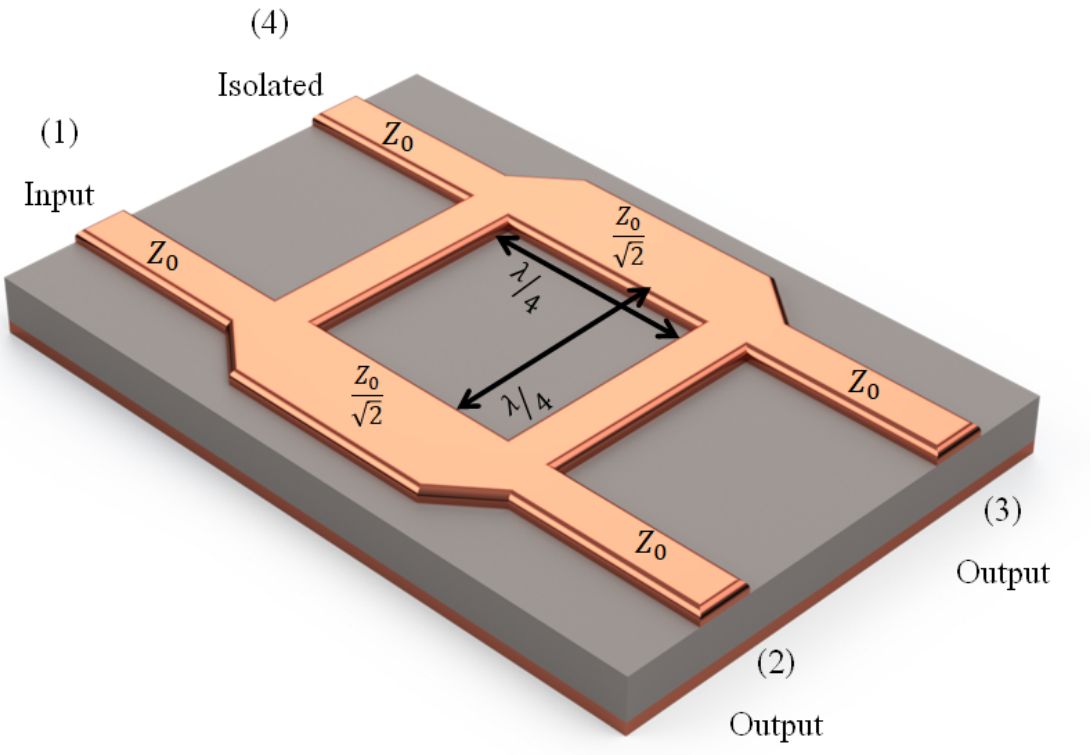

Figure 2.11: Setup of a microstrip branch-line coupler.

There are a few structural conditions to setting up this transmission line-based coupler. Firstly, a 50 Ohm transition is required to feed into the 4-port network. Secondly a quarter-

wavelength transmission line is required between the 4 junctions. Thirdly, an impedance of $Z0/\sqrt{2}$ is required from ports 1-2 and ports 3-4. Given that the antenna target designs have been in the WiFi and Bluetooth frequency ranges, it was decided that a centre frequency for the design would be 2.2 GHz, targeting 3G type application around this region, with the aim of extending to the lower end of the Wifi allocated spectrum.

Making reference back to Figure 2.3, for impedance as a function of wire radius using the exact WOGP stack-up presented earlier, a 50 Ohm impedance may be achieved by using a 0.1 mm wire radius and 50 mm length, $Z0/\sqrt{2} = 35.35$ Ohms, may be closely achieved by using a wire of radius 0.25 mm. It was found from EM simulation, that the $\lambda/4$ length required, as per Figure 2.11, is 24 mm to achieve centre frequency operation at 2.2 GHz.

Shown in Figure 2.12 is the HFSS simulated design with the critical dimensions. The s-parameters extracted from the simulation in HFSS are presented in Figure 2.13. It can be seen from the S11 response, that a minimum is achieved close to 2.2 GHz. It can be seen from the S21 and S31 responses that a close to 3 dB split is seen between the ports. The results there do show a difference of approximately 0.5 dB. It must be stated that the transitions between the $Z0$ and $Z0/\sqrt{2}$ impedance sections are quite abrupt, which may give rise to the varied amplitude response between the ports. It may be useful in a future iteration to possibly taper the section, or model lump of solder, which may be used physically join the section in a practical implementation. For the treatment here, the model was sufficient to generate a response for the underlying behaviour. Analysis of the phase response from Figure 2.14, shows a close to 90 degree phase difference, quadrature, between ports 2 and 3. The bandwidth over which this phase difference closely occurs is from approximately 2 to 2.5 GHz, at which point the quadrature phase difference between the ports 2 and 3 rapidly diminishes.

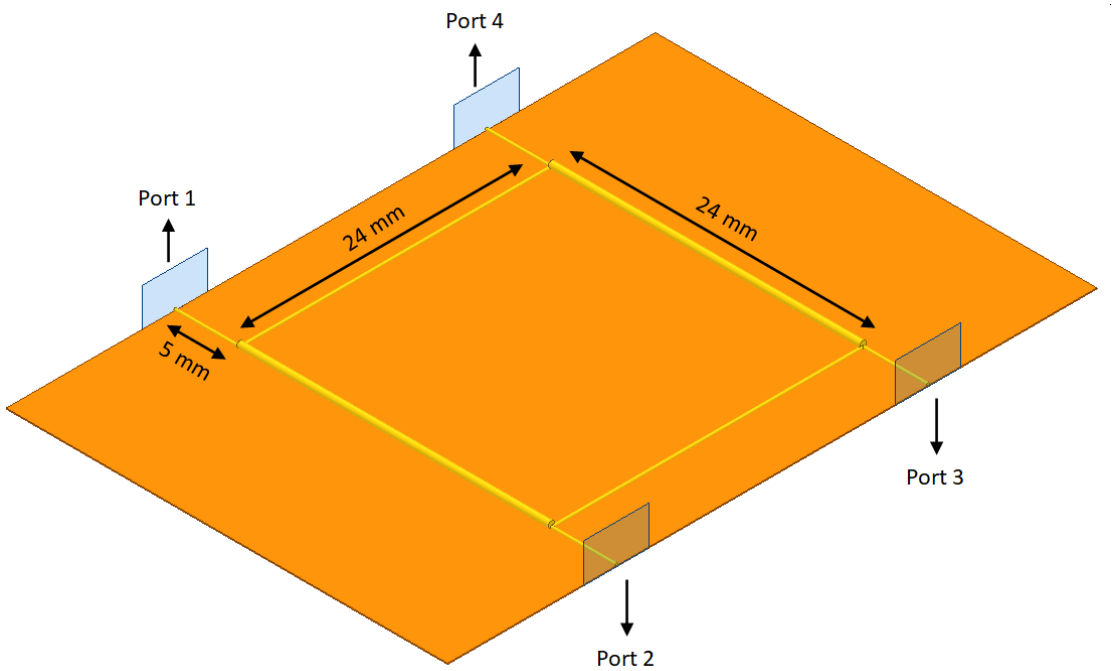

Figure 2.12: HFSS model of the simulated branchline coupler.

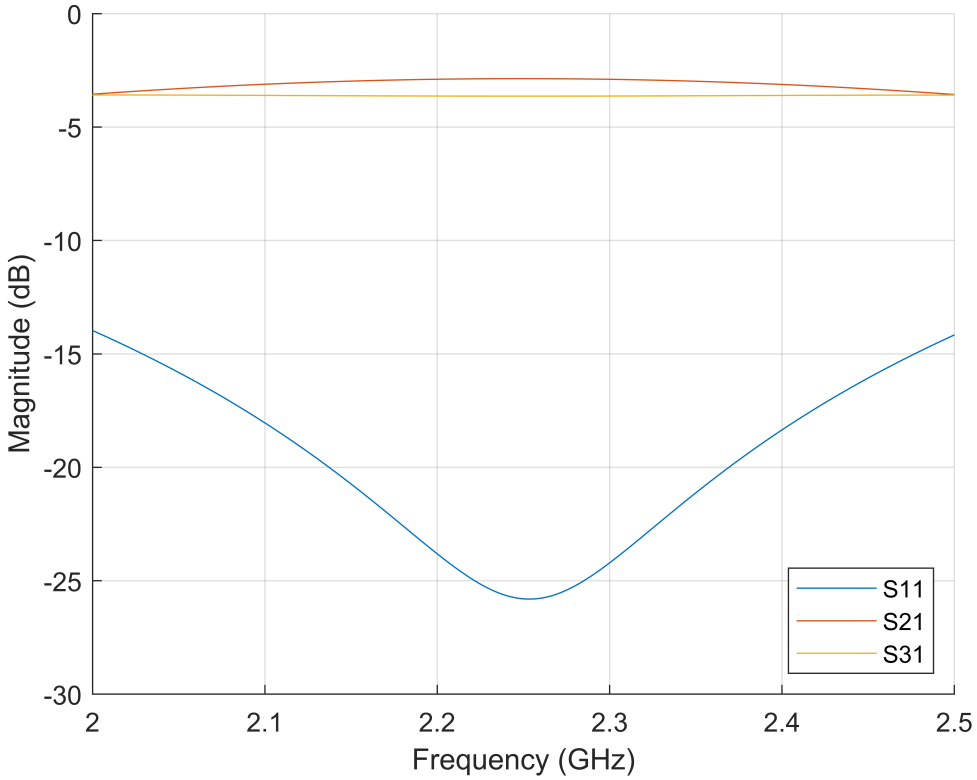

Figure 2.13: Amplitude Response for a WOGP implementation of the branch-line coupler.

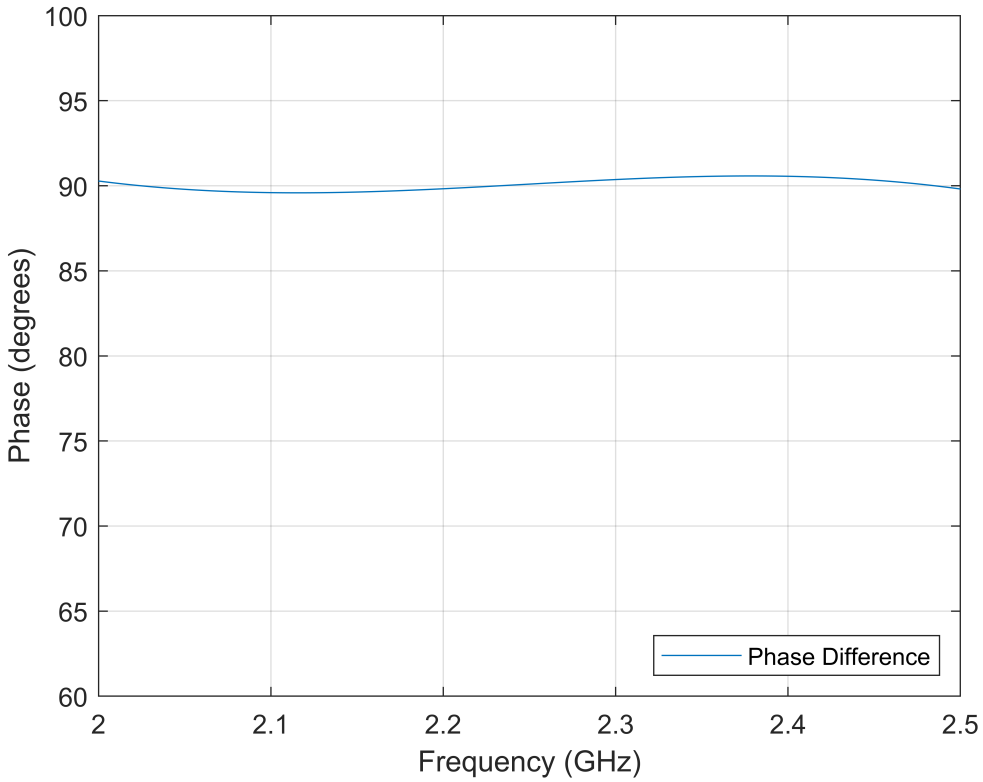

Figure 2.14: Phase Response for a WOGP implementation of the branch-line coupler.

2.4 WOGP Implementation of a Modified-Marchand Balun

Balanced to unbalanced transitions are useful in situations, such as that of the feeding of dipole antenna from a coaxial cable, where a differential feed is required at the dipole inputs. Aligned with the motivation of this thesis, the aim of this section is to demonstrate a means of providing this differential feed whilst also achieving a planar, mechanically flexible structure. The Marchand balun is one such type of balun design, which can be implemented using transmission lines, such as planar microstrip lines. Analysis of this modified Marchand balun from Sun et al. [7], yields a principle of operation reliant on the coupling between $\lambda/4$ lengths of transmission line. It is proposed that a controlled coupling be achieved through means of a WOGP implementation. Using a series of coupled WOGP transmission line, one may be able to replicate behaviour achieved by Sun et al. The following sub-sections presents the idea, and demonstrates through EM simulation, the operation of the proposed structure. Once more, as per the previous section, the intended design centre-frequency is 2.2 GHz.

2.4.1 Design Idea and Principle of Operation

The principle of operation of a transmission line Marchand balun is to effectively isolate [8], or float the ground from the unbalanced input port. Using the modified Marchand approach [7], $\lambda/4$ lengths of transmission line, shorted on either end to ground, are coupled to the unbalanced transmission line. The differential outputs are then drawn from the respective coupled section of transmission line.

The modified Marchand balun presented by Sun et al. [7], makes use of the lines cross-coupling over lengths of $\lambda/4$ and $3\lambda/4$, making for a $\lambda/2$ or 180 degree difference between the lines. The $3\lambda/4$ path is achieved via the reflection off the short circuit to ground on the far side and thereafter travelling the additional $\lambda/4$ to accumulate the additional phase difference, prior to differential energy extraction at the center of the structure. The results from Sun et al. [7] present VSWR 2:1 bandwidth extending from 1.9 GHz up to 4 GHz, whilst simultaneously achieving differential behaviour across this bandwidth.

The translation to a WOGP implementation may be made in a straight forward manner. In that, by appropriately selecting the wire radius, the impedance of the transmission lines may be chosen appropriately, and the phase may be adjusted by varying the length of the line. A critical feature of the Marchand balun arrangement, is the coupling between the transmission lines. It was thought that, instead of using bare copper wire, as had been done previously to realise the transmission line, insulated copper wire, having appropriate jacket thickness, would be used instead. Selecting wire of appropriate core and jacket diameters would ensure for accurate coupling distances between the transmission lines. Furthermore the physical implementation may be simplified, and made more elegant in realisation, if these geometries equated to standard AWG sized wire that could be simply placed alongside each other.

Figure 2.15 presents a graphical realisation of this idea. The variables below express the various geometries related to Figure 2.15.

$W1, W2, W3$ - Total wire diameter per respective wire

$S1$ - Distance between midpoints of left and centre conductor

$S2$ - Distance between midpoints of right and centre conductor

$H1$ - Substrate height

$H2$ - Copper-Tape height

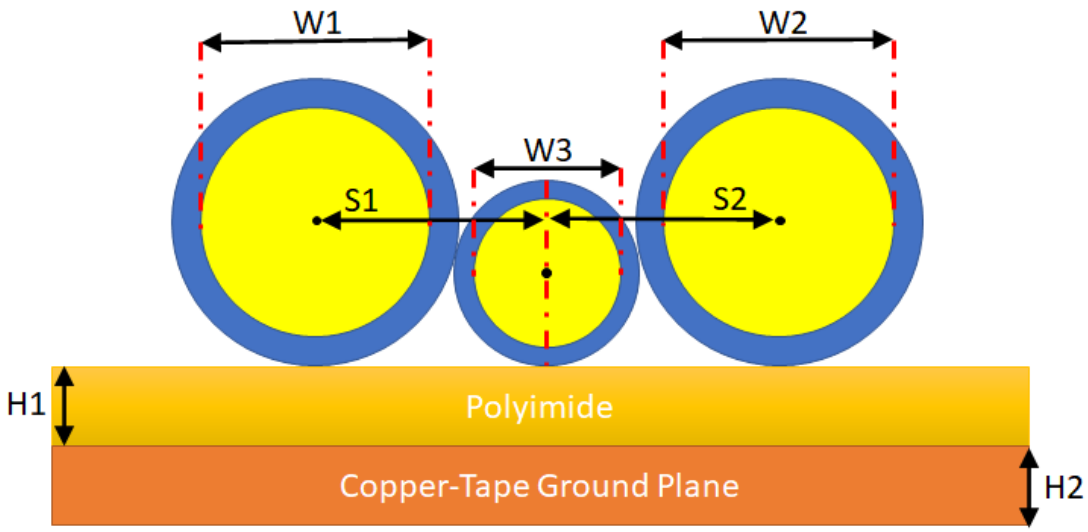

Figure 2.15: Proposed design idea for a modified Marchand balun utilizing a WOGP realization.

2.4.2 WOGP Modified Marchand Balun Design Method

The design idea described above was then used to implement a 3D model in HFSS. Hard-rubber was used to model the jack dielectric, which has a relative permittivity of 3. Given that the polyimide section below has a relative permittivity of 3.5, means that there is relatively small difference between the 2 neighbouring dielectrics. However, referring back to Figure 2.15, upon examining the cross-section of dielectrics across the coupled structure, there exist a small cross-section of air, through which the electric field must travel prior to terminating on the ground plane. We notice as well that the modified Marchand design implemented by Sun et al.[7] contained bond wires on the open-sectioned ends of the coupled $\lambda/4$ sections. This may have been done to equalize the potentials on either side of the unbalanced transmission lines, and to short out any unwanted modal setup on the coupled transmission line structure. The same has been implemented on the WOGP design, as shown in Figure 2.16, by placing a copper-block between the coupled line. The WOGP design has been modified further to isolate the differential outputs, by extracting the output from either side of the transmission line, from a 50 Ohm transmission line, connected bonded to the coupled section. By spatially separating the two signals, a greater amount of signal isolation is achieved between the output ports. Further, given that the electrical distance the reflected signal must travel is identical, leads to an unchanged differential setup.

As per Figure 2.15, the variables describing the design are per follows

$W1, W2$ - 0.45 mm

$W3$ - 0.3 mm

$S1, S2$ - 0.375 mm

$H1$ - 0.07 mm

$H2$ - 0.066 mm

The unbalanced transmission line had been designed to operate as a 50 Ohm line. From the analysis conducted earlier, in Section 2.2, it was found that this equated to a conductor radius of 0.1 mm. In this instance the wire insulation forces the inner copper wire to sit a certain distance above the polyimide substrate. The wire insulation between the copper cores were optimised and set to 12.5 um. This modification equated to a slightly larger wire radius of 0.15 mm for this design, to maintain a 50 Ohm impedance. In this instance, priority was placed on optimising the coupling between the transmission lines to obtain an appropriate signal split from the unbalanced transmission line. There is a minimal air gap between the copper wire insulators at its nearest point, in the HFSS model, of order less than 10 um. This was done to avoid unnecessary complexity in the overlapping of edges and the dielectric insulation of the wires. For the purposes of modelling the behaviour and operation of this structure, it had been assumed that there would be minimal impact on the electrical behaviour, given that this distance is of order magnitudes less than the wavelength of operation at 2.2 GHz. For simplicity, a design was derived which locked the dimensions of S1 with S2 and W1 with W2. This was done to simplify potential construction of this transmission line. Through EM simulation in HFSS, it was found that the required impedance of the coupled lines is approximately 35 Ohms. Once more, through simulation, the optimal diameter of W1 and W2 were found to be 0.375 mm. The total length of the transmission line structure is 34 mm, which allowed for a centre frequency of 2.2 GHz. The quarter-wavelength coupled lines, were set to 16.5 mm to accommodate for the break between the sections. The break in between the quarter-wave sections was set to 1 mm. To further illustrate the behaviour of the WOGP structure, the current density on the surface of the ground plane is plotted, as per Figure 2.17. From this visual representation of the current density, with excitation from Port 1 on the left, one may see the propagation of current down the coupled section of transmission line. This wave couples to the first $\lambda/4$ section, which then branches off to a 50 Ohm line, propagating up to its respective termination on Port 2. Secondly, the wave along the second $\lambda/4$ section travels to the end of the open circuit termination, reflects off the termination as can be seen by the saturation of current on the right, displayed in red-orange, and is then coupled out of this section, which branches to its 50 Ohm line, thereafter propagating down to its respective termination on Port 3.

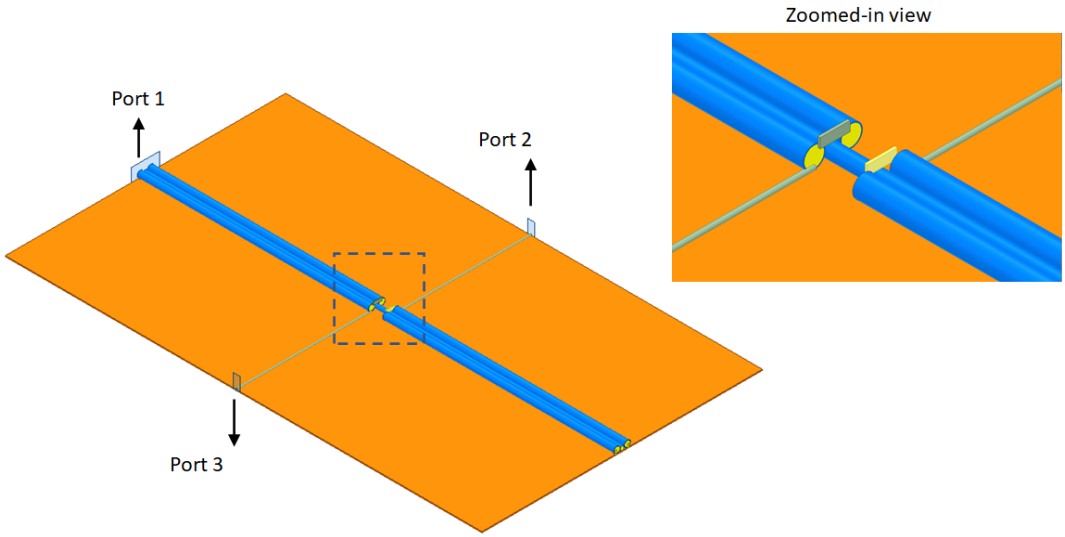

Figure 2.16: 3D illustration of the modified Marchand balun WOGP implementation.

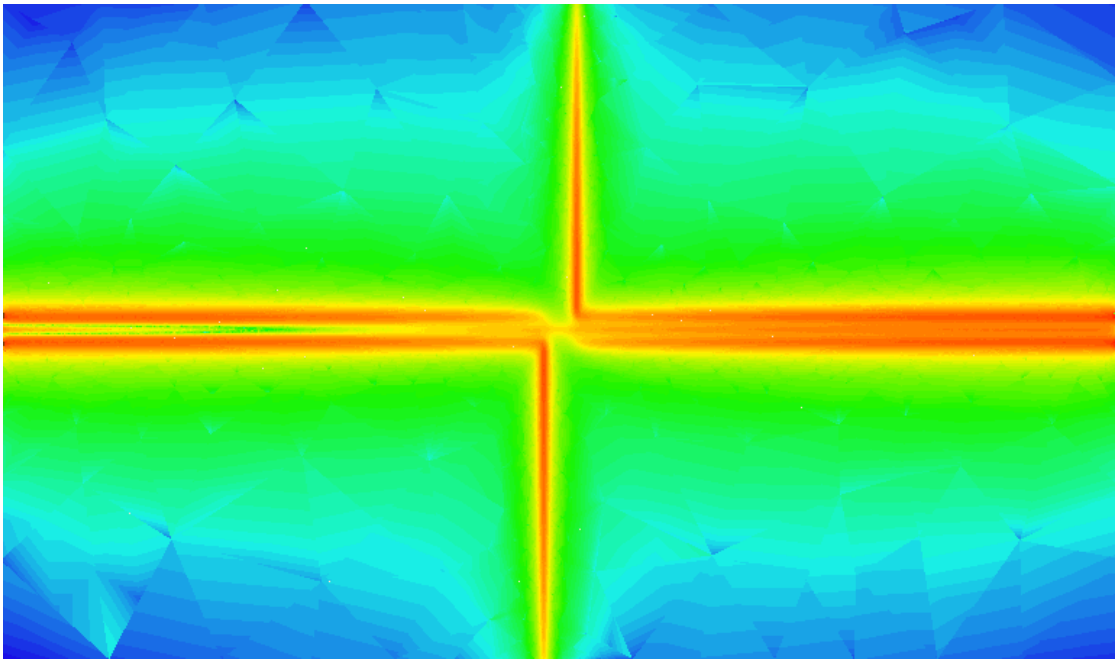

Figure 2.17: Current density magnitude on the surface of the ground plane.

Figures 2.18 and 2.19, present the s-parameters and the phase difference between the 2 output ports. One may observe from the s-parameters, that the reflection coefficient, from port 1 has a minimum at 2.2 GHz, indicating that the total length of the design has been set appropriately. Also, the coupling from the unbalanced transmission line to the balanced outputs is slightly less

than 3 dB. This would be expected due to dielectric losses in the substrate and the hard-rubber insulation. The loss-tangent for polyimide and hard-rubber are 0.006 [9] and 0.01 [10]. The design shows a VSWR of less than 2:1 from 2.02 to 2.4 GHz, indicating a percentage bandwidth ratio of 17.27 %. The phase difference represented in Figure 2.19, shows that the phase difference between the outputs is less than 5°. Further optimization here may be made with reference to the length of the quarter-wave transmission lines to get this offset even closer to 180°. In comparison to the results produced by Sun et al.,[7], the usable bandwidth here is approximately 398 MHz for a centre frequency of 2.201 GHz, which corresponded to a fractional bandwidth of 18 %. It must be stated that the bandwidth result obtained here is significantly less than the planar design from which the WOGP implementation is derived. This is informative in the sense that the setup, geometry, and structure of the WOGP implementation, inherently restricts wider band operation.

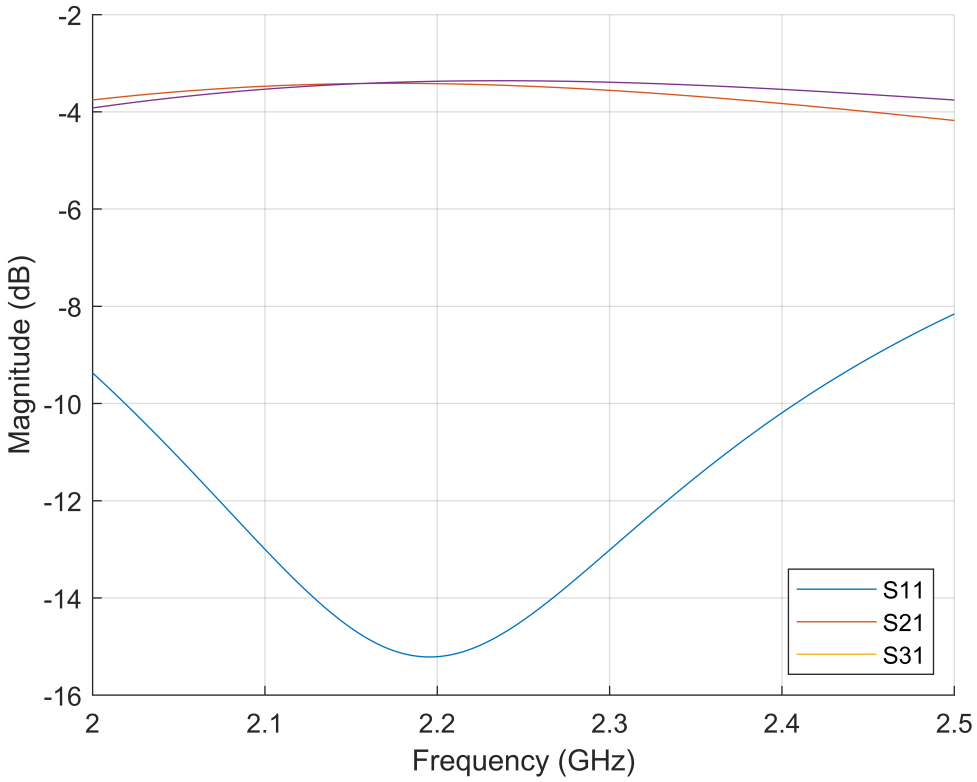

Figure 2.18: S11, S21 and S31 for the WOGP implementation of a modified Marchand balun.

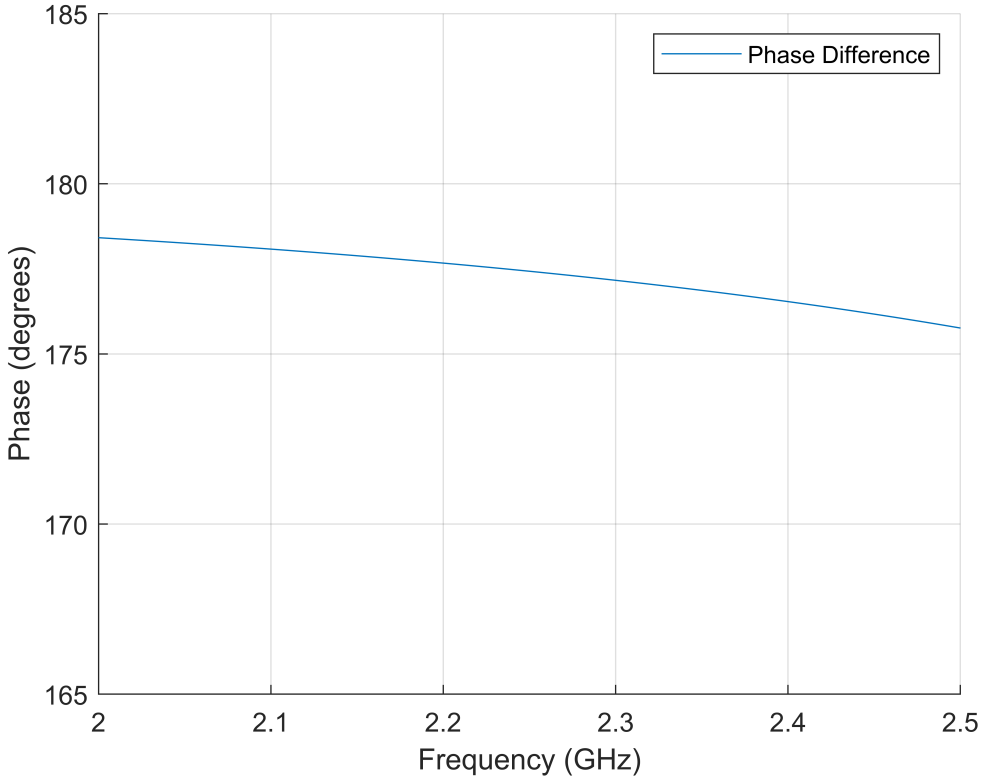

Figure 2.19: Phase difference between the balanced output ports.

2.5 Practical Considerations

Practically, a means of connecting to the WOGP transmission line from a suitable RF connector for example, SMA, MMCX, SMP is required to generate an end-to-end connectivity solution. Further treatment is required to develop a mechanism for physical connection to the line. A connection that forms a seamless electrical and physical connection with the line would be an ideal approach. The centre-conductor diameter, 100 um, makes this a complicated procedure, due to the fragility of the wire to establish reliable connectivity. A means of connectivity from a rigid to a flexible section of transmission line may need to be considered. The design idea illustrated in Figure 2.20, demonstrates one potential approach. Here a SMA connector is attached to a rigid PCB with a metal layer beneath and a narrow conductive strip above, to effectively serve as a microstrip line. The flexible WOGP section is then attached to the opposite end. It is imagined that the wire is soldered to the active microstrip terminal. The polyimide section, coated with conductor on it's bottom surface, is attached to the board through vias providing electrical connection to the microstrip ground plane.

2.6 Conclusion

From the simulated results obtained from the WOGP structure on the polyimide layer, a few important findings have been made. Firstly, it has been proven that it is quite possible to design a transmission line capable of operation of up to 5 GHz using this type of WOGP transmission line. Secondly, the impedance of the line can be controlled through the selection of wire of appropriate diameter over a 66 um thin substrate with ground-plane beneath. This condition allows one to control the signal amplitude. Thirdly, the phase of the line can be controlled by simply tuning the total length of the line. Control of amplitude and phase parameters enables the design of passive RF structures such as the branch-line coupler and the modified Marchand balun, as proved through simulation in previous sections. In the case of the modified Marchand balun implementation, there is nevertheless a considerable reduction in usable bandwidth. However, the electrical characteristics deem that the structure can nevertheless be quite useful over an appreciable bandwidth. The components used can be purchased off-the-shelf including the AWG standard wire, polyimide and copper-tape, which are readily produced by manufacturers such as 3M, [11][12]. These attributes make for potentially readily available low-cost flexible PCB alternatives. In order to realise an end-to-end solution, a means of robust connectivity to the transmission line is required.

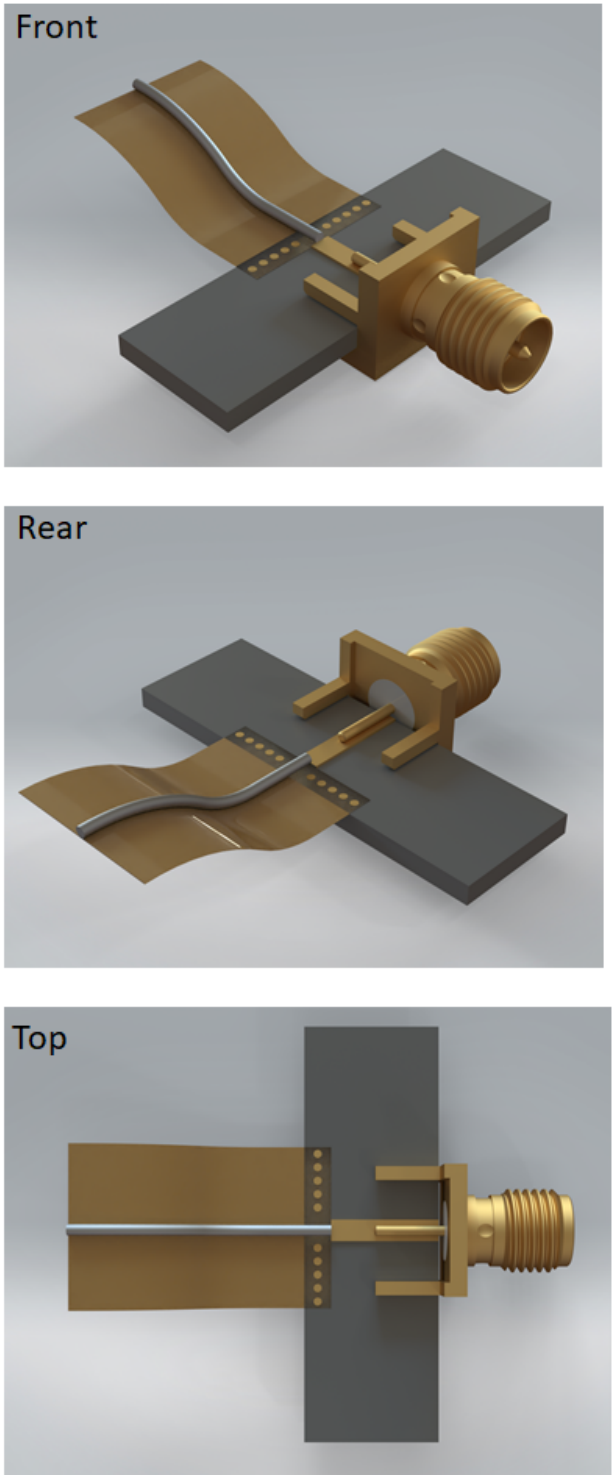

Figure 2.20: Illustration of a design idea for rigid to flexible WOGP transition.

Bibliography

[1] David M Pozar. Microwave Engineering. *Fourth Editions, University of Massachusetts at Amherst, John Wiley & Sons, Inc*, 2012.

[2] Haider R Khaleel, Hussain M Al-Rizzo, Daniel G Rucker, and Seshadri Mohan. A compact polyimide-based uwb antenna for flexible electronics. *IEEE Antennas and Wireless Propagation Letters*, 11:564–567, 2012.

[3] Joshua A Spechler, Tae-Wook Koh, Jake T Herb, Barry P Rand, and Craig B Arnold. A transparent, smooth, thermally robust, conductive polyimide for flexible electronics. *Advanced Functional Materials*, 25(48):7428–7434, 2015.

[4] Suhui Lee, Daun Jeong, Mallory Mativenga, and Jin Jang. Highly robust bendable oxide thin-film transistors on polyimide substrates via mesh and strip patterning of device layers. *Advanced Functional Materials*, 27(29):1700437, 2017.

[5] Brian C Wadell. *Transmission line design handbook*. Artech House, 1991.

[6] AF Osman and N Mohd Noh. Wideband lna design for sdr radio using balanced amplifier topology. In *2012 4th Asia Symposium on Quality Electronic Design (ASQED)*, pages 86–90. IEEE, 2012.

[7] Jwo-Shiun Sun and Tsung-Lin Lee. Design of a planar microstrip balun at s-band. *Microwave Journal*, 44(8):132–132, 2001.

[8] Doug Jorgesen and Christopher Marki. Balun basics primer, 2014.

[9] George E Ponchak and Alan N Downey. Characterization of thin film microstrip lines on polyimide. *IEEE Transactions on Components, Packaging, and Manufacturing Technology: Part B*, 21(2):171–176, 1998.

[10] Kouya Oohira. Development of an antenna material based on rubber that has flexibility and high impact resistance. *NTN Technical Rev*, (76), 2008.

[11] *3M Polyimide Film Tape 5413*. 3M, 9 2014. Datasheet 70-0703-2532-2.

[12] *3M Copper Foil Tape 1181*. 3M, 4 2010. Datasheet 78-8127-9953-0 A.

Chapter 3

Radio Frequency Performance and Strain Testing of an Iron-On Fabric Shielded Stripline

3.1 Statement of Authorship

Statement of Authorship

Title of Paper	Radio Frequency Performance and Strain Testing of an Iron-On Fabric Shielded Stripline
Publication Status	☑ Published ☐ Accepted for Publication ☐ Submitted for Publication ☐ Unpublished and Unsubmitted w ork w ritten in manuscript style
Publication Details	Deshan Govender, Jon Arnold, and Wayne Martinsen. Radio frequency performance and strain testing of an iron-on fabric shielded stripline. In 2015 International Symposium on Antennas and Propagation (ISAP), pages 1–4. IEEE, 2015.

Principal Author

Name of Principal Author (Candidate)	Deshan Govender		
Contribution to the Paper	Derived the design. Involved in the fabrication. Performed the experiment to extract the measured data. Performed critical analysis and contributed to the paper.		
Overall percentage (%)	80		
Certification:	This paper reports on original research I conducted during the period of my Higher Degree by Research candidature and is not subject to any obligations or contractual agreements with a third party that would constrain its inclusion in this thesis. I am the primary author of this paper.		
Signature		Date	04/08/2021

Co-Author Contributions

By signing the Statement of Authorship, each author certifies that:

i. the candidate's stated contribution to the publication is accurate (as detailed above);

ii. permission is granted for the candidate in include the publication in the thesis; and

iii. the sum of all co-author contributions is equal to 100% less the candidate's stated contribution.

Name of Co-Author			
Contribution to the Paper	Arnold, Jon Digitally signed by Arnold, Jon Date: 2021.08.19 08:47:10 +09'30'		
Signature		Date	

Name of Co-Author			
Contribution to the Paper			
Signature		Date	

Please cut and paste additional co-author panels here as required.

3.2 Introduction

Here we continue to pursue the ideas of creating flexible transmission lines, focusing the design of RF transmission lines with materials commonly used in the manufacture of clothing [1] [2] [3]. It is worth restating that should one require a body worn antenna, a conformal feed structure may be required to accommodate for natural user movements and for personal comfort. The optimum locations of the antennas may be high up on the wearer and could be embedded within clothing - the RF transceiver may not be closely located to the antenna. To accommodate these requirements requires highly flexible RF distribution transmission lines and robust interconnections. These interconnections need to survive repeated attachment and detachment with minimal performance degradation. Motivated by the wearable shielded stripline produced by Kaufman et.al [4], the fabrication of a similar shielded stripline using iron-on fabrication techniques and the evaluation of its measured RF performance over the range of 10 MHz to 7 GHz was investigated. Presented are the simulated and measured return loss and forward transmission characteristics. Also investigated are attachment techniques by which SMA connectors are bonded to the flexible shielded stripline. Four bonding techniques; three solder and one epoxy were evaluated for bond strength by being subjected to precise mechanical loading. A total of sixteen strain tests were undertaken with the mean force to failure and standard deviation reported for each approach. The contents of this chapter have been published [5] by the IEEE in the 2015 International Symposium on Antennas and Propagation (ISAP).

3.3 Shielded Stripline Design

The transmission line presented in this paper, as shown in Figure 3.1, has been fabricated using fleece for the substrate plane and an " iron-on " rip-stop metal plated nylon fabric for the conductive plane. Fleece is a commonly used fabric for clothing, is easily available and relatively inexpensive. The conductive iron-on fabric is known as " Shieldit Super " [6] and is made by weaving Nickel and Copper plated nylon threads. The manufacturer specified conductivity of the "Shieldit Super" fabric is 0.5 Ohms/square. A hot-melt adhesive has been applied to one side of the woven conductive fabric. The adhesive activates at 130°C and is well suited to being ironed onto the fleece.

Figure 3.1: Flexible shielded stripline fabricated using " Shieldit Super " and fleece.

3.4 Iron On Fabrication

The stripline was fabricated by ironing a narrow conductive strip onto the centreline of a length of fleece. Another fleece strip was placed on top sandwiching the conductive strip. The structure was shielded by ironing a single sheet of " Shieldit Super " onto the outer surface. To seal the conductive ground layer, the sheet was wrapped over onto itself and ironed up the seam, as shown in Figure 3.2. An electrical connection bridging the length of the seam is not necessary as shown by the excellent radio frequency performance in Section II-B. The stripline length and

total width (a) Figure 3.3, were chosen to be 100 mm and 20 mm respectively. The thickness of the conductive fabric (t) minus the hot-melt adhesive is 0.07 mm and the total thickness of the two layers of fleece (b) is 4.6 mm. The relative permittivity (r) of the fleece fabric was determined by measuring the characteristic impedance of a stripline constructed with a 5 mm wide conductive strip. With all the physical dimensions of the stripline known, equation 3.1, [7] pg. 61, was used to calculate the ε_r of 1.28.

$$Z_0 = \frac{377}{4\pi\varepsilon_r}\left(\frac{1}{\frac{w/b}{1-t/b} + \frac{2}{\pi}\ln\left(\frac{1}{1-t/b} + \coth\frac{\pi a}{2b}\right)}\right) \tag{3.1}$$

Figure 3.2: Shielded stripline ironed seam.

A Keysight PNA was used to measure the line's characteristic impedance in the GHz region. The calculated ε_r was then used to determine that a 5.5 mm wide conductive strip was needed to create a 50 Ohm line. A diagram representing the stripline cross section is shown in Figure 3.3.

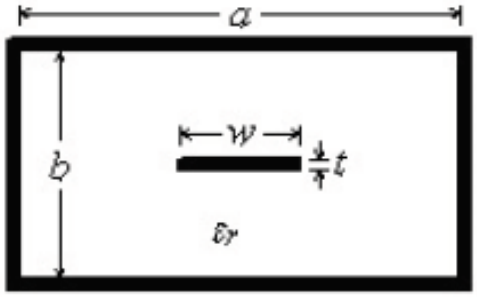

Figure 3.3: Shielded stripline cross section design parameters.

3.5 Simulations and Measurements

To confirm the analytical solution, a 3D model was developed in Ansys HFSS V15 and a numerical analysis conducted. The constructed 50 Ohm stripline model was measured on a Keysight PNA and the measured s–parameters were compared against those obtained in the numerical solution. Figure 3.4 and 3.5 present the measured and simulation results for S11 and S21 for the copper laden solder stripline. A DC conductivity of 90000 S/m was applied to the simulation of the stripline model to achieve good correlation between the measured and simulated results. The measured S11 is better than -18 dB and S21 is within 0.2 dB of the simulation from 10 MHz to 7 GHz.

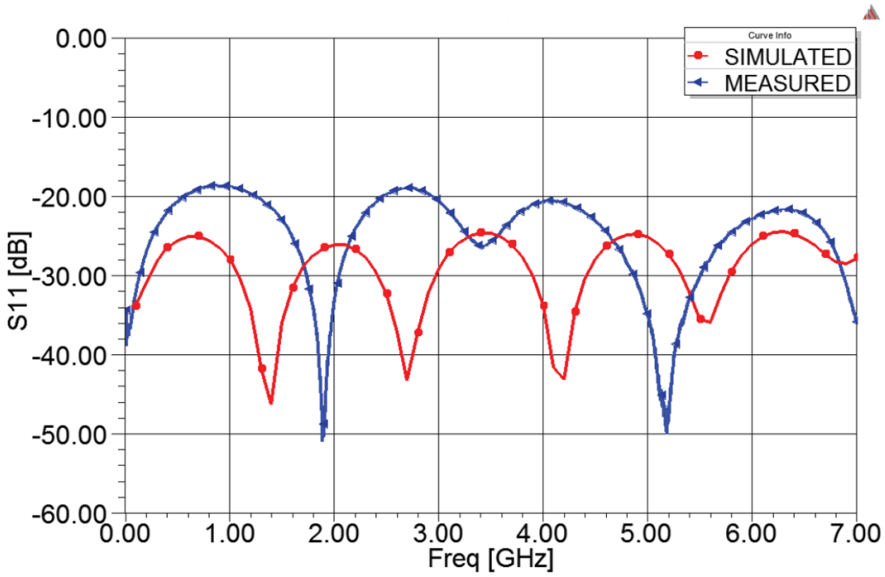

Figure 3.4: Shielded stripline simulated and measured reflection coefficient.

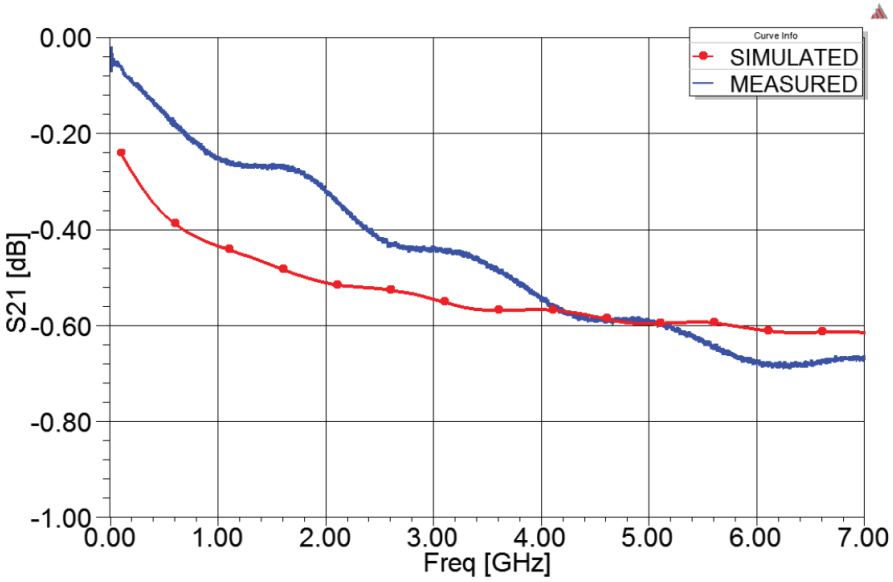

Figure 3.5: Shielded stripline simulated and measured forward transmission coefficient.

3.6 Connector Pull Strain Tests

In order to evaluate the strain of the solder bond between the conductive fabric and the SMA connector, a pull strain test was conducted using the Condor XYZTEC pull measurement unit, see Figure 3.6.

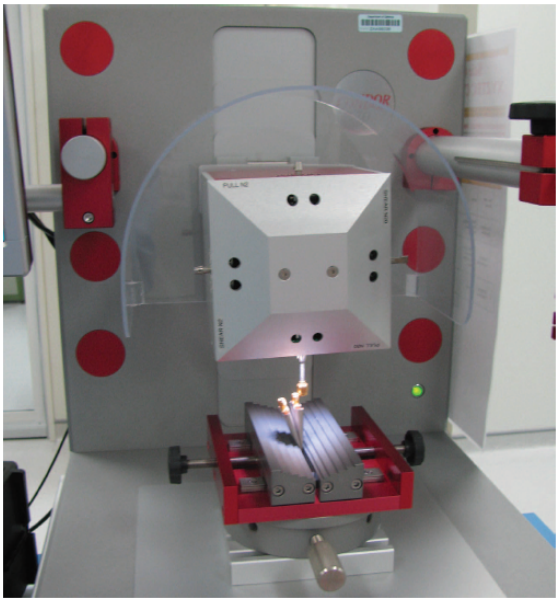

Figure 3.6: Condor load pull configuration.

The test was performed by firstly, securing and clamping the transmission line in a vice. Secondly, in order to vertically align the stripline, a male SMA fixture was attached to the machine head. Thirdly, the male SMA fixture was screwed onto the female connector of the stripline, Figure 3.7. During the pull measurement, the unit exerts up to 8800 grams force (gf) over a test distance of 4000 um in the vertical direction at a velocity of 250 m/s. The measurement continues irrespective of the connector breaking off the stripline during testing. A peak force is generated from the measurement and is used for comparison. These tests were performed on transmission lines bonded with Tin-Lead solder, Indium solder, conductive Silver epoxy and Copper laden Tin-Lead solder. The bonding agents were applied using the manufacturer's guidelines for their respective application. A total of 16 tests were performed. Each bonding agent was applied to four of the SMA stripline connections.

Table 3.1: PULL STRAIN TEST RESULTS.

Bonding Agent	Mean Force Applied	Standard Deviation
Tin Lead Solder	6152	1571
Indium Solder	6311	3090
Silver Epoxy	6607	1302
Copper Laden Solder	7379	1825

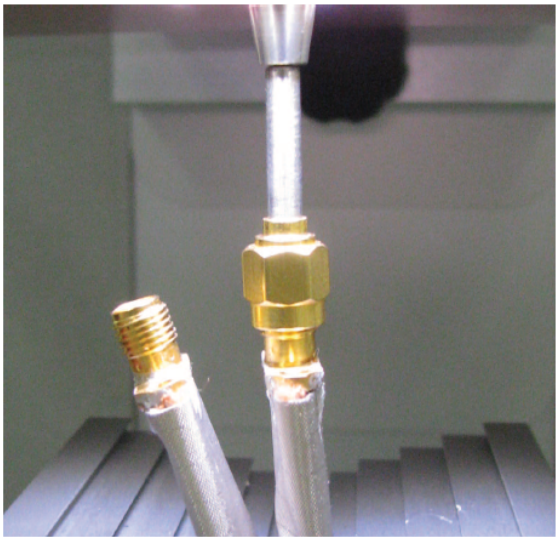

Figure 3.7: Condor load pull jig.

The mean and standard deviation of the results have been tabulated in Table 3.1 for each of the bonds. From Table 3.1, the Copper laden solder demonstrates the strongest average bond to the iron-on conductive fabric. This has been attributed to the solder being laden with copper. This minimises the dissolution of the copper atoms from the thin metallic plating on the fibres of the " Shieldit Super " during the application of heat whilst the solder was in the liquid state [8]. The electron microscope photo clearly depicts the excellent bond attachment, Figure 3.8. The weakest is the standard Tin-Lead based solder due to the copper dissolution thinning the fibre plating, Figure 3.9. The Indium bond demonstrated significant variation in the applied force-to-failure measurement. There was difficulty in the application of the Indium solder paste due to a large flux to solder ratio. Figure 3.10 clearly shows the residual flux from the soldering process. This flux had wicked into the absorbent fleece during soldering, carrying with it micro particles of solder, shorting out the centre pin of the SMA connector. The silver epoxy samples showed, after the pull test, that the epoxy did not bond well to the conductive fabric leaving little indication of the epoxy ever being applied. The silver epoxy failed to adhere to the conductive mesh, Figure 3.11, yet adhered to the gold plating of the SMA connectors.

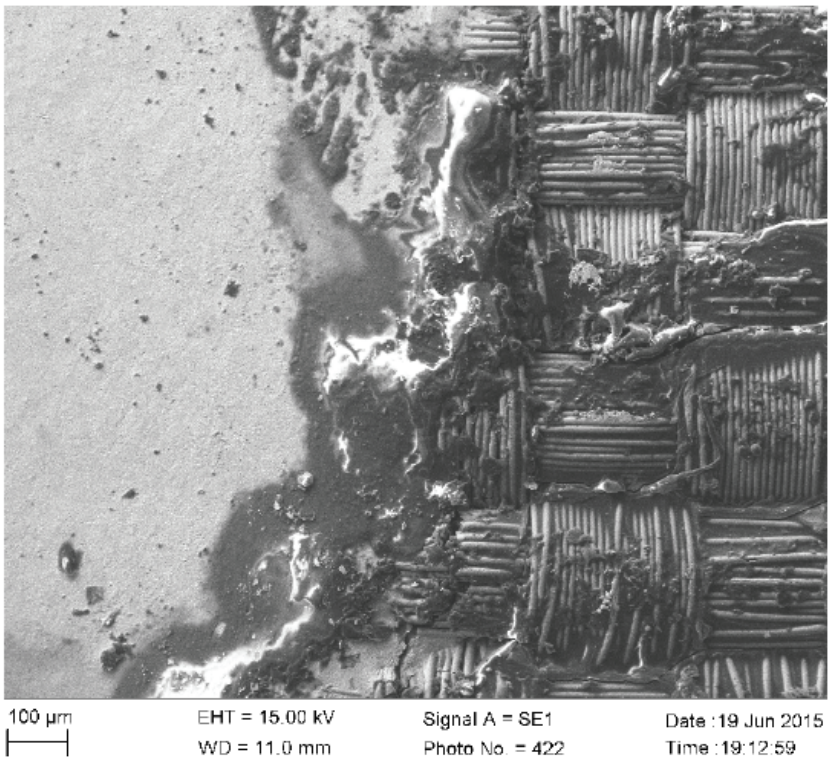

Figure 3.8: Copper laden solder bond.

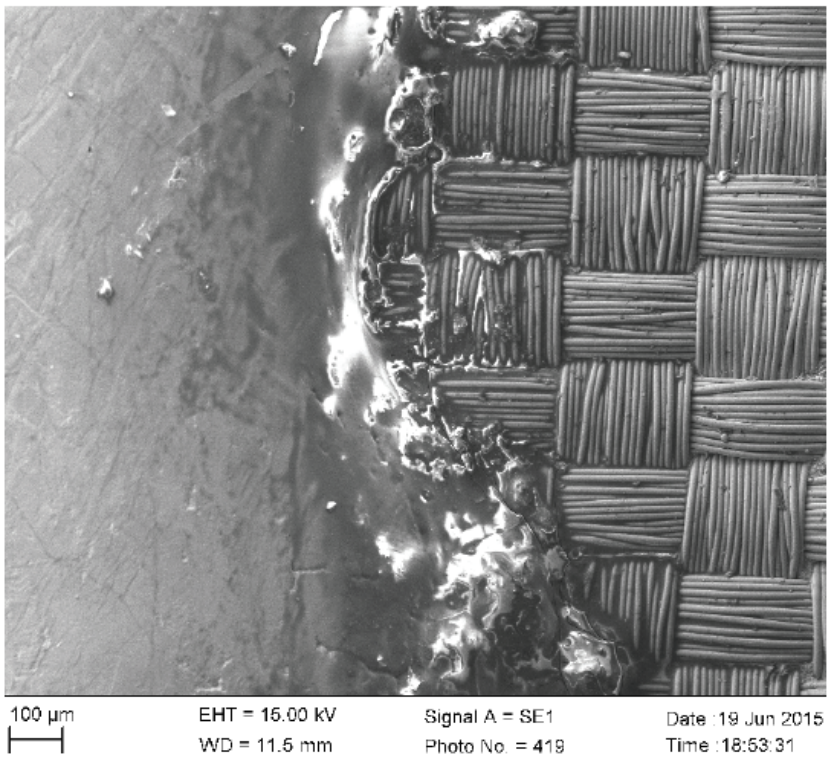

Figure 3.9: Tin Lead solder bond.

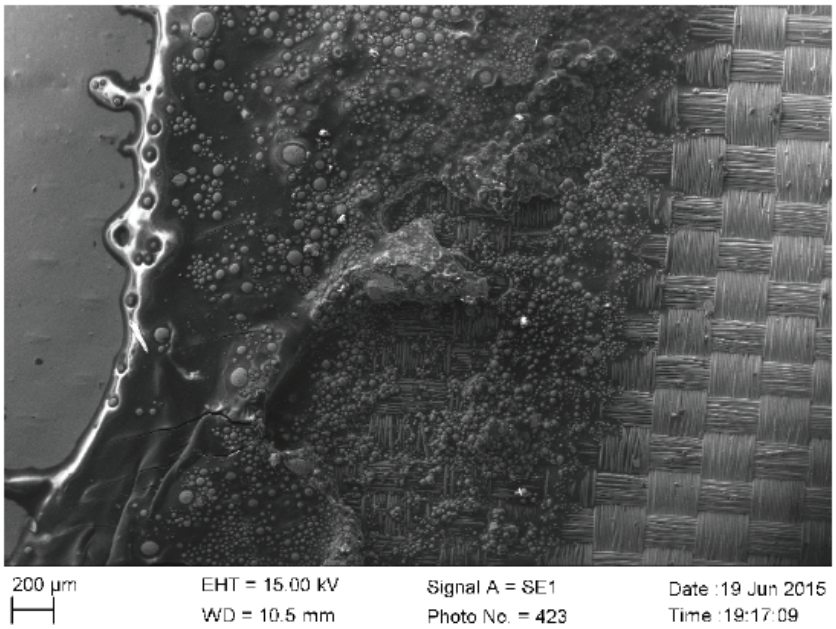

Figure 3.10: Excessive indium solder flux residue with micro particles of solder visible in suspension.

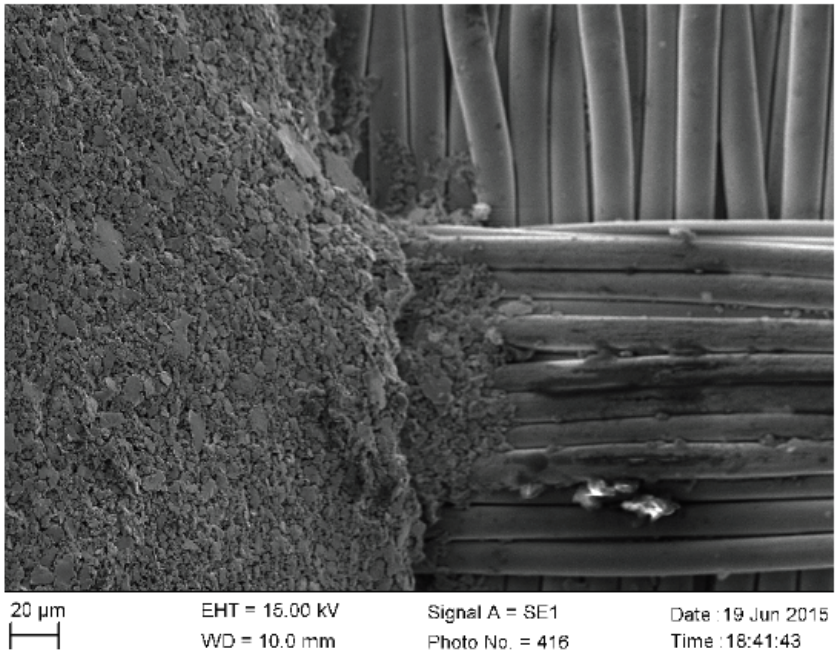

Figure 3.11: Photo of the poorly bonded silver epoxy.

3.7 Conclusion

A method for creating an iron-on shielded stripline transmission line constructed from fleece and an iron-on conductive fabric has been demonstrated. The stripline is capable of broadband operation to 7 GHz and demonstrates a low insertion loss of 0.063 dB/cm at 7 GHz. The bond strength tests carried out have indicated that conductive fabric can be bonded to a connector using solder. The strength of the bond is dependent upon the solder or epoxy used. It has been shown that using a Copper laden solder produces a bond that requires a mean force of 7379 gf to break the joint and demonstrated to be the preferred method of bonding. Finally, further examination of all solder bond methods under the electron microscope, revealed that a large amount of flux had been left behind during the soldering process. Care needs to be taken during the soldering process to ensure that the flux does not wick into the fleece altering its permittivity at that location and hence creating a localized change in the characteristic impedance of the line. The conclusion has been drawn that the conductive Silver epoxy is not compatible with the nickel and copper content of the plating on the nylon threads thus preventing adequate bonding.

3.8 Acknowledgements

I would like to thank Shyam Mehta and Igor Switala for their help in conducting the load pull tests and producing the electron microscope pictures.

Bibliography

[1] Leah Buechley and Michael Eisenberg. Fabric PCBs, electronic sequins, and socket buttons: techniques for e-textile craft. *Personal and Ubiquitous Computing*, 13(2):133–150, 2009.

[2] JCG Matthews and G Pettitt. Development of flexible, wearable antennas. In *2009 3rd European Conference on Antennas and Propagation*, pages 273–277. IEEE, 2009.

[3] Rita Salvado, Caroline Loss, Ricardo Gonçalves, and Pedro Pinho. Textile materials for the design of wearable antennas: A survey. *Sensors*, 12(11):15841–15857, 2012.

[4] Thomas Kaufmann and Christophe Fumeaux. Wearable textile half-mode substrate-integrated cavity antenna using embroidered vias. *IEEE Antennas and Wireless Propagation Letters*, 12:805–808, 2013.

[5] Deshan Govender, Jon Arnold, and Wayne Martinsen. Radio frequency performance and strain testing of an iron-on fabric shielded stripline. In *2015 International Symposium on Antennas and Propagation (ISAP)*, pages 1–4. IEEE, 2015.

[6] LessEMF. Shieldit super. http://lessemf.com/fabric.html1220. URL `http://lessemf.com/fabric.html1220.`

[7] Brian C Wadell. *Transmission line design handbook*. Artech House, 1991.

[8] Po-Yi Yeh, Jenn-Ming Song, and Kwang-Lung Lin. Dissolution behavior of cu and ag substrates in molten solders. *Journal of electronic materials*, 35(5):978–987, 2006.

Chapter 4

Helically Counterpoised-Monopole Antenna

4.1 Statement of Authorship

Statement of Authorship

Title of Paper	Helically Counter-Poised Monopole Antenna
Publication Status	☑ Published ☐ Accepted for Publication ☐ Submitted for Publication ☐ Unpublished and Unsubmitted w ork w ritten in manuscript style
Publication Details	D Govender, J Magarelli, A Caldow, and C Fumeaux. Helically counter-poised monopole antenna. In 2016 IEEE-APS Topical Conference on Antennas and Propagation in Wireless Communications (APWC), pages 170–172. IEEE, 2016.

Principal Author

Name of Principal Author (Candidate)	Deshan Govender		
Contribution to the Paper	Derived the design. Involved in the fabrication. Performed the experiment to extract the measured data. Performed critical analysis and contributed to the paper.		
Overall percentage (%)	80		
Certification:	This paper reports on original research I conducted during the period of my Higher Degree by Research candidature and is not subject to any obligations or contractual agreements with a third party that would constrain its inclusion in this thesis. I am the primary author of this paper.		
Signature		Date	02/08/2021

Co-Author Contributions

By signing the Statement of Authorship, each author certifies that:

i. the candidate's stated contribution to the publication is accurate (as detailed above);

ii. permission is granted for the candidate in include the publication in the thesis; and

iii. the sum of all co-author contributions is equal to 100% less the candidate's stated contribution.

Name of Co-Author	JOSEPH MAGARELLI		
Contribution to the Paper	HELPED WITH FABRICATION PERFORMED MEASUREMENTS		
Signature		Date	11/08/2021

Name of Co-Author			
Contribution to the Paper			
Signature		Date	

Please cut and paste additional co-author panels here as required.

Statement of Authorship

Title of Paper	Helically Counter-Poised Monopole Antenna
Publication Status	☑ Published ☐ Accepted for Publication ☐ Submitted for Publication ☐ Unpublished and Unsubmitted work written in manuscript style
Publication Details	D Govender, J Magarelli, A Caldow, and C Fumeaux. Helically counter-poised monopole antenna. In 2016 IEEE-APS Topical Conference on Antennas and Propagation in Wireless Communications (APWC), pages 170–172. IEEE, 2016.

Principal Author

Name of Principal Author (Candidate)	Deshan Govender		
Contribution to the Paper	Derived the design. Involved in the fabrication. Performed the experiment to extract the measured data. Performed critical analysis and contributed to the paper.		
Overall percentage (%)	80		
Certification:	This paper reports on original research I conducted during the period of my Higher Degree by Research candidature and is not subject to any obligations or contractual agreements with a third party that would constrain its inclusion in this thesis. I am the primary author of this paper.		
Signature		Date	02/08/2021

Co-Author Contributions

By signing the Statement of Authorship, each author certifies that:

i. the candidate's stated contribution to the publication is accurate (as detailed above);

ii. permission is granted for the candidate in include the publication in the thesis; and

iii. the sum of all co-author contributions is equal to 100% less the candidate's stated contribution.

Name of Co-Author	Christophe Fumeaux		
Contribution to the Paper	Advisory contribution		
Signature		Date	02/08/2021

Name of Co-Author	Adrian Caldow		
Contribution to the Paper	Advisory contribution to the design and joint contributor to the paper writeup.		
Signature		Date	11/08/21

Please cut and paste additional co-author panels here as required.

4.2 Introduction

Exploring one of the core thesis research tenets, antenna miniaturisation, we pursue an avenue of experimental antenna research, taking the approach of asymmetrical dipole manipulation. Here we introduce a novel method of reducing the size of a conventional dipole antenna by means of replacing one of the dipole arms with a helical element. Interest in small antennas is not new [1] [2], and there are a number of well known techniques that make the electrical length appear greater than the maximum dimension. The obvious choice is to reduce the antenna size by folding the radiating elements [3]. Capacitive loading can be used to reduce the length of monopole or dipole elements [4] through the use of top loading discs. Performance of electrically short monopoles and dipoles can be improved by placing an inductive loading coil in series with wire elements [5]. The use of slow wave structures such as meandering or zigzag of wire elements can also be used to shorten a dipole axial length [6]. To date, most researchers have used these techniques as part of symmetrical antenna structures when attempting to miniaturise dipole antennas. Similarly, symmetry is implicitly enforced by image theory when considering miniaturisation of monopoles [7]. It has been however shown in [8] [9] that asymmetric elements may offer opportunities for performance improvement, but there has been no comprehensive investigation into asymmetrical dipole designs. In this research, the use of asymmetrical design will be examined, where one arm of the dipole is replaced by a helical coil to effectively form a counter-poised monopole. The contents of this chapter have been published [10] by the IEEE, in the 2016 IEEE-APS Topical Conference on Antennas and Propagation in Wireless Communications (APWC).

4.3 Design and Simulation

The motivation behind the design of the counterpoised monopole antenna structure is to investigate a method of antenna miniaturisation by means of asymmetrically reducing the size of the structure. Dipole miniaturisation by means of meander line techniques or capacitive top hats [4] has conventionally been applied in a balanced manner. Given that meander lines and zigzag lines have been used previously [6], it is proposed here that a 3D helical element be used to replace one of the dipole arms.

4.3.1 Counter-Poised Monopole Design

A numerical simulation was conducted in HFSS, with the geometry shown in Figure 4.1, to evaluate the feasibility of this design. Firstly, a simple dipole antenna was designed at a frequency of 965 MHz. Through simulation, it was found that each arm of the dipole is a length of 75 mm at 965 MHz. From that design, one of the dipole arms was removed and then replaced by a helical structure. After a parametric simulation, suitable helix pitch, diameter and number of turns were found to be 1.2 mm, 4.57 mm and 7.5 turns respectively. It was found that when the helical structure replaced one of the dipole arms, the antenna continued to perform, however it radiated efficiently at a higher frequency. In order to account for the shift higher in frequency, the length of the wire was increased by 20 mm to bring it back to the intended frequency of operation of 965 MHz. The total length of the straight wire arm is 95 mm. In this instance, the dimensions of the helical element were kept constant and the length of wire changed. It can be seen in Figure 4.2 that the antenna reflection coefficient is below -20 dB and from Figure 4.3 that the gain is 2 dBi for the counter-poised monopole. It must be noted that a HFSS lumped excitation was used to excite the structure in the simulation, therefore any losses from a practical balun implementation have not been taken into account in these simulations.

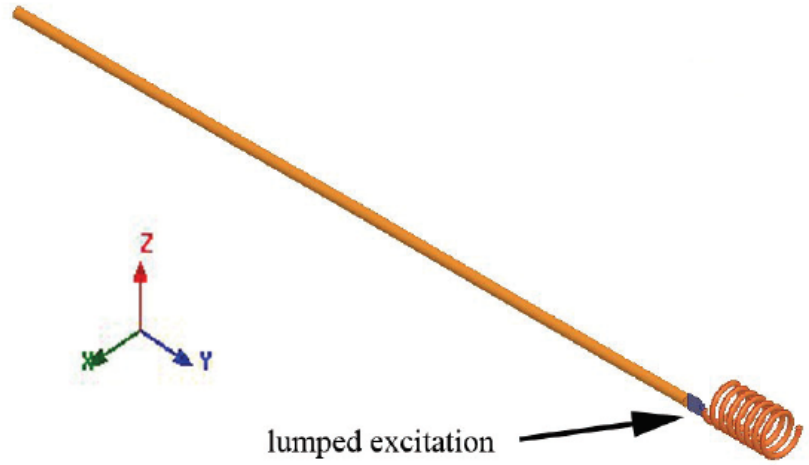

Figure 4.1: Counter-poised monopole HFSS model.

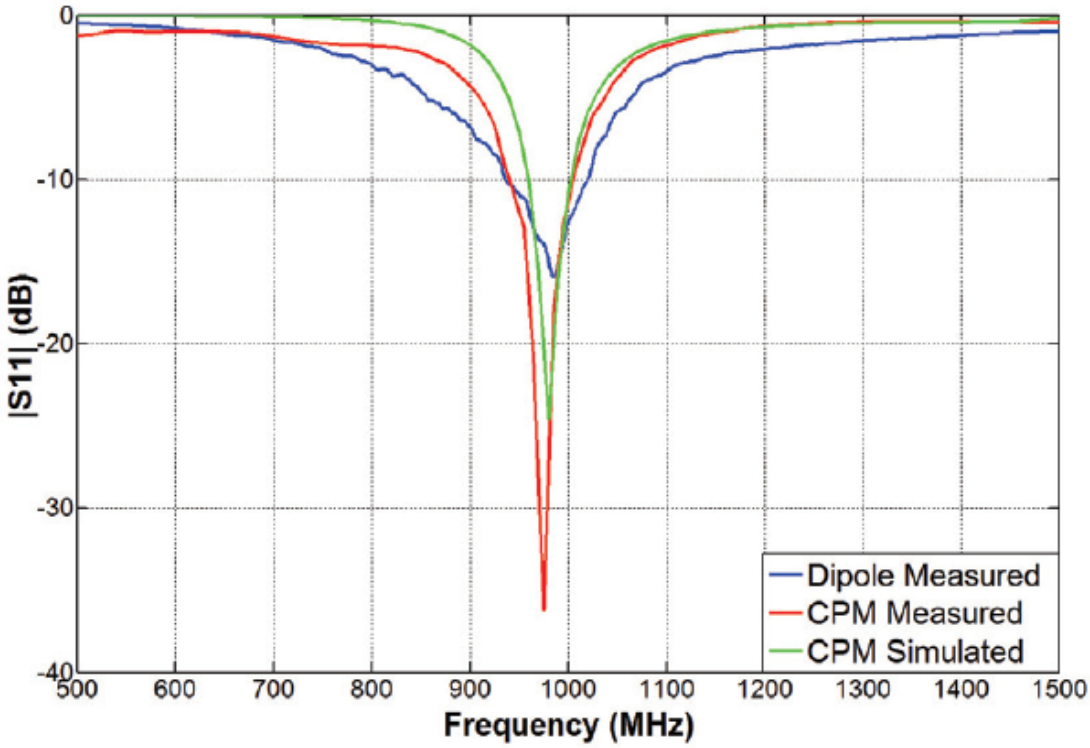

Figure 4.2: Measured versus simulated reflection coefficient for the dipole and the counter-poised monopole (CPM). The simulated results do not consider the losses of the balun.

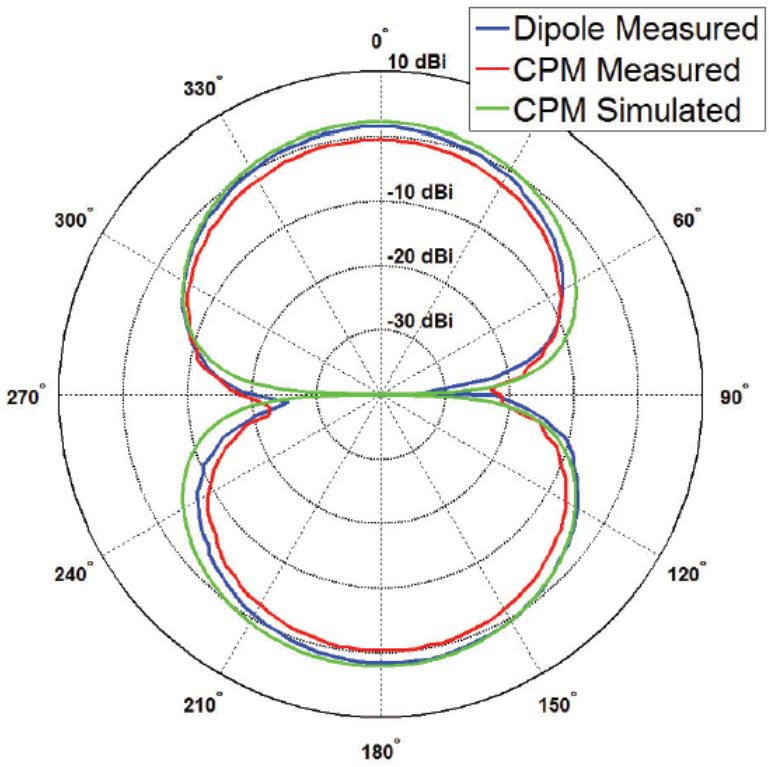

Figure 4.3: Simulated and measured gain co-polarized patterns in the yz-plane.

4.4 Fabrication and Measurements

4.4.1 Fabrication

The dipole was fabricated using wire of radius 0.65 mm. A Printed Circuit Board (PCB) was then constructed to solder the dipole arms to a RF transformer balun which was used to feed the dipole arms differentially. The model number of the balun used is Mini-Circuits, TC1-1-13MA+. Typical insertion loss through the balun at 1 GHz is quoted at 0.68 dB. It is assumed that this is the worst case loss through the balun used in the feed structure developed here, since the device has been designed to operate at a frequency of 965 MHz. Figure 4.4 shows the constructed dipole prototype with the balun feed structure. The same structure used to feed the dipole antenna was then used to feed the counter-poised helical antenna. The helix was created by winding wire of radius 0.32 mm on an M4.5 screw, with the same number of turns as per the simulation. The M4.5 screw provided a convenient method of winding the helical element whilst also achieving the dimensional specifications that had been simulated.

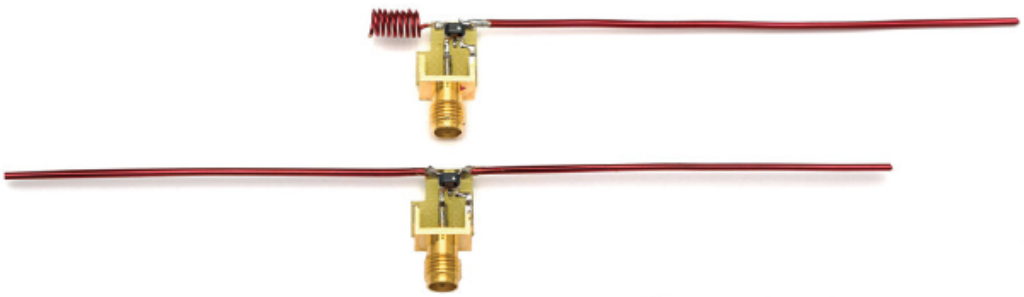

Figure 4.4: Fabricated monopole and dipole.

4.4.2 Measurement

The reflection coefficient, S11, was measured on an Agilent Vector Network Analyser. The radiation patterns were measured in an ETS-Lindgren 8050 anechoic chamber. The antenna gain was measured for both the dipole antenna and the counter-poised monopole antenna. A cross-polarisation measurement was also conducted for both the dipole and counter-poised monopole antenna to ensure that the co-axial cable feeding the antenna was not responsible for the radiation. The results of the measurements are discussed in the following.

4.5 Analysis of results

The reflection coefficient of the counter-poised monopole is shown in Figure 4.2. The measured 10 dB bandwidth for the dipole and counter-poised monopole are 72 MHz and 60 MHz respectively. This represents a 17% reduction in bandwidth in comparison to the corresponding results for the dipole antenna, also shown in the figure. The plot of the gain measurement (Figure 4.3) shows the counter-poised monopole antenna to exhibit a similar pattern to that of the dipole antenna. However there is a modest reduction in gain in comparison to the measured dipole antenna, of approximately 1.8 dB. Both the dipole and counter-poised monopole antennas were fed with an identical balun arrangement. In order to verify that the counterpoised monopole antenna itself was responsible for the radiation and not the coaxial cable feeding the antenna due to any unbalance, a cross polarisation measurement was conducted, with the results shown in Figure 4.5. In the case of the dipole, the cross polarisation measurement is well below -20 dB. For the counter-poised monopole, the cross-polarisation remains below -10 dB. This is an acceptable result for this type of antenna, given the inherent asymmetry of the structure.

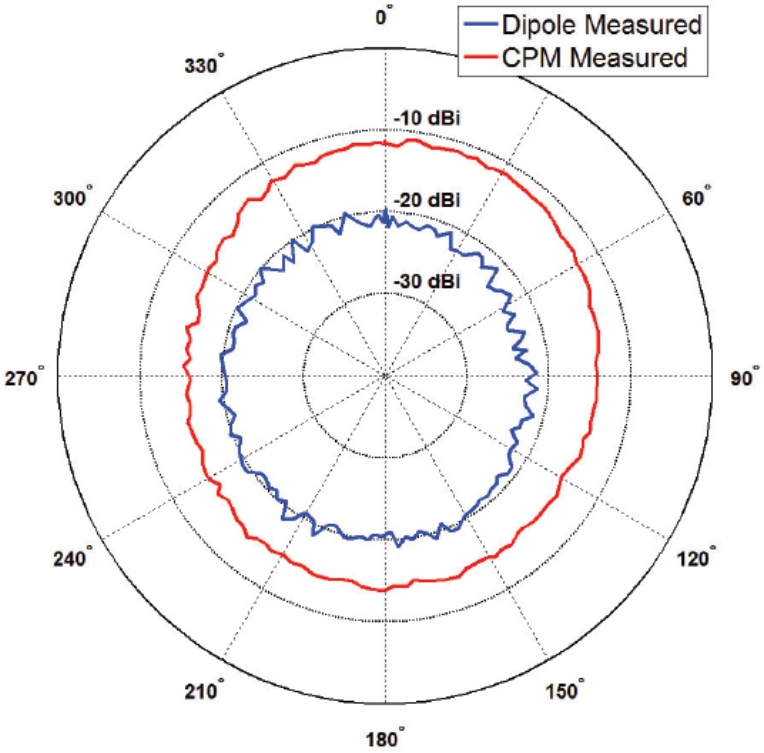

Figure 4.5: Simulated and measured gain cross-polarized patterns in the yz-plane.

4.6 Conclusion

From the results, it can be concluded that the investigated helically counter-poised monopole antenna still operates reasonably well when one of the arms has been replaced with a helix. The radiation pattern indicates that the counter-poised monopole is still well balanced, though not as well as the dipole, and this is confirmed by the cross-polarisation measurement. It has also been found that there are modest reductions in gain and bandwidth, which can be expected given the antenna has been reduced in size by approximately 30%. It has also been proven that a helix can be used as ground plane for a monopole antenna and this arrangement produces a radiation pattern similar to that of a dipole. Further studies will consider a predictive modelling of the findings and further optimization of the helical counter-poise.

Bibliography

[1] Lan Jen Chu. Physical limitations of omni-directional antennas. *Journal of applied physics*, 19(12):1163–1175, 1948.

[2] Harold A Wheeler. Fundamental limitations of small antennas. *Proceedings of the IRE*, 35 (12):1479–1484, 1947.

[3] Bengt Josephson. The quarter-wave dipole. In *WESCON/57 Conference Record*, volume 1, pages 77–90. IEEE, 1957.

[4] Kyohei Fujimoto and Hisashi Morishita. *Modern small antennas*. Cambridge University Press, 2013.

[5] R Hansen. Efficiency and matching tradeoffs for inductively loaded short antennas. *IEEE Transactions on Communications*, 23(4):430–435, 1975.

[6] Hisamatsu Nakano, Hitoyuki Tagami, Akihiro Yoshizawa, and Junji Yamauchi. Shortening ratios of modified dipole antennas. *IEEE Transactions on Antennas and Propagation*, 32 (4):385–386, 1984.

[7] S Zhao, C Fumeaux, and C Coleman. Miniaturised high-frequency and very-high-frequency antennas based on optimised non-uniform helical structures. *IET microwaves, antennas & propagation*, 6(6):603–610, 2012.

[8] John D Kraus. The helical antenna. *Proceedings of the IRE*, 37(3):263–272, 1949.

[9] Christos I Kolitsidas, B Lars G Jonsson, P Persson, and A Stjerman. Exploiting asymmetry in a capacitively loaded strongly coupled dipole array. In *2014 Loughborough Antennas and Propagation Conference (LAPC)*, pages 723–726. IEEE, 2014.

[10] D Govender, J Magarelli, A Caldow, and C Fumeaux. Helically counter-poised monopole antenna. In *2016 IEEE-APS Topical Conference on Antennas and Propagation in Wireless Communications (APWC)*, pages 170–172. IEEE, 2016.

Chapter 5

Planar Counter-Poised Monopole Antenna with Uni-Planar Feed

5.1 Introduction

Building from the experimental research performed in Chapter 4, this chapter focuses on developing an understanding of the antenna's counter-poise and the antenna's overall behaviour once the counter-poise is applied to the antenna. Further, a method to predictably design the counter-poise to match the opposing arm is analysed and presented. Design emphasis is placed on miniaturization and planar realisation of the antenna and its feed. The intent is to achieve a structure that can be entirely fabricated using a PCB fabrication process. A planar design lends itself to the possibility of flexible implementation in future design iterations. The frequency of operation of the antenna analysed here is 2.45 GHz, a frequency within the ISM band, and which is additionally compatible with commercial wireless technologies, such as Bluetooth and Wi-Fi.

In comparison to the counter-poised antenna structure presented in Chapter 4, a planar balun is designed here. The balun implementation is achieved through planar realisation by means of a uni-planar transition, which by design is comparatively compact in nature. This structure is analysed and designed to operate across the pass-band of the antenna.

Three prototypes are designed, fabricated, and analysed prior to achieving the final design iteration. All three designs make use of the planar uni-planar balun structure. The first design is a dipole design. This design serves as a reference design upon which further changes are made. The second design iterates on this first design through replacement of one of the dipole arms with a coil counter-poise. The third design replaces the coil-counterpoise of the second design with a "planar coil" implementation.

5.2 Counter-poise Operation

To further try and understand the behaviour of the counter-poised monopole and thereafter derive a method for design, one must try and understand the behaviour of the counter-poise.

To do this, reference is made to the physical model of a coil. A coil is a fundamental circuit element used to generate inductance. The coil's behavior is well understood, and the inductance generated from a coil can be calculated from well-known formulas [1]. Figure 5.1 [1] illustrates the the equivalent circuit model which accounts for the inductance, parasitic capacitance and resistance of the coil. Important to note is the frequency-dependent inductance of the coil. As the frequency increases, one would expect non-linearity in the transfer function to appear because of cancellation between the inductive and parasitic capacitance reactances. As the number of turns of the coil is increased, so too would the inductance of the coil however along with that inductive increase would be a parasitic capacitance between the turns. This may have an overall effect on reducing the self-resonant frequency of the coil. This interaction is made known because one may ultimately select to avoid this region of operation due to the non-linearity in the inductance across frequency.

An initial starting point for the coil design is to develop a coil of inductance, which at the very

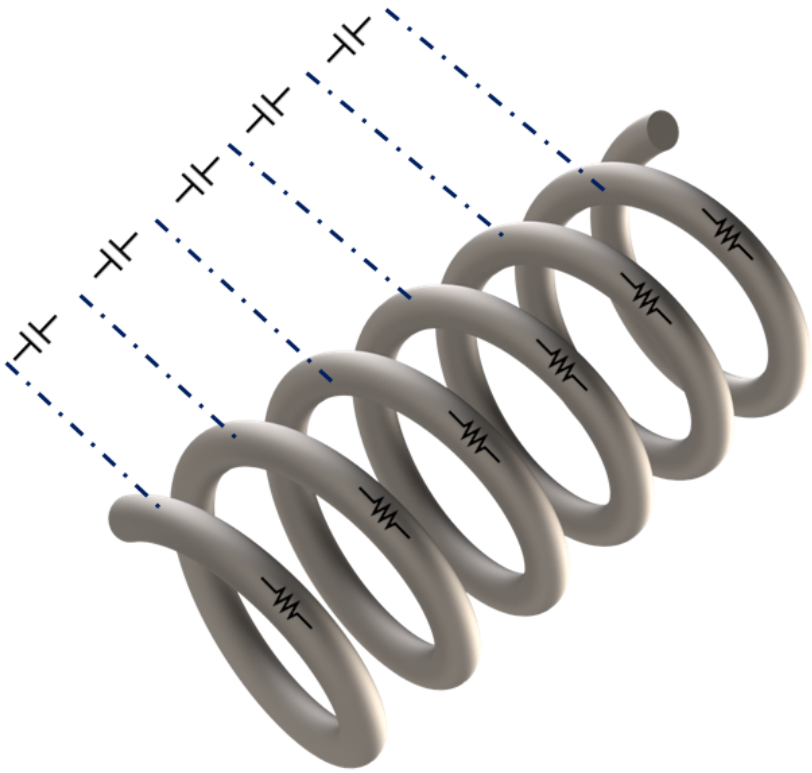

Figure 5.1: Equivalent RF circuit for a coil.

least is an equivalent inductive substitution for the dipole arm it replaces. Here an assumption is made that the straight wire geometry of the dipole generates a level of self-inductance and that an equivalent inductor can replace it. Referring to Figure 5.2 [2] helps one to form an intuitive understanding of dipole operation from a circuit perspective. Here one may see that the description presents the arms of the dipole as series inductors, and between these differential arms exists a capacitance. This is not too dissimilar to a LC resonator setup. The capacitance between a single dipole arm and the coil will certainly affect the overall antenna behaviour. Therefore an antenna optimisation is performed numerically to account for this behaviour once an initial model description is developed. To evaluate the amount of inductance required as a starting point for the design, the self-inductance of a straight wire length must be evaluated. Here the focus is on planar implementation, hence for a straight, flat wire, the inductance may be calculated in a straightforward manner [3]:

$$L_{flat} = 2 * 10^{-4} * l[ln(\frac{2l}{w+t}) + 0.5 + 0.2235(\frac{w+t}{l})][u\mathbf{H}] \tag{5.1}$$

l - line length [mm]

w - conductor width [mm]

t - conductor thickness [mm]

Figure 5.3a clearly shows the original dipole setup, thereafter Figure 5.3b displays the substitution made with the counter-poise for one of the dipole arms.

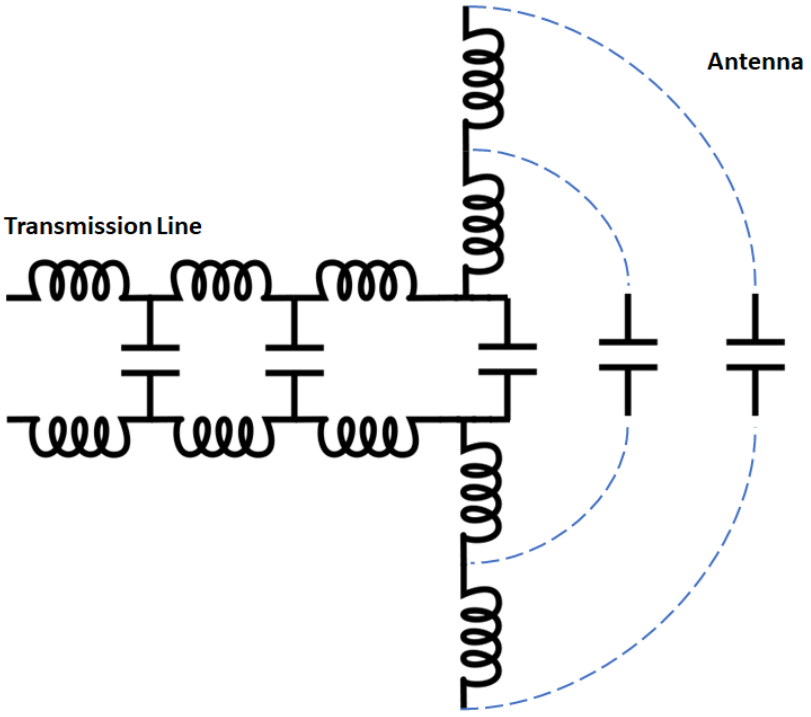

Figure 5.2: Circuit based realization of a dipole.

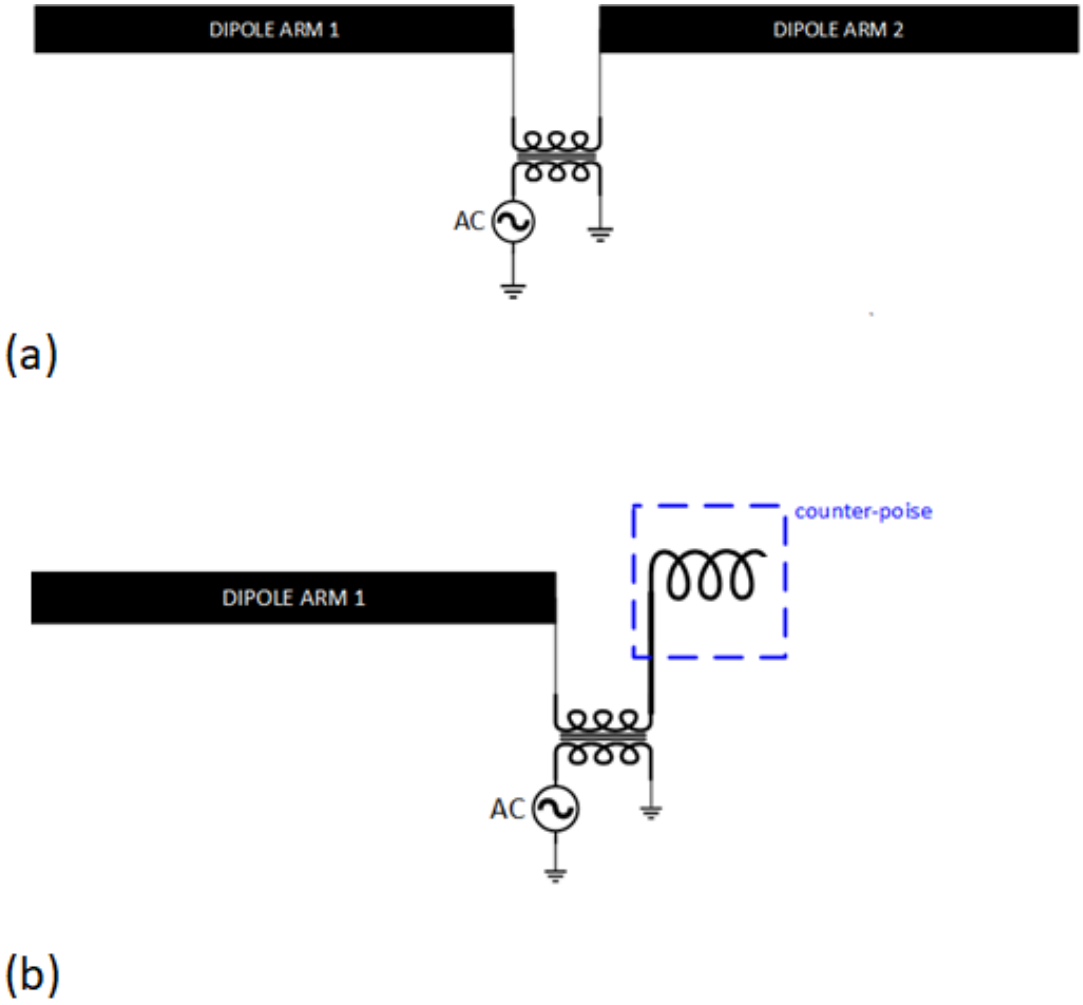

Figure 5.3: (a) Dipole structure with balun. (b) Monopole with counter-poised coil, used as an equivalent replacement for one of the dipole arms.

5.3 Planar Coil Design

To begin the design process, the effective length of a planar $\lambda/2$ dipole antenna on a substrate must first be evaluated. Once this effective length is calculated, the dimensions of the coil may then be calculated to deduce the inductance required to replace the opposing dipole arm. To develop the coil using a PCB fabrication process, a coil model is required whose geometry is suitable for fabrication using this PCB process. The design equations of a circular coil in free-space are well known [1], these equations help generate a starting point for the antenna counter-poise, with further fine-tuning carried out through optimisation of its parameters in HFSS to account for frequency-dependent parasitic behaviours. In this work, presented is the design of a rectangular coil implemented in planar technologies to behave as suitable counter-poise for the antenna.

Figure 5.4 presents a design for the proposed rectangular coil. The antenna substrate will effectively be used as the structure around which the turns of the inductor are wound. Within the PCB fabrication process, the turns are realised by either etching or milling away at the top and bottom conductor surfaces between the inductor turns. To connect the top and bottom layers or turns, circular through-hole vias are used to connect the turns of the inductor to complete the loops. The conductor width, length, and number of turns are the primary levers by which the inductance can be adjusted for the design. The overall inductor height is fixed by the height of the substrate.

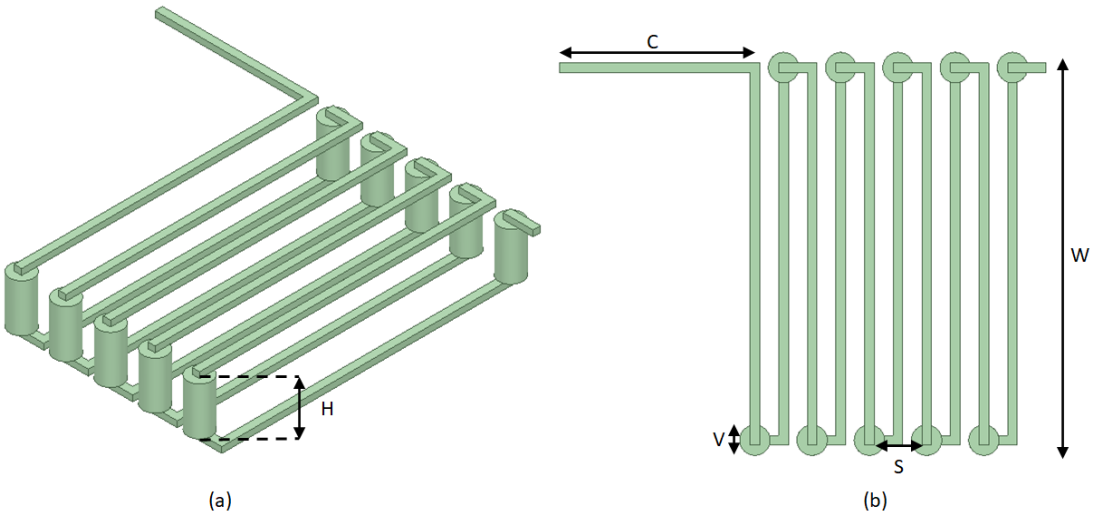

Figure 5.4: (a) Isometric View of the rectangular counter-poise. (b) Top view of rectangular counter-poise.

InductorDimensions

H - Height

C - Connector length from the balun

W - Total Width

S - Spacing between turns

V - Via Diameter

To evaluate the inductance of the rectangular coil, a model was created in HFSS. For purpose of demonstrating operation of the model, a simulation was conducted varying the number of turns on the inductor, and thereafter observing the variation in inductance across frequency. It was expected, that as the number of turns increased, so too would the parasitic capacitance between the turns, which would lead to an overall decrease in the self-resonant frequency of the coil. Standard PCB fabrication tolerances were applied to the model parameters to evaluate model behaviour. The values applied for *H, C, W, S, V,* are 1.6, 2.25, 5, 1.95, 0.8 mm respectively. Turns on the inductor were varied from 2 to 4 in increments of 1. Figure 5.5 presents the results of the simulation. One may observe from the result, that as the number of turns increase, so too does the inductance across frequency. At the intended design frequency of operation, 2.45 GHz, the inductance for 2, 3 and 4 turns are 22.45, 44 and 120.8 nH respectively. Notice, that at 4 turns of the coil, the self-resonant frequency appears at 2.73 GHz. An aspect concerning the design, is the position of the self-resonant frequency of the coil. A consideration of the overall antenna design is that the coil must be designed to keep the self resonant frequency of the coil far from the desired antenna operating frequency.

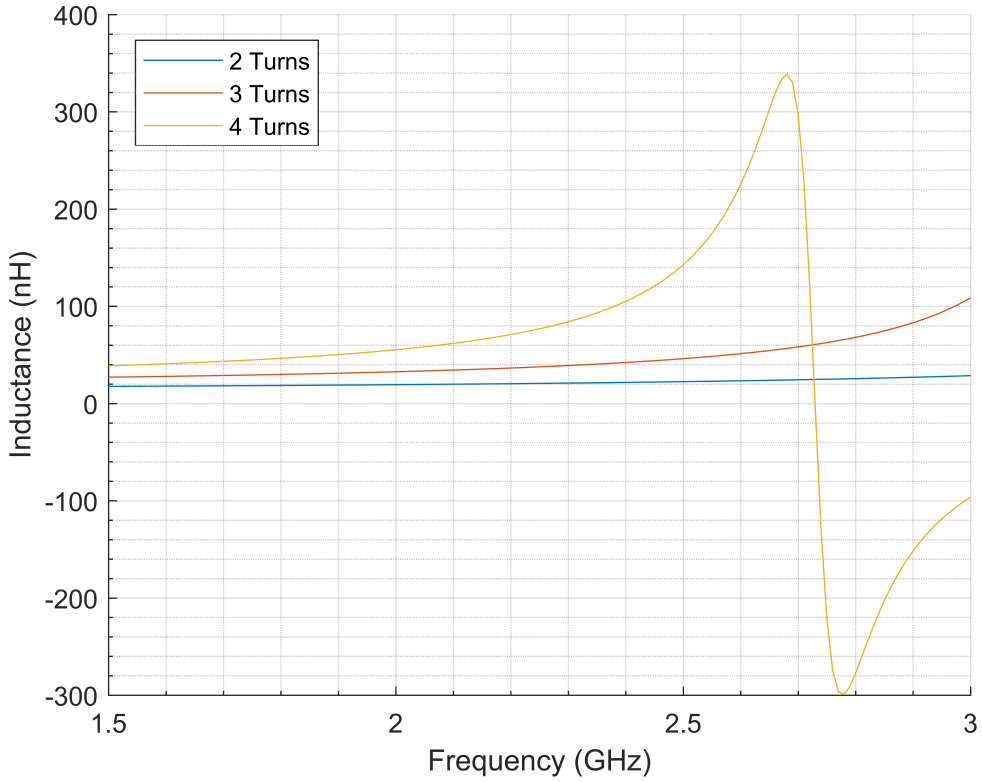

Figure 5.5: Inductance of the 3D rectangular inductor as a function of frequency for different number of turns.

5.4 Planar Balun Design

The balun is an integral aspect of the entire antenna design, in that it must provide accurate differential excitation to the opposing arms of the dipole. The balun found in the first experimental design, chapter 3, is a discrete commercial-off-the-shelf balun designed to be soldered onto a PCB. Since the objective here is to design a planar balun, a more suitable implementation is sought.

Baluns commonly found in a planar implementation are typically wavelength dependent structures [4] [1], more specifically their physical dimensions scale with the wavelength of operation. Some examples of these balun structures are the bazooka balun, Marchand balun, or a Wilkinson power divider used to split the power evenly, followed by a lumped element network to induce a differential phase shift required for a dipole antenna.

Figure 5.6, adopted from Lin et al.,[5] demonstrates an alternative means of achieving this differential setup, whilst significantly reducing the size of this differential transformation. By feeding the antenna from a coplanar waveguide and thereafter applying a resonator between the balanced and unbalanced sides of the transmission line, Lin et al., achieve differential signals on the balanced output. The resonator in this case is realised by means of an inter-digitated capacitor and inductive taper in parallel with this capacitor. Through careful design of this structure, a resonator may be designed to resonate at a given frequency by adjusting the spacing and size of the inductive taper, the inter-digitated capacitive structure or both structures together. In the case of the antenna, the resonator must be designed to operate at the resonant frequency of the antenna.

The principle of operation of this resonant mechanism used to achieve differential signalling is similar to that of a $\lambda/4$ transformer. By utilisation of a $\lambda/4$ length of line, a match is achieved by transforming the load impedance to a real impedance, thereby reducing reflection back to the source at a given frequency of operation. Looking forwards into the transmission line section, it would appear that the line is terminated in its characteristic impedance. From the perspective of the load looking back into the transmission line, it would appear to be conjugately matched. The authors have demonstrated an alternative means of realising this transformation through the use of planar lumped elements.

Here, in Figure 5.6 [6], a diagram and physical setup are presented for the planar configuration. To short-out the unwanted odd mode at the transition, a bond wire or bridge conductor is used to maintain the same potential on either side of the CPW transmission line. This is necessary to prevent the RF current from splitting into parasitic modes thereby aiding in maintaining a high degree of overall antenna efficiency.

The structure was modelled and simulated in HFSS to evaluate behaviour. Figure 5.7 presents the designed structure. The RF current density magnitudes have been plotted on the surface of the model. It may be observed that on the CPW side of the line, the currents are unbalanced. However, on the CPS side of the resonator, the currents may be seen to be visually similar - this is an expected result since this section is balanced. Bond-wires looping across ground planes are added to equalise potentials on the CPW grounds, hence shorting out any unwanted modal excitation.

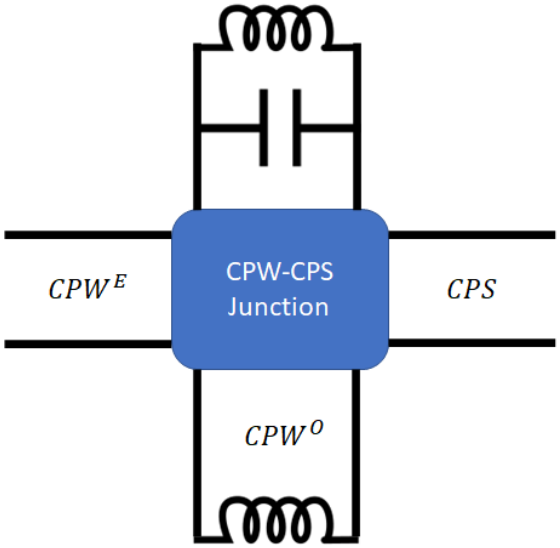

Figure 5.6: CPW to CPS Transition. Adopted from [6].

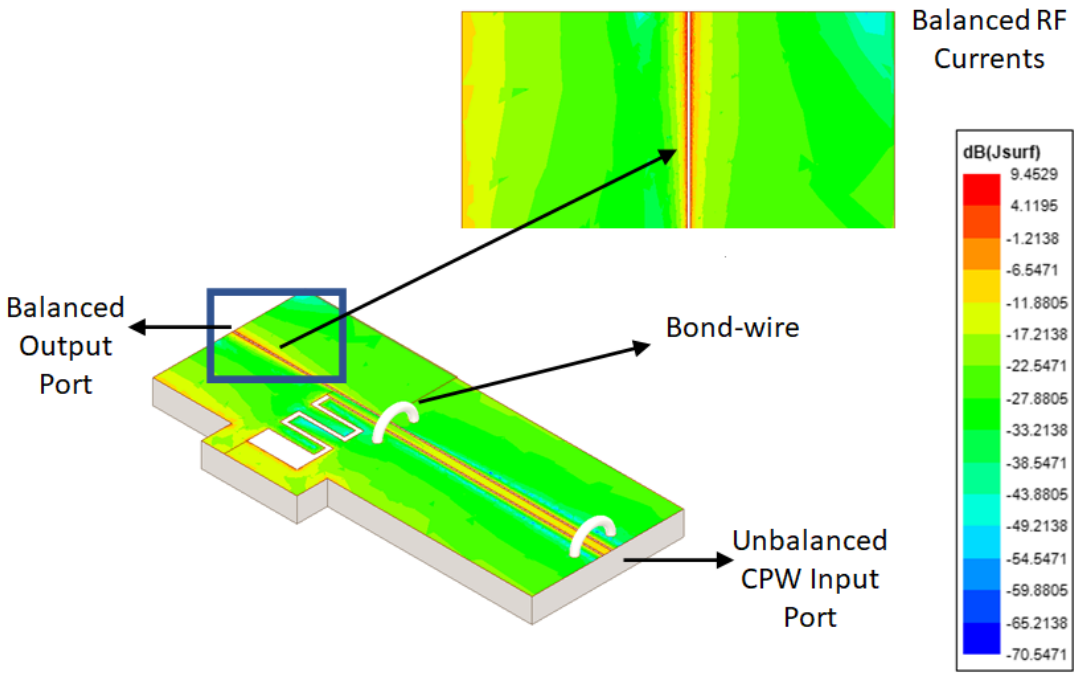

Figure 5.7: Resonant structure design for the CPW to CPS transition.

5.4.1 Design of Balun Resonant Structure

A key requirement of the balun structure from [6], is the effective design of the resonator to enable a balanced transition. The capacitance is physically controlled by the dimensions of the inter-digitated fingers, and the inductance is tuned through the meander joining the inter-digitated sections. From the model presented in Figure 5.6, one may see that this LC setup is an equivalent arrangement to a parallel LC resonator. To design the structure, this resonator was modelled numerically in HFSS. The aim of the design is to position the self-resonant frequency of the balun-resonator at 2.45 GHz. This was done by appropriately controlling the parameters of the balun-resonator model. This model is presented in Figure 5.8 with associated parameters in Table 5.1.

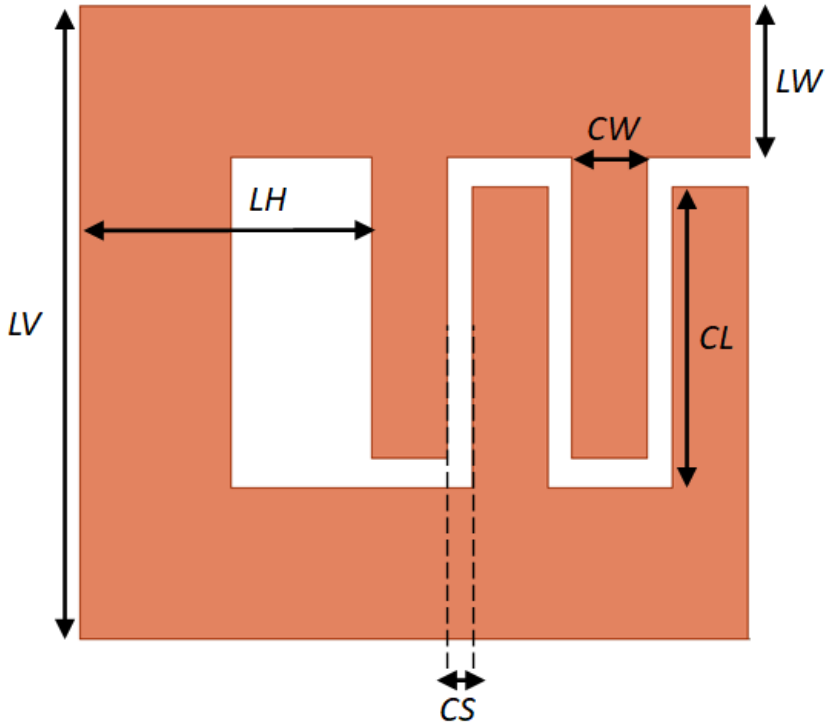

Figure 5.8: Resonant structure design for the CPW to CPS transition.

Table 5.1: Balun Resonator Parameters.

LH	Inductor horizontal length
LV	Inductor vertical length
LW	Inductor width
CS	Capacitive-finger spacing
CW	Capacitive-finger width
CL	Capacitive-finger length

A simulation model is designed and evaluated in HFSS and thereafter the impedance of the

structure extracted. The resonator is excited by placing an excitation port between the inductive meander and the capacitve finger. By setting the values of *LH, LV, LW, CS, CW, CL,* to 2.9, 6.3, 1.5, 0.25, 0.75 and 3 mm respectively, a self-resonant frequency of 2.47 GHz is achieved. A plot of the real and imaginary impedance components are displayed in Figures 5.9 & 5.10. One would expect a parallel LC circuit to exhibit a maximum impedance at the self-resonant frequency. It can be clearly seen from Figure 5.9, that a maximum occurs at 2.47 GHz. The imaginary component confirms a zero crossing at this frequency, confirming the requisite conditions for resonance. Now that the balun-resonator closely meets the design goal, the following step is to incorporate this model into the overall feed structure.

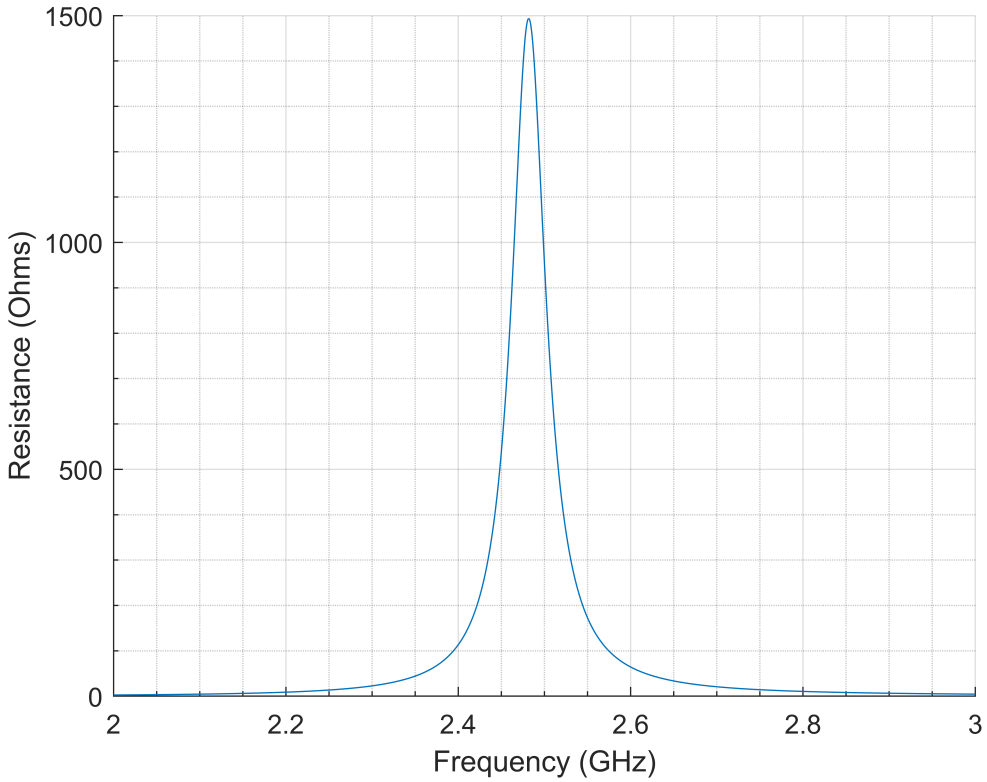

Figure 5.9: Real-component of the resonator impedance across frequency.

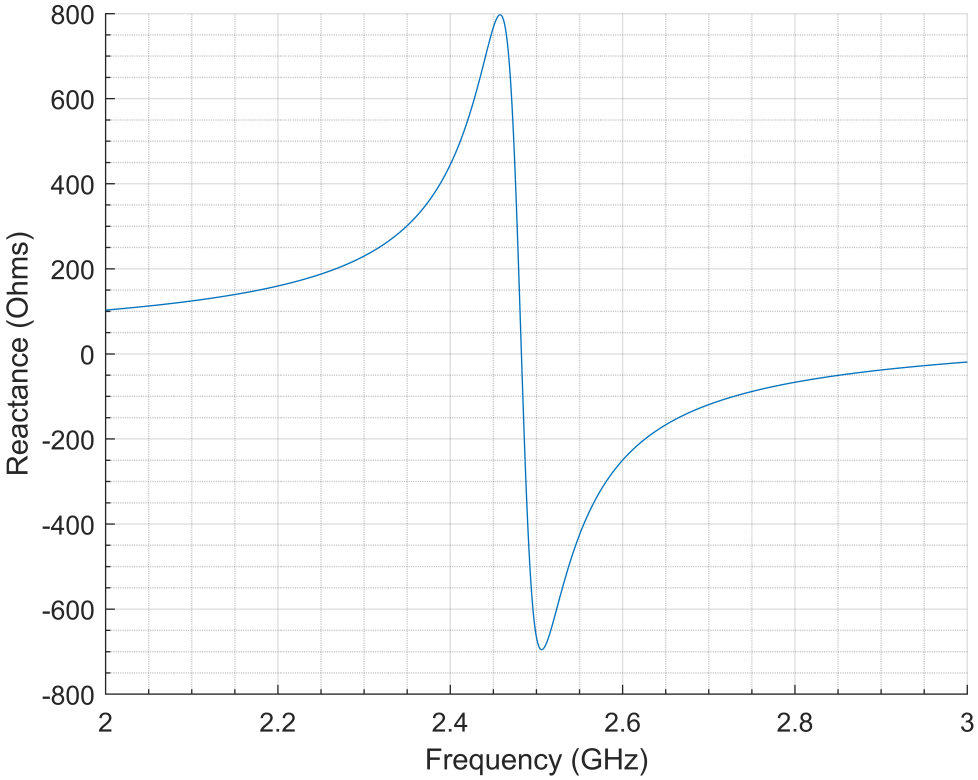

Figure 5.10: Imaginary-component of the resonator impedance across frequency.

5.4.2 Integration of Resonant Balun into the Transmission Line

Now that the balun resonant structure is designed, the next step is to integrate this design into the transition from an unbalanced CPW to a balanced CPS transmission line. The CPW transmission line section is designed to operate as 50 Ohm line with a centre-conductor width of 0.55 mm and with a spacing of 0.08 mm to the adjacent ground planes on either side. The width of the ground plane on either side is 4.65 mm. This ground plane width was chosen to suit an edge-mount SMA connector. The conductor thickness of the entire structure is 18 um. A Rogers 4003 substrate is used with a relative permittivity of 3 and a thickness of 1.6 mm. The loss tangent of this substrate is 0.002. Referring to Figure 5.8, a 50 Ohm CPW line is fed in alongside the balun-resonator. This allows for excitation of the balun and the impedance transformation to occur as the line transitions into a balanced arrangement. The separation between the balanced conductors is maintained as the same as that of the CPW ground spacing, 0.08 mm, to allow for a seamless balanced transition. The width of the balanced conductors is 5.275 mm. It is important to notice that the resonator itself is placed on the left-hand side of the transmission line, leading to an overall asymmetrical geometry in the feed. In this analysis, there are bond-wires placed to connect up the ground planes to equalize potentials on either side of the CPW section and short out the parasitic odd mode that may result with the introduction of the planar balun. This arrangement can be seen in Figure 5.7. Plotted in Figure 5.7 are the RF surface currents on the conductor. This is done to crucially inspect the currents on the balanced section of the feed. Visually, one may see that the currents on the opposing conductors are quite similar along the adjacent sides. This generates a degree of confidence that the balun is having the intended effect.

Further analysis of the feed structure is carried out numerically in HFSS by parametric variation of dimension LH on the resonator. This was done to inform overall behaviour of the balun as when selected dimensions are varied. As can be seen from Figure 5.11, as LH is varied from 2.9 to 5.9 mm, one may observe an overall frequency shift lower in the response. This is consistent with increasing the inductance of the resonator, hence shifting its self-resonant frequency lower. In the case of LH set to 2.9 mm, VSWR is better than 2:1 from approximately 2 to 5 GHz. The simulation registers an insertion loss for the antenna feed of 0.33 dB at 2.45 GHz. Although the transmission line exhibits operation across 3 GHz of bandwidth, the phase response across this bandwidth is difficult to extract numerically given this arrangement. Once the feed structure is connected to the dipole arms, it will be possible to deduce how well the feed performs in setting up the differential currents on the dipole arms. Given that this is close to the ideal dipole case, one would expect total gain to be quite close to the ideal case. If this is not the case and total gain or antenna efficiency exhibit unusually low levels, one may attribute this lack in performance to an incorrect electrical setup on the antenna, for which the balun is responsible. Accordingly, one may expect that cross-polarization levels would appear considerably higher due to the unbalanced currents on the feed. The variable LH is chosen to remain at 2.9 mm because the intent here is to preserve the self-resonant frequency and phase response of the balun at the antenna's frequency of operation 2.45 GHz.

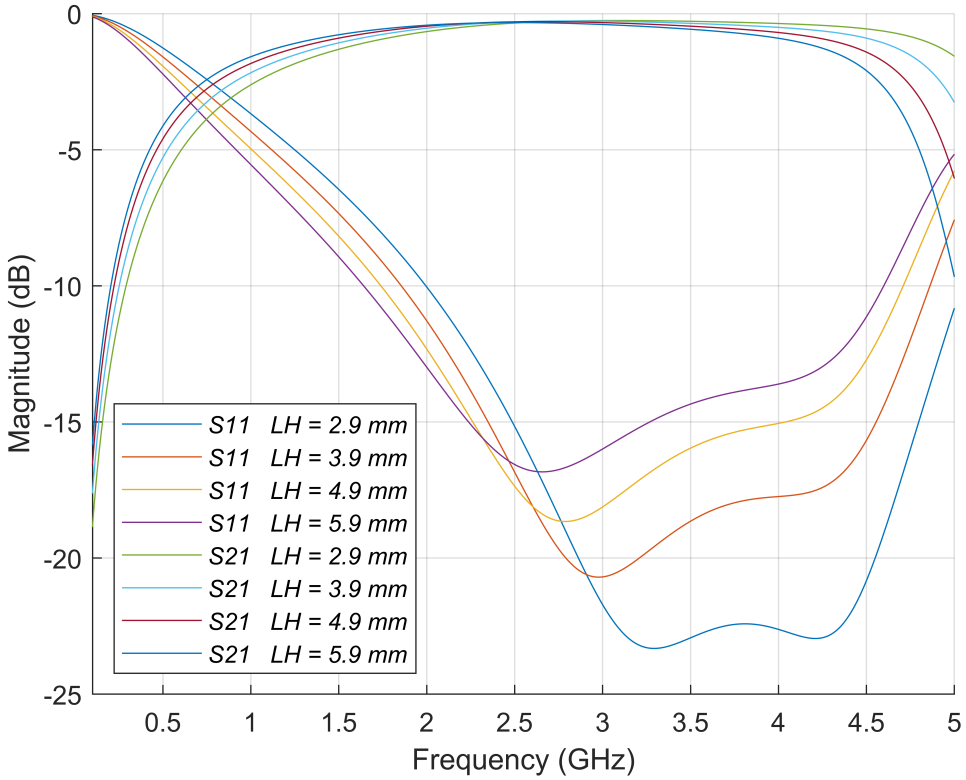

Figure 5.11: S-Parameters for the CPW to CPS balun. S11 and S21 are plotted whilst varying dimension LH.

5.5 Design and simulation of a planar $\lambda/2$ dipole with integrated balun

Now that the feed-structure has been designed in the previous section, the next step in the design process is to design a $\lambda/2$ dipole using the balun to provide a differential feed to the antenna. The creation of a dipole is useful in that it gives one a reference to which other derivative designs may be compared.

To examine if there is any interaction between the length of the balun on either side of the resonator, and the dipole antenna, the lengths before and after the resonator are varied in length. Figure 5.12 is a representation of the dipole setup with feed. The lengths varied are denoted as M and N on the diagram. The total length of the dipole is denoted L.

The antenna was simulated on a Rogers 4003 substrate, with a relative permittivity of 3 and a loss tangent of 0.002. The intended design frequency for this dipole is 2.45 GHz. The free-space wavelength at this frequency is 122 mm, equating to a $\lambda/2$ of 61 mm. Each corresponding dipole arm in a free-space model is 31.25 mm. The electric fields around the antenna in this setup, pass through both the substrate and air, leading to a higher effective permittivity. Hence, a shorter effective length for the $\lambda/2$ is realized in this case. From the dipole model in Figure 5.12, the bond-wires that were previously use to short out the unwanted modes have been replaced by vias which pass through the substrate to the bottom of the board and are bridged by a planar metal trace on the under-side of the board. This allows for construction of the entire antenna in a single fabrication run in standard planar technologies.

The lengths, M and N are parametrically evaluated to generate insight into variation of the antenna's reflection coefficient.

'L' was optimized separately and a value of 27.28 mm for each arm was found to achieve antenna resonance close to 2.45 GHz. Variables, M and N are then varied whilst fixing the total antenna length.

Firstly, the dimension M, was varied from 0.2 to 3.2 mm in 0.5 mm increments whilst fixing N to 9 mm. The reflection coefficient is graphed in Figure 5.13 to capture this variation. One can see that the dimension M certainly influences the antenna match. The resonant dip between each variation exhibits minimal shift in frequency, however there is significant variation in the depth of this notch. It must be noted that when designing this antenna using such a balun, it is imperative that this length be considered because it affects the antenna match. For the final prototype models, M is fixed at a length of 2.2 mm. This trade-off offers good antenna match with a reduction in overall antenna size.

To evaluate the variation in N, dimension M was fixed to 2.2 mm, thereafter N was varied from 9 to 13 mm in 1 mm increments. The antenna's reflection coefficient is graphed in Figure 5.14 across this variation. Here one may observe that there is only a minor deviation in responses of the reflection coefficient between variation in 'N'. This result allows one to see that the currents along the dipole are fairly well balanced. Had this not been the case, variation of this length would have significantly shifted the antenna's resonant frequency. Given the minor effect this length has on antenna operation, it is decided that the length N be fixed to 9 mm to reduce total antenna size for this and subsequent designs.

The co- and cross-polarization radiation patterns, in the yz plane, are plotted in Figure 5.15. The dipole antenna is superimposed on this diagram to help analyse and attribute aspects of the antenna geometry that affect the radiation pattern. The co-polarization pattern is quite symmetrical with maximum gain of 2.29 dB and half-power-beam-width (HPBW) of 80 degrees. In comparison to an ideal dipole which has 2.15 dB of gain and HPBW of 78 degrees, the result presented here is extremely close to this ideal case. The cross polarization reaches a maximum

of -14.09 dB. Of note is that this cross-polarization maximum occurs on the side of the antenna on which the balun is placed. The placement of this balun certainly has an impact on the cross-polarization pattern, however it is still well below -10 dB.

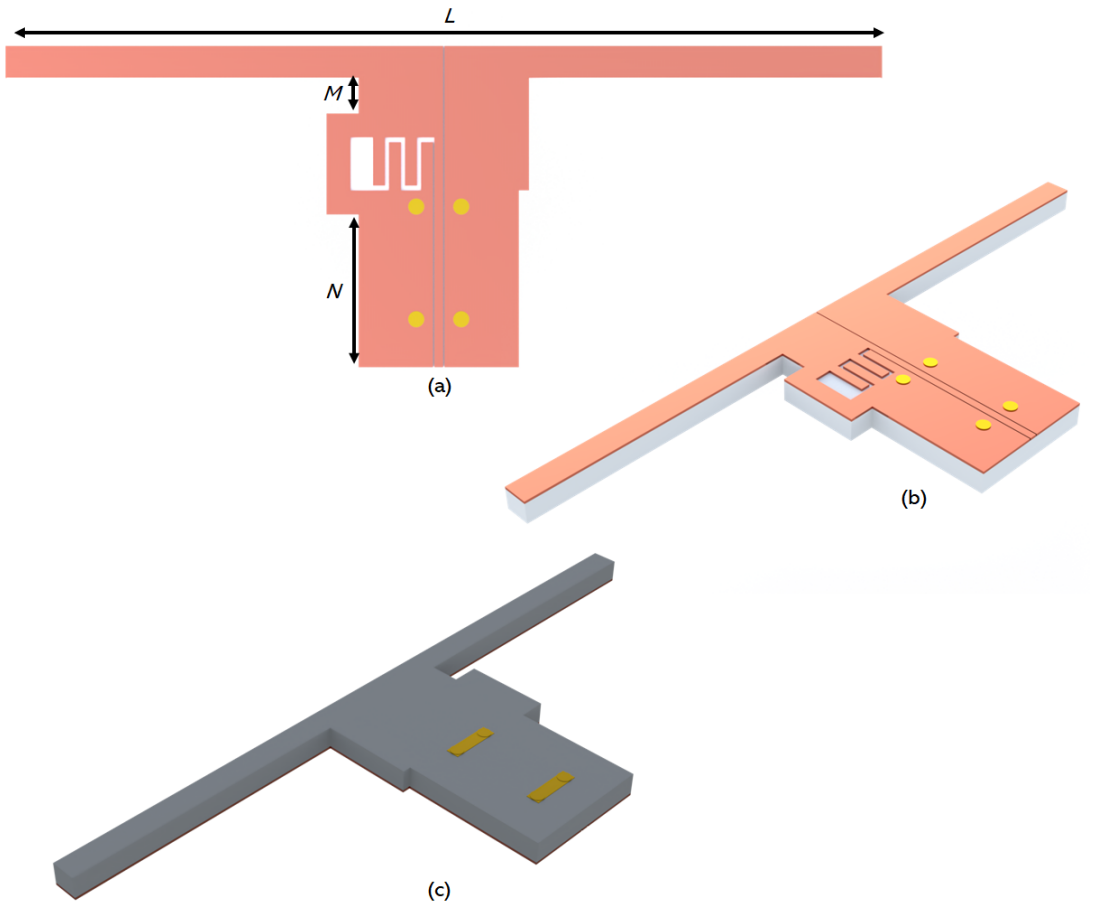

Figure 5.12: (a) Top view of the dipole with integrated balun. (b) Top isometric view of the dipole, showing yellow grounding vias on either side of the CPW. (c) Bottom isometric view showing the via-bridge on the beneath the substrate, connecting vias on either side of the CPW.

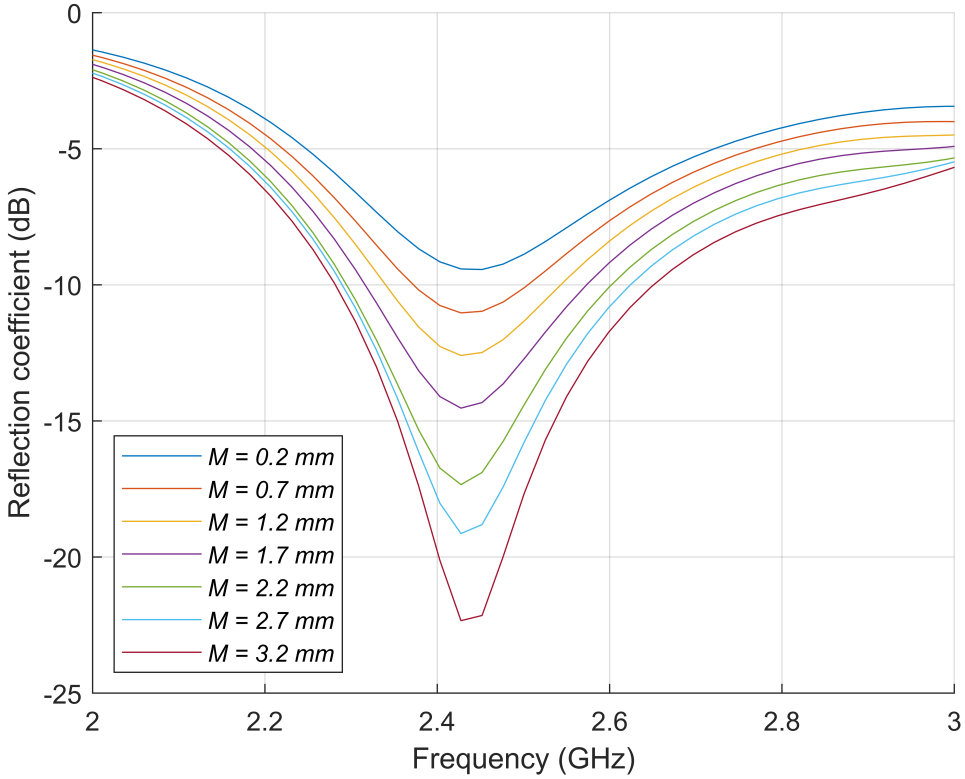

Figure 5.13: Reflection coefficient of the planar dipole showing the variation in dipole frequency response as M is varied.

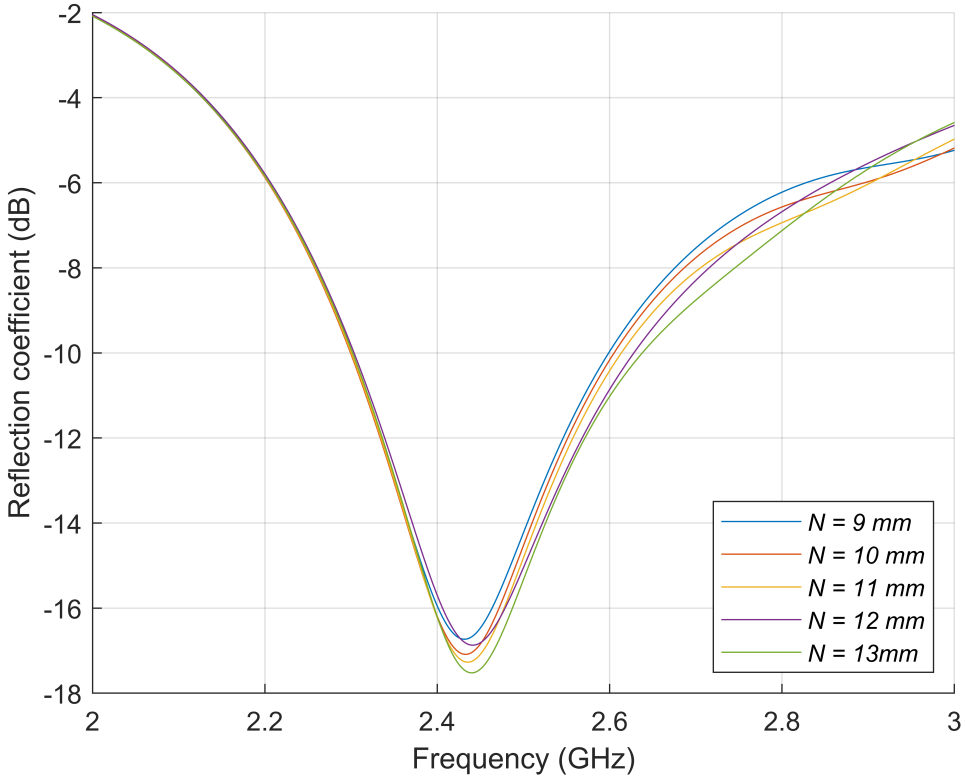

Figure 5.14: Reflection coefficient of the planar dipole showing the variation in dipole frequency response as N is varied.

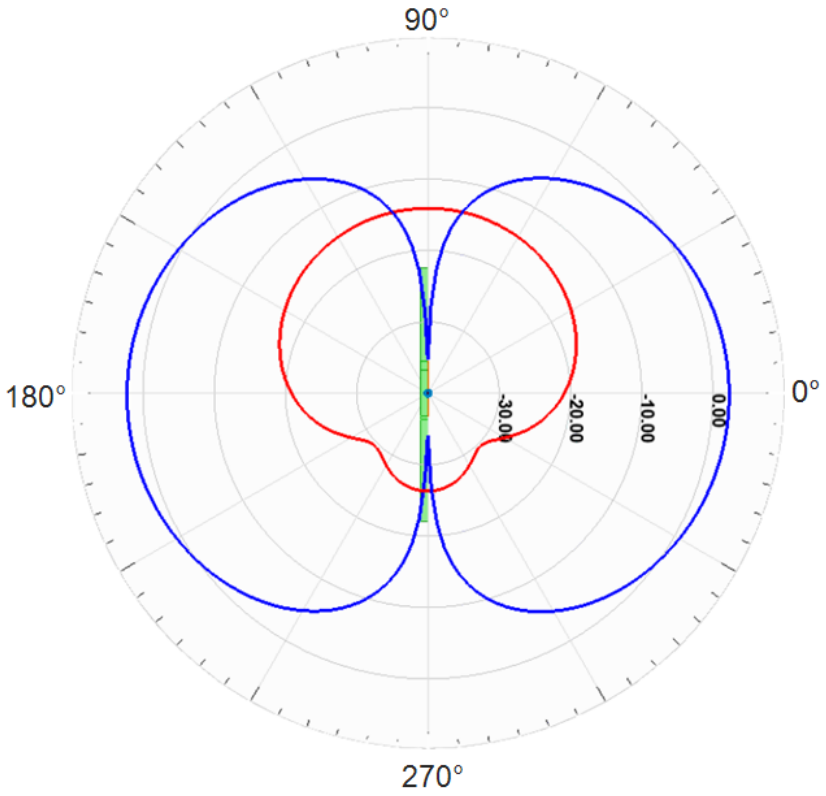

Figure 5.15: Simulated co- and cross-polarization dipole radiation patterns overlayed onto the dipole antenna model.

5.6 Counter-poise monopole antenna, combining planar coil and balun structures

Following the design of the feed structure, balun and dipole, focus is applied on replacing one of the dipole arms with a suitable counterpoise. Design of the coil and planar counterpoise follow the design procedure outlined below:

1. Maintain the existing length of the straight dipole arm.
2. Determine an initial starting point to generate a value of inductance for the counter-poise. One may refer to Equation 5.1 [7] [8] to calculate the value of inductance required for a flat inductor of rectangular cross-section.
3. Design the counter-poise to match this inductance.
4. Remove the opposing arm of the dipole and replace with a counter-poise. Numerically optimize the counter-poise until it matches the intended design frequency of 2.45 GHz.

Figure 5.16 illustrates the setup of the model. The counter-poise replaces the dipole arm in the top-right of the model and is connected to the feed-structure where the arm was positioned previously. An arm length of 27.275 mm leads to a value of self-inductance 20.75 nH. Referring to section 5.3, a counter-poise geometry to achieve this level of inductance is developed as shown previously. To optimize the antenna model, the number of turns on the counter-poise is increased until a close-to 50 Ohm match is achieved to the antenna. To gather information on how the antenna match varies with the number of turns, a simulation is firstly conducted without the counter-poise, and thereafter with counter-poises re-introduced with the number of turns spanning from 1 to 3. The resulting impedance of each state is plotted for a frequency of 2.45 GHz on the impedance plane of the Smith-chart, Figure 5.17. The impedance of the dipole designed herein is plotted there for reference. One may notice from Figure 5.17 that in the case where no counter-poise is present, the antenna is highly unmatched and is quite close to a short-circuit condition, hence a significant amount of power incident on the input of the antenna is reflected back to the load. Introducing a counter-poise with a single turn, transforms the match along the inductance contour of the smith chart. Here the antenna is still highly inductively loaded thus a negative reactance is required to bring the antenna closer to a 50 Ohm matched condition. Increasing the number of turns on the counter-poise subsequently introduces more negative reactance to the antenna, thereby bringing down the impedance match closer to 50 Ohms, as required. Comparing the impedance of the dipole and the 3-turn counter-poised monopole shows that they are quite close in impedance, indicated by the ellipse drawn around their respective impedance points. At this point, the counter-poised monopole is well matched, and the design considered complete. An overshoot condition at 4 turns is plotted for comparison. Observed is a heightened sensitivity to mismatch above 3 turns, with the antenna returning to a highly inductive match. A comparison between simulation and fabricated antennas is made in the proceeding section.

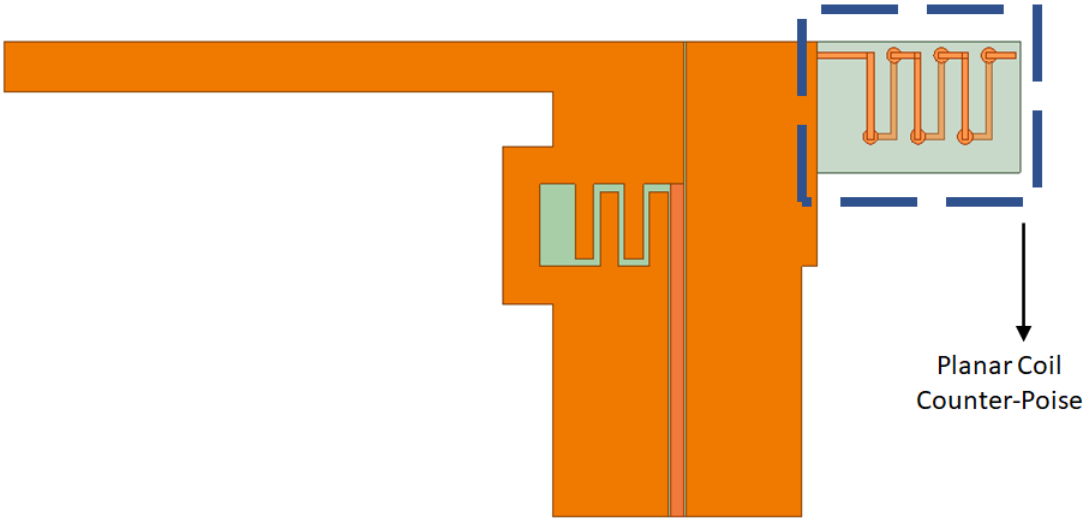

Figure 5.16: Planar Counter-poise monopole antenna, illustrating analysis of the connecting balanced arm.

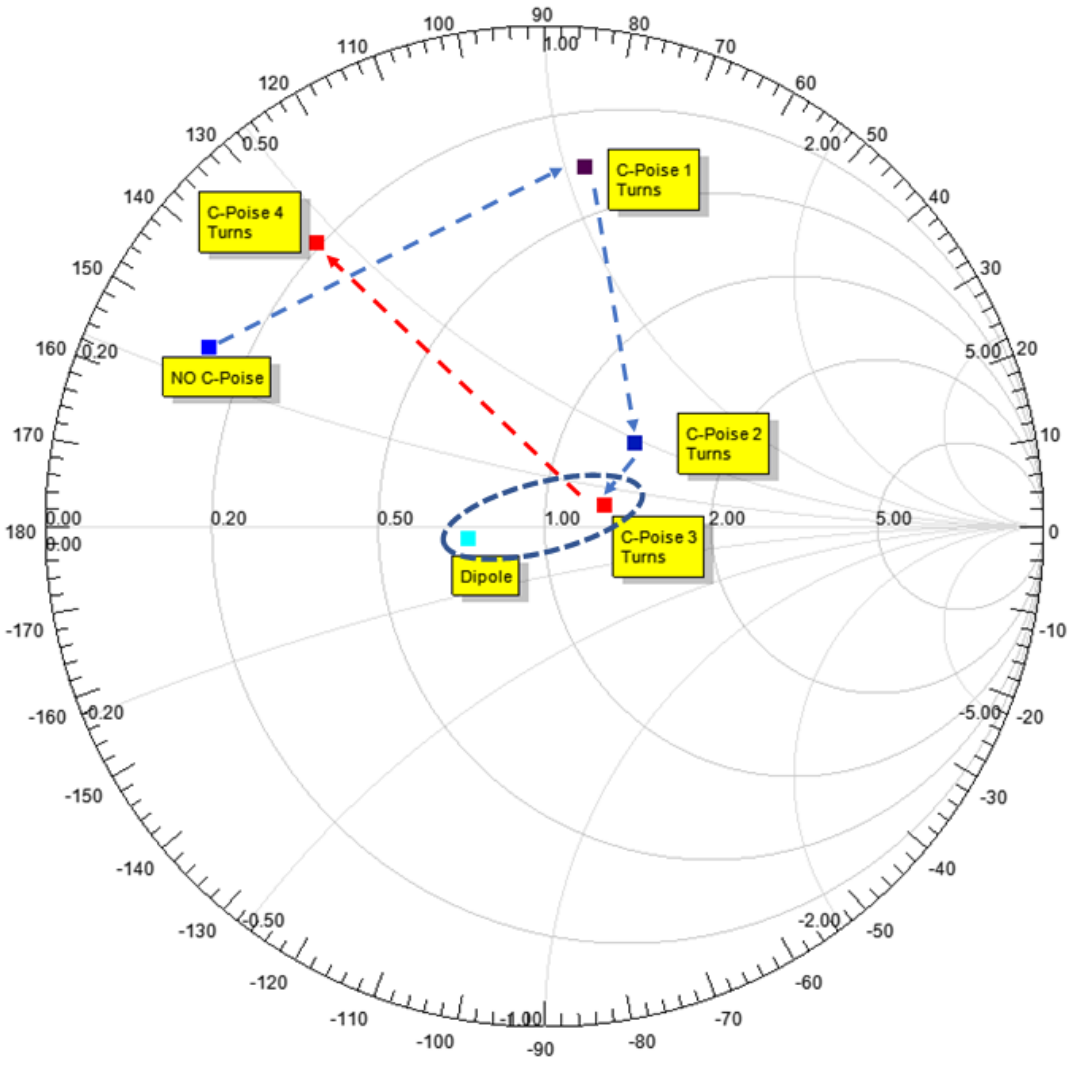

Figure 5.17: Smith-Chart illustrating impedance transformation from no counter-poise to achieving an effective match with a 3-turn counter-poise. The dotted line in red points to the overshoot from the optimally matched impedance.

5.7 Results

Three antennas were constructed to experimentally validate the design. Figure 5.18 shows the fabricated designs. A summary of the key measured results may be found in Table 5.2. The first is a dipole antenna with integrated balun and feed structure. The second a 3D coil counter-poised monopole. The third a planar counter-poised monopole. The antennas are respectively measured to evaluate the input impedance, gain and radiation pattern in the XY and XZ planes. On the fabricated antennas, it can be observed that the edge-mount connector fits almost perfectly alongside the CPW feed of the antenna.

Firstly, comparing the simulated and measured dipole reflection coefficients, shown in Figure 5.19, a strong correlation between simulation and measurement is observed. The simulated and measured results show, a centre frequency of 2.425 and 2.414 GHz, with a 2:1 VSWR bandwidth of 300 MHz and 240 MHz, respectively. The maximum antenna gain is measured at 1.53 dBi, which is quite close to the simulated response of 2.29 dBi. The HPBW in the simulated and measured cases are 78 and 80 degrees, respectively. Importantly, from the dipole radiation measurement, Figure 5.20(a), the cross-polarization level is below -10 dB in the XY and XZ planes.

Secondly, comparing the simulated and measured coil counter-poised monopole reflection coefficients, Figure 5.21, the centre frequencies from the measured and simulated results are 2.43 GHz and 2.48 GHz respectively. The measured case shows a negative frequency shift of 53 MHz and a 2:1 VSWR bandwidth of 120 MHz from 2.38 GHz to 2.5 GHz. The equivalent simulated 2:1 VSWR bandwidth is also 120 MHz. The centre frequency red shift is attributed to an inconsistency in the 3D circular coil geometry. We can observe in Figure 5.18(b) a varying pitch between successive turns on the coil. In practise, there is an inherent difficulty in maintaining the pitch between successive turns. Inevitably there is some movement due to the spring-like nature the coil and as a result there is some variation in parasitic capacitance between turns. In this instance the antenna shifts lower in frequency, leading to a determination that there is an increase in capacitance due to reduced pitch between turns of the coil. Maximum gain for the simulated and measured results are 1.785 and 1.221 dBi respectively. Referring to Figure 5.20(b), the cross-polarization level is below -10 dB in the XY and XZ planes. The HPBW in the simulated and measured results are 86 and 81 degrees, respectively.

Thirdly, for the planar counter-poised monopole antenna design, Figure 5.18(c), results show that there is good correlation between simulated and measured results. Comparing simulated and measured reflection coefficients, the centre frequencies are 2.481 GHz and 2.478 GHz, with a 2:1 VSWR bandwidth of 176 MHz 180 MHz respectively. Notice in this case that the responses are largely overlapping, proving that the practical constraints imposed using a circular coil is remedied through the accurate implementation of a rigid counter-poise in planar technologies. There is a 3 MHz difference between centre frequencies, indicating that there is potentially minor variation in the material properties and manufacture of the antenna. Maximum antenna gain from the simulated and measured results are 1.82 and 1.316 dBi respectively. The HPBW from the simulated and measured results are 84 and 82 degrees, respectively.

Referring to Figure 5.20, all antennas display measured results matching their simulated performances to within 0.8 dB, cover frequency of operation across the intended band of operation from 2.4 - 2.5 GHz and show a slightly reduced gain in comparison to the simulated performances. This discrepancy in measurement may be attributed to increased material losses, SMA connector losses and minor measurement inaccuracies. Comparing maximum gain between the measured dipole and the counter-poised antennas, shows a reduction in gain at worst of 0.3 dB. There is also a slight increase in HPBW in the counter-poised antennas by approximately 1 to 2 degrees. The 2:1 VSWR bandwidth is reduced considerably in the counter-poised antenna cases. The coil-

Table 5.2: Measured antenna comparison.

Antenna	Gain (dBi) max.	Bandwidth (MHz)	Cross-pol. (dBi) max.
Dipole	1.53	240	-10.25
Coil counter-poised monopole	1.22	120	-11.61
Planar counter-poised monopole	1.31	180	-12

counterpoise sees its bandwidth reduced by 50% compared to the measured dipole, whereas the planar-counterpoise antenna sees a reduction by 25% in comparison to the measured dipole. The larger bandwidth achieved in the planar counter-poise design is attributed to a more effective matched impedance through accurate design and control of the counter-poise. Both counter-poised antennas still have good dipolar pattern at 2.45 GHz despite modest reduction in gain.

5.8 Summary

From the results, it can be concluded that the design method used, initially employing an analytical approach to roughly guide the counter-poise design and thereafter employing a numerical approach to refine the overall antenna design works well. Demonstrated as well, is the ability to construct an antenna at higher frequency using this counter-poise method in relation to the antenna presented in Chapter 4 operating at 965 MHz. Referring to the design objectives of miniaturization and planar realization, the planar counter-poised antenna meets both objectives and offers potential of a future flexible variant. In applications where there are space and size constraints, this antenna serves as an alternative offering dipole radiation pattern, with a minor reduction in gain and bandwidth.

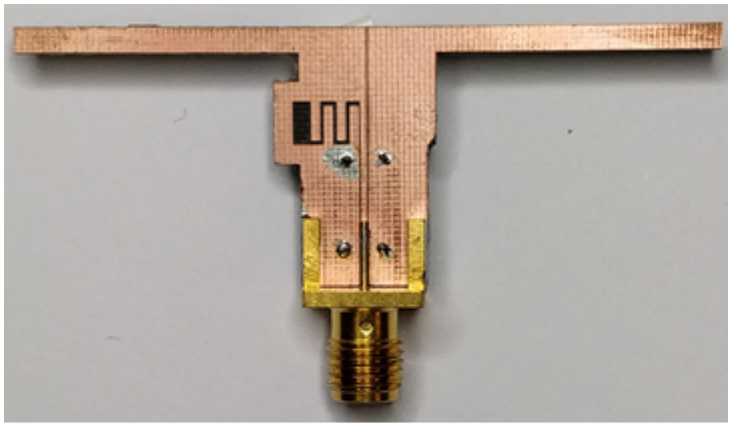

(a)

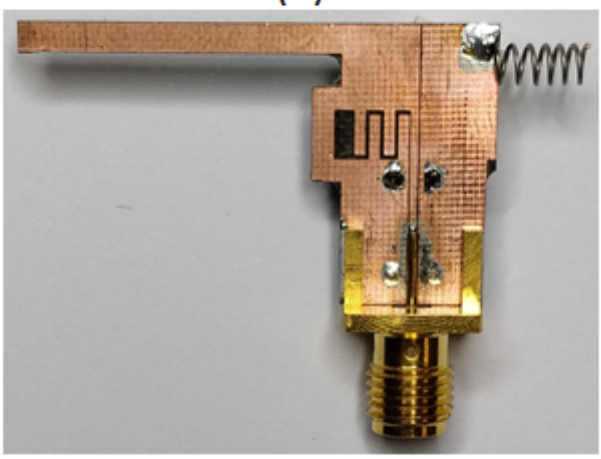

(b)

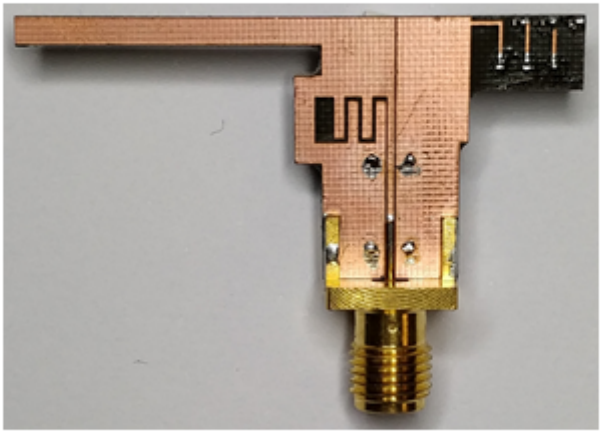

(c)

Figure 5.18: (a) Dipole antenna. (b) Coil counter-poised monopole antenna. (c) Planar counter-poised monopole antenna.

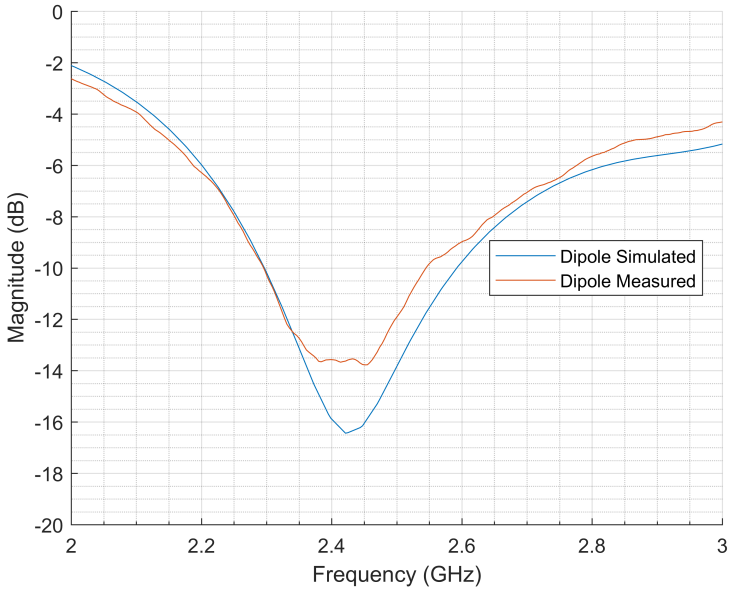

Figure 5.19: Simulated and measured dipole reflection coefficients.

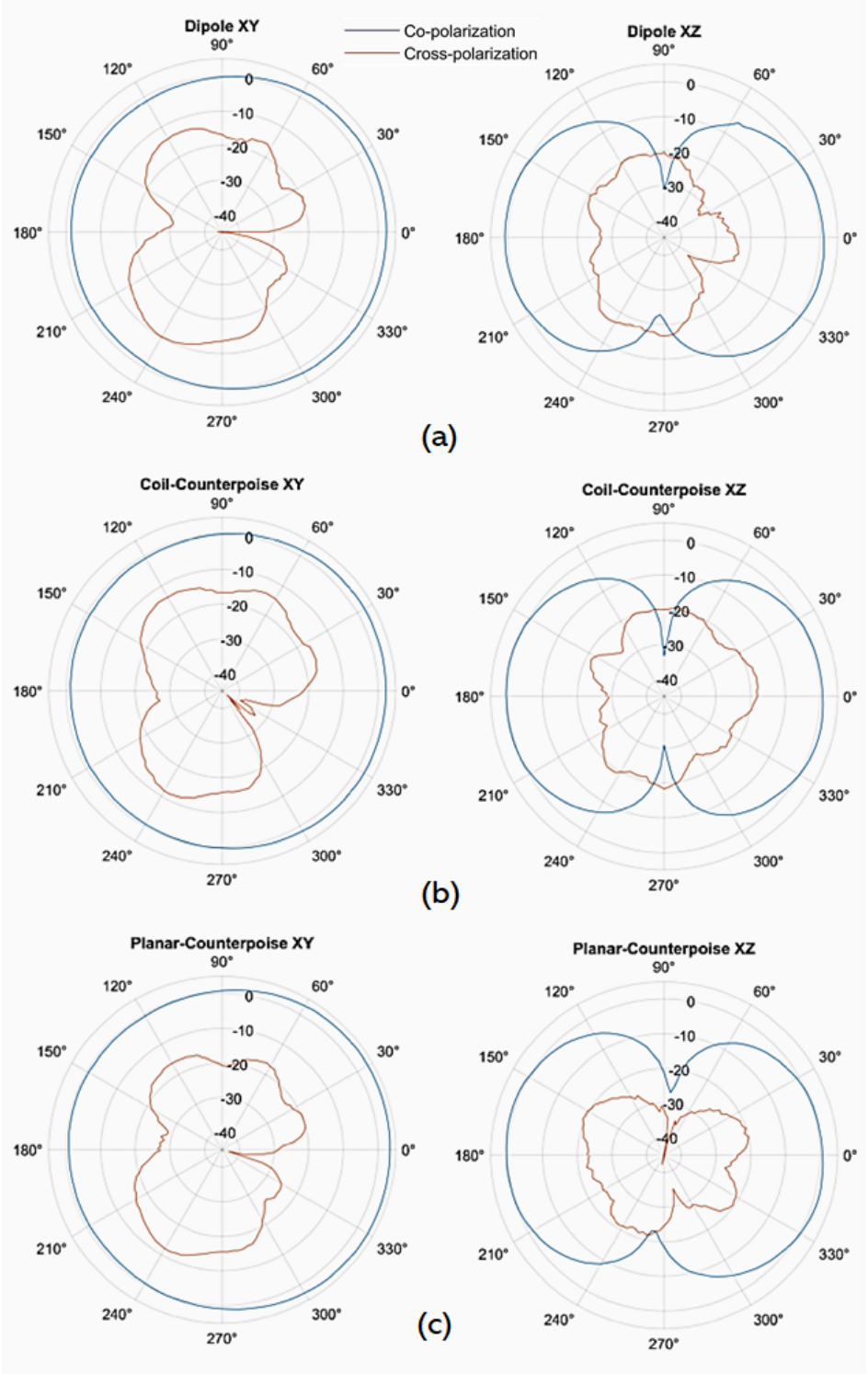

Figure 5.20: Measured antenna co- and cross-polarization plots in the XY and XZ planes. (a) Dipole. (b) 3D counterpoised monopole. (c) Planar counterpoised monopole.

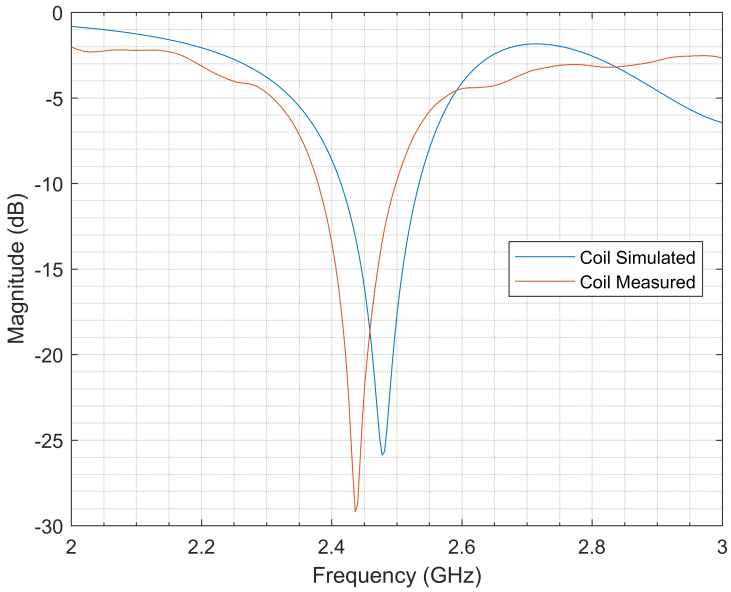

Figure 5.21: Simulated and measured coil counter-poised reflection coefficients.

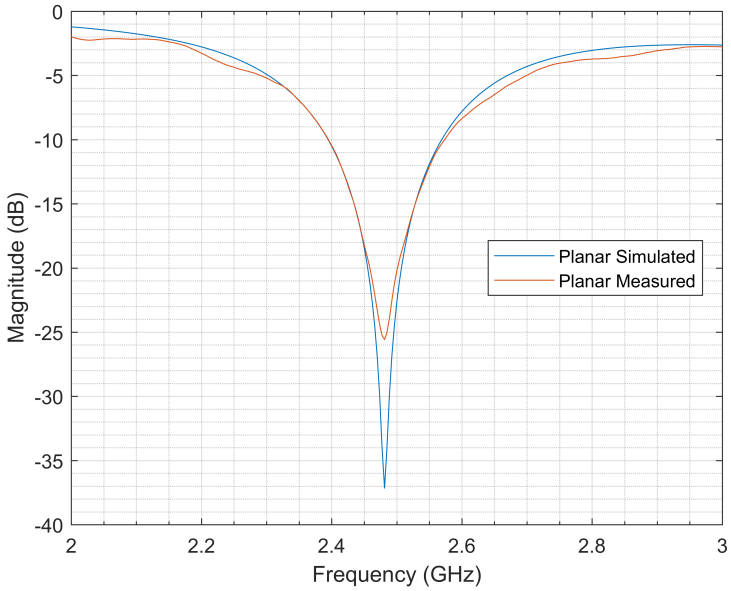

Figure 5.22: Simulated and measured planar counter-poised reflection coefficients.

Bibliography

[1] Reinhold Ludwig and Pavel Bretchko. RF circuit design, 2000.

[2] Christopher Coleman. *An Introduction to Radio Frequency Engineering*. Cambridge University Press, Cambridge, 2004.

[3] Spartaco Caniggia and Francescaromana Maradei. *Signal Integrity and Radiated Emission*. Wiley Online Library, 2008.

[4] David M Pozar. Microwave Engineering. *Fourth Editions, University of Massachusetts at Amherst, John Wiley & Sons, Inc*, 2012.

[5] Shengjian Jammy Chen, Thomas Kaufmann, Roderick Shepherd, Benjamin Chivers, Bo Weng, Anthony Vassallo, Andrew Minett, and Christophe Fumeaux. A compact, highly efficient and flexible polymer ultra-wideband antenna. *IEEE Antennas and Wireless Propagation Letters*, 14:1207–1210, 2015.

[6] Yo-Shen Lin and Chun Hsiung Chen. Novel lumped-element uniplanar transitions. *IEEE transactions on microwave theory and techniques*, 49(12):2322–2330, 2001.

[7] Brian C Wadell. *Transmission line design handbook*. Artech House, 1991.

[8] Frederick Warren Grover. *Inductance calculations*. Van Nostrand, 1946.

Chapter 6

Reconfigurable Varactor-Counter-Poised Monopole Antenna with Uni-Planar Feed

6.1 Introduction

After a fixed frequency counter-poised monopole has been designed and experimentally validated in the previous chapter, the aim of the present chapter is to focus on the design of a frequency-reconfigurable variant. One of the core tenets of antenna design in this thesis, is the development of a frequency-agile antenna, which is beneficial to an operator in a varying environmental context. The ability of maintaining high antenna efficiency through physical environment change is crucial. In Chapter 1, it was outlined that reconfigurability can be achieved through an electrical manipulation of the antenna structure. Since the passive counter-poise possesses an equivalent inductance and capacitance, the most straightforward place to introduce an active element is around the counter-poise.

6.2 Counter-poise Modification and Varactor Placement

As a starting point for the design, we revisit the planar counter-poise monopole antenna developed in chapter 5 and shown in Figure 6.1. It is from this point on-wards that further modifications to the design are performed. Apart from design of the active counter-poise section, the intent for the rest of the antenna structure - feed, balun and the straight arm of the antenna - is maintained as per the design illustrated in Figure 6.1. Given the good standard of operation demonstrated in the previous chapter, we wished to maintain the basis of the design, whilst exploring counter-poise modification alone for frequency-reconfigurability. To implement the antenna reconfigurability feature, a varactor is added to the planar counter-poise, as shown in Figure 6.1. The position considered for placement of the varactor is in shunt with the counter-poise. This has been done for two reasons. Firstly, from the analysis performed in chapter 5, the inductance increases non-linearly as the number of turns on the counter-poise are increased as illustrated in Figure 5.5. The idea here is that by exploiting this non-linear characteristic a larger frequency shift may result for a smaller applied capacitance. Secondly, placement of the varactor in this location provides a convenient point at which to tap into the counterpoise, where supporting electronics may be included, whilst minimally interfering with antenna behaviour.

6.3 Reconfigurable Antenna Simulation

Once the placement of the varactor is decided, the next step in the process is to optimize the fixed section of the counter-poise with the addition of the varactor, RF coupling capacitor, choke resistor and inductor. The simulation will also consider parasitic contributions from each component. The proximity of these components has an overall effect on the frequency response

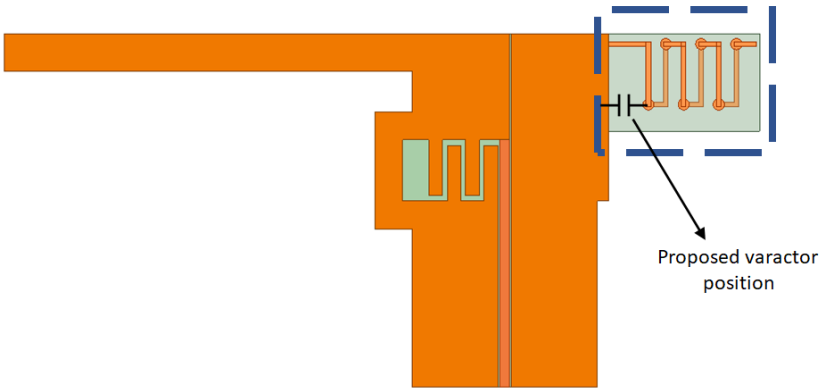

Figure 6.1: Varactor placement around the counter-poise.

and must be accounted for during simulation and optimisation. Figure 6.2 shows the setup of the simulation and the position of the respective circuit elements. The orange shaded region represents the top conductor, the light-green region the substrate under the top layer, and the non-shaded region outlined in orange the conductive traces of the counter-poise beneath the substrate. For the simulation, a value of 1 K Ohm was applied to the resistor, 820 nH for the inductor, 22 nF for the RF coupling capacitor and the varactor was varied from 0.01 to 10 pF. Since the antenna presents as a DC short, the RF coupling capacitor provides DC isolation to the rest of the antenna from the varactor bias. A combination of an electrically large resistor and inductor is used to maximally prevent stray RF currents from travelling through the DC bias path. The pads for the resistor and inductor are designed to accommodate soldering of 0603 size components. For the RF coupling capacitor and varactor, the pads are designed to accommodate 0402 components. Figure 6.3 displays an isometric projection of the proposed setup with surface mount components with vias connecting the top and bottom electrical layers.

To design for the frequency range over which the antenna is configurable, one must first observe the frequency response of the balun. Shown in Figure 5.10, it is observed that the balun performs well over the range of 2.3 to 3 GHz. It is for this reason that we choose to design for reconfigurability over this bandwidth. The target here is to achieve at minimum 15% reconfigurability, therefore the fixed section of the counter-poise along with the associated circuit components are firstly designed to achieve an upper resonant frequency of 2.75 GHz. Thereafter additional capacitance provided by the varactor will shift the resonant frequency of the antenna down to 2.3 GHz.

To design for an upper frequency limit of 2.75 GHz, referring to Figure 5.4, the fixed section of the counter-poise was modified to have a value of $H = 1.6$ mm, $C = 2$ mm , $W = 3.75$ mm, $S = 1.9$ mm, and $V = 0.6$ mm respectively. Upon completion of this antenna optimization, a logarithmic sweep of an hypothetical varactor capacitance is then conducted from 0.01 to 10 pF. These simulations are conducted to evaluate the frequency reconfigurability of the antenna and to aid in identifying an appropriately specified varactor to achieve the desired frequency reconfigurability. Figure 6.4 shows this sweep in resonant frequency across capacitance. One may observe from the graph that the antenna may be tuned from an upper limit of 2.77 GHz down to 1.33 GHz. However, this result must be taken with a degree of caution, given the frequency response of the balun breaks down below 2.2 GHz, as shown in Figure 5.11. The dotted orange lines superimposed on Figure 6.4 indicates the range of usable bandwidth of the balun. The degradation in antenna performance is further illustrated in Figure 6.5, which shows the

frequency response across capacitance with a colour-map for the return loss. As can be noticed from the plot, at 2.31 GHz and below, subsequent pixels show a significant degradation in return loss to below 6 dB. We attribute this degradation in return loss to bandwidth limitations of the balun. With the current balun design, one may achieve 460 MHz of frequency reconfigurability with better than 2:1 VSWR, as shown by the orange ellipse in Figure 6.5. However, if one were to implement a broadband frequency balun down to 1.4 GHz, as shown by the dotted blue line on Figure 6.4 and the white ellipse in Figure 6.5, it may be possible to achieve a reconfigurable percentage bandwidth of at least 40%. In the first instance, we shall maintain the balun design to confirm frequency reconfigurability in the counterpoised-monopole antenna, and thereafter in a future work seek to extend the frequency reconfigurability through further extending the balun bandwidth. The plot in Figure 6.5 also shows that as the capacitance increases, the bandwidth of the antenna decreases, as can be observed from the yellow-band becoming increasingly narrow, as the antenna is tuned lower in frequency. This characteristic will be analyzed in detail in the proceeding sections. Notice at 1 pF and above the appearance of a mode between 2.8 and 3 GHz. This artefact is presently outside the intended design specification and can be ignored for now, however in a future iteration of the design an attempt to keep these modes outside of the band of operation will be required. Analyzing Figure 6.4, a value of a 0.54 pF is required to shift the resonant frequency to 2.29 GHz. Therefore, this particular antenna design requires a varactor capable of producing at least 0.54 pF. For this reason, a MACOM MA46H120 varactor is chosen as it is capable of producing a variable capacitance of up to 0.9 pF.

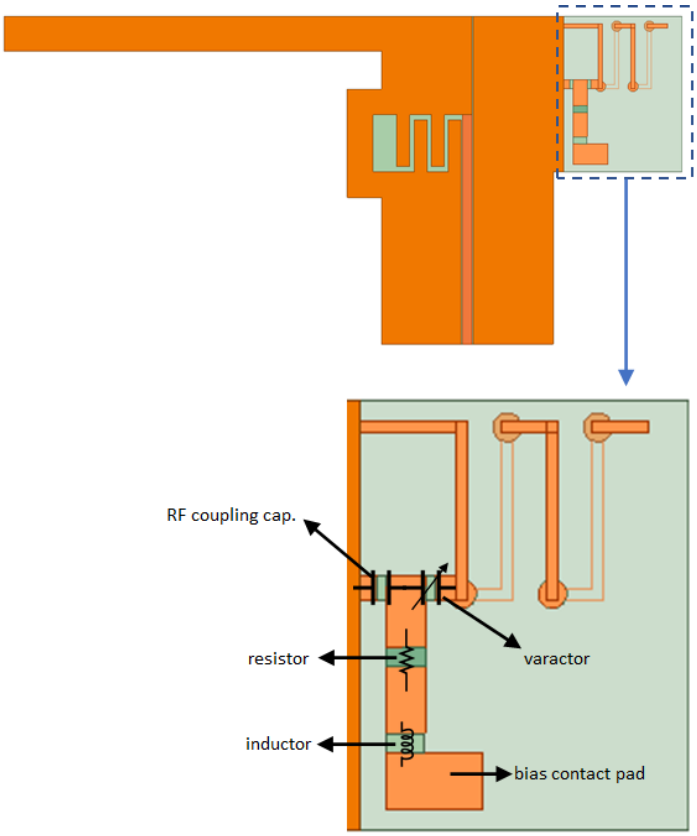

Figure 6.2: Simulated varactor counter-poise antenna, inclusive of active counter-poise electronics and associated pad parasitics.

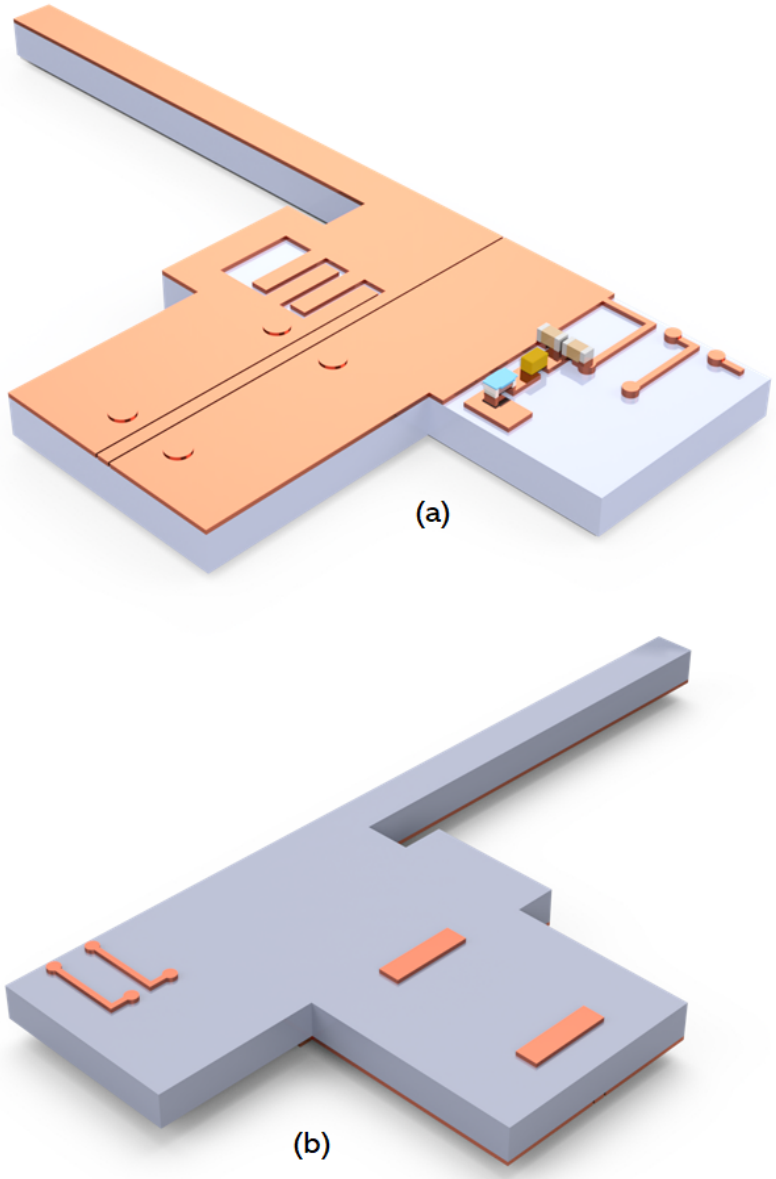

Figure 6.3: (a) Illustration of the top isometric view of the antenna with representative surface mount components. (b) Illustration of the rear isometric view of the antenna, displaying bridging traces connecting grounding vias, and rear counter-poise tracks.

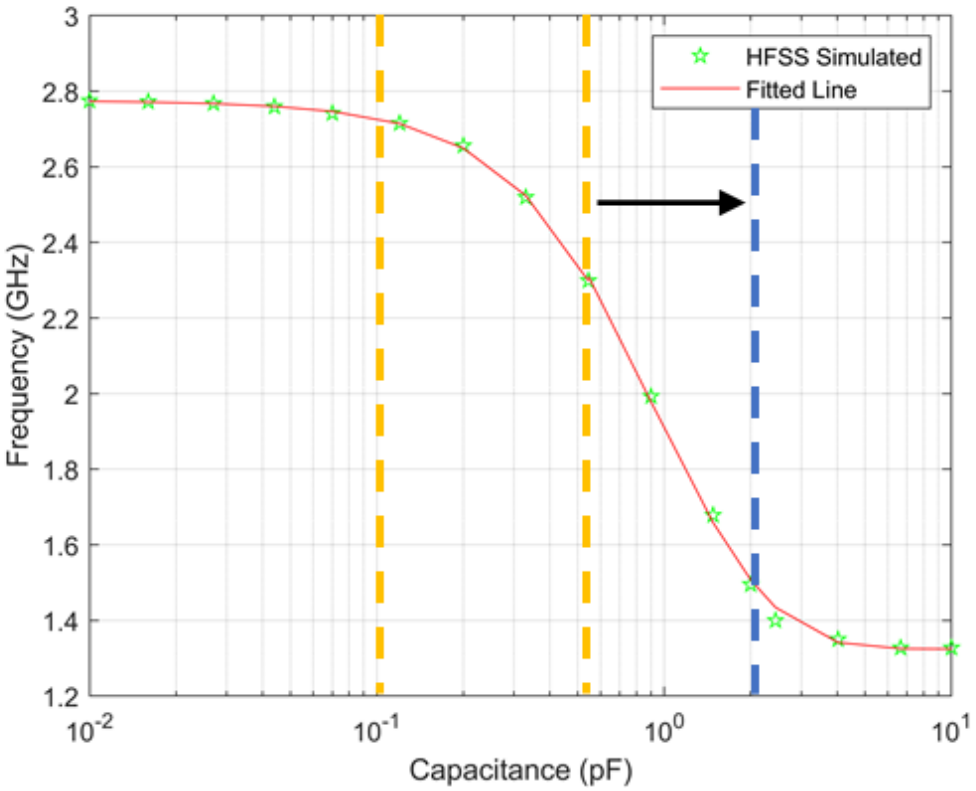

Figure 6.4: Resonant frequency as a function of capacitance.

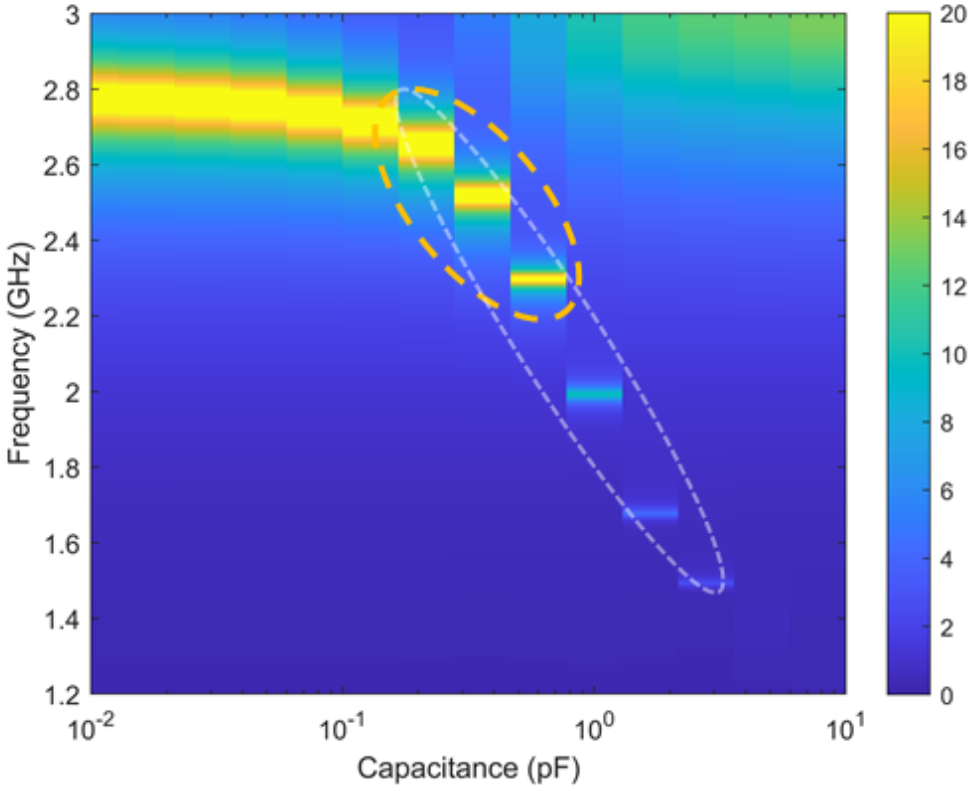

Figure 6.5: Frequency sweep as capacitance is varied, with colour-mapping intensity for return loss.

6.4 Reconfigurable Antenna Fabrication

With the antenna design complete, the next step is to fabricate the antenna. For direct comparison, the reconfigurable antenna is manufactured using the same PCB fabrication process for the antennas designed in the previous chapter. The antenna is fabricated on a Rogers 4003 substrate, with relative permittivity of 3.0 and loss tangent 0.002. An edge-mount SMA connector is soldered to the antenna feed. Figure 6.6, shows the front and rear views of the manufactured prototype. All electronic components are surface-mount packaged, which makes for straightforward electrical attachment of these components to the antenna PCB. A tinned copper wire is then soldered to the PCB to provide the DC bias required for the varactor. A closeup of the setup is shown in Figure 6.7 with components soldered to the antenna PCB. There are minute amounts of excess solder around the joints where vias and components were connected, however these excess contributions should have minimal impact on the measured antenna performance.

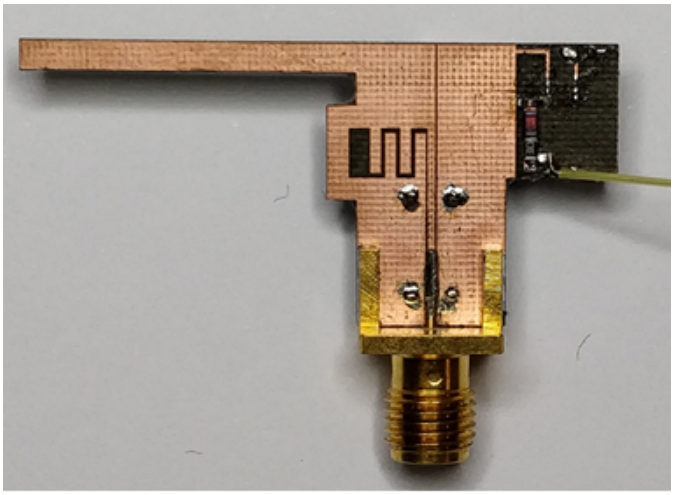

(a)

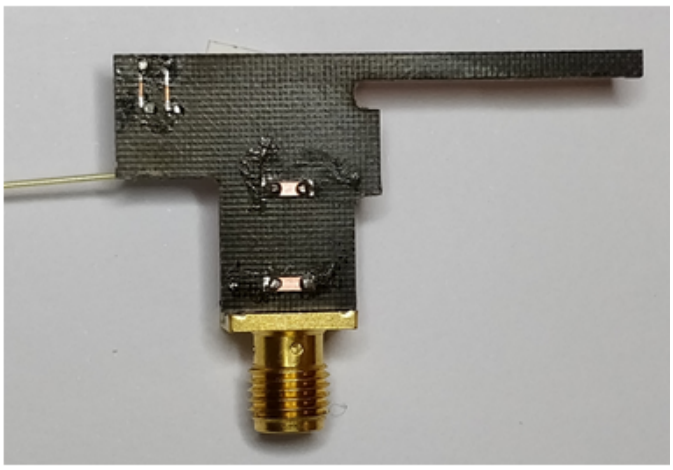

(b)

Figure 6.6: (a) Varactor counter-poised monopole antenna front. (b) Varactor counter-poised monopole antenna rear.

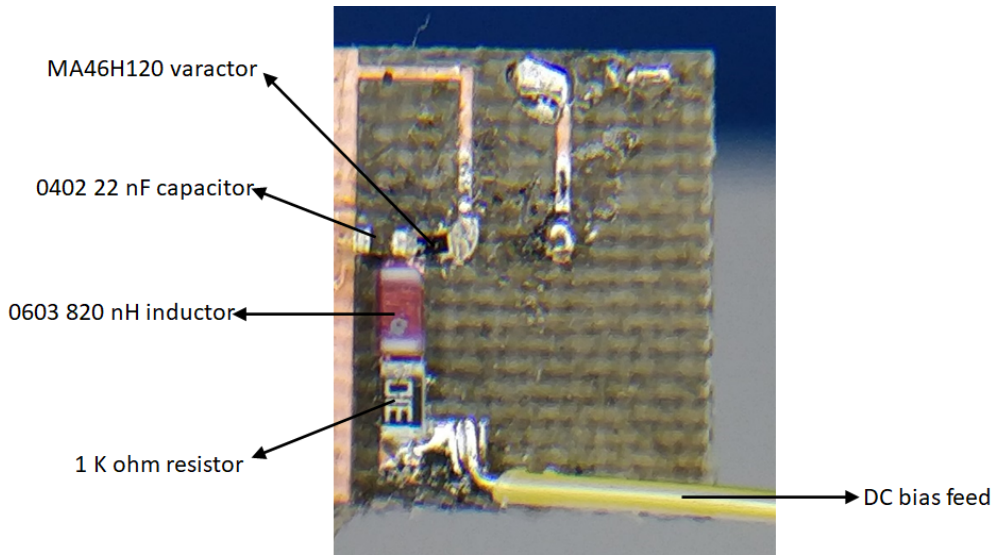

Figure 6.7: Zoomed in section of the active counter-poise section with associated electronics.

6.5 Results

The reconfigurable antenna is measured across 3 varactor settings and thereafter comparisons are drawn to their respective simulations. Measurements are made of the antenna input impedance, gain and antenna radiation pattern in the XY and XZ planes. The varactor is set to 0.15, 0.33 and 0.54 pF, requiring a bias voltage across the varactor of 18, 4.5 and 2.5 volts, respectively.

Firstly, comparing the simulated and measured reflection co-efficient when the varactor is set to 2.5 V, generating a capacitance of 0.54 pF, Figure 6.8, the simulated and measured centre frequencies are 2.29 and 2.30 GHz respectively. These results correlate well, however the depth of the responses differs considerably. The measured response is not as well matched in comparison to the simulation, with a measured input reflection coefficient at the centre frequency of -9 dB. The simulated 2:1 VSWR bandwidth is 56 MHz. There are two reasons that are attributed to this measured shortfall. The first is that the resonant frequency is now shifted to the lower frequency edge of the balun's operating range resulting in performance degradation. A secondary contribution is from the parasitic resistance associated with the varactor, leading to further antenna mismatch. The maximum antenna gain is measured at -4.64 dBi, Figure 6.10, which differs considerably from the simulated gain of 0.005 dBi - albeit the simulation did not account for the parasitic losses associated with the varactor. The HPBW in the simulated and measured cases are 86 and 69 degrees, respectively. The cross-polarization level, Figure 6.9, is below -10 dB across most of the XY and XZ planes. However, there are narrow regions over which the cross-polarization crosses this boundary, with a maximum reaching -5 dB.

Secondly, comparing the simulated and measured reflection co-efficient when the varactor is set to 4.5 V, generating a capacitance of 0.33 pF, Figure 6.8, the simulated and measured centre frequencies are 2.48 and 2.5 GHz respectively. The simulated and measured 2:1 VSWR bandwidths are 123 and 112 MHz, respectively. Both centre frequency and 2:1 VSWR bandwidth results correlate well. This is to be expected given the balun is now in operating at close to the intended design frequency of 2.45 GHz. The peak antenna gain is measured at -1.33 dBi, Figure 6.11, which is close to 2 dB below the simulated gain of 1.29 dBi. The HPBW in the simulated and measured cases are 86 and 80 degrees, respectively. The cross polarization levels across the XY and XZ planes, Figure 6.9, measure less than -10 dB across the majority of these regions with narrow regions rising above this level with a maximum of -6.38 dB.

Thirdly, comparing the simulated and measured reflection co-efficient when the varactor is set to 18 V, generating a capacitance of 0.15 pF, Figure 6.8, the simulated and measured centre frequencies are 2.77 and 2.74 GHz respectively. The simulated and measured 2:1 VSWR bandwidths are 278 and 146 MHz, respectively. In this case the simulated result is greater than the measured result by 132 MHz. The frequency entry points of the 2:1 VSWR bandwidth specification are quite close, 2.63 GHz for the measured result and 2.65 GHz for the simulated result. The exit points for the 2:1 VSWR bandwidth specification differ significantly, 2.8 GHz for the measured result and 2.9 for the simulated result. This reduction in bandwidth is potentially attributed to the balun, in that the upper frequency of operation is curtailed by the usable operational bandwidth of the balun. Additionally, the parasitic resistances of the varactor and RF coupling capacitor may lead to antenna mismatch, limiting the bandwidth in practise. The peak antenna gain is measured at -2.54 dBi, Figure 6.12, in comparison to the simulated gain of 1.65 dBi. The HPBW in the simulated and measured cases are 84 and 96 degrees, respectively. The cross polarization levels across the XY and XZ planes, Figure 6.9, are below -10 dB across the majority of these regions with some regions rising above this level with a maximum of -6 dB.

6.6 Future Work

The simulated results shown in Figures 6.4 & 6.5, indicate that there is potential for significant improvement to the reconfigurable frequency range of the counter-poised monopole antenna. Now that it has been experimentally proven that the antenna is capable of frequency agile operation, through modification of the counter-poise, we can shift focus towards further optimisation in a future iteration of the design. To improve the reconfigurable antenna design, a few areas could potentially be explored to exploit the region of maximal variation, encircled by the white ellipse in Figure 6.5. The first would be to design a balun with additional resonator stages across the intended band of the antenna - this would aid in balancing the currents on the antenna across frequency. The parasitic effect of these additional resonator stages may have effect on the counter-poise, which would require further optimization. It was observed in simulation that as higher levels of capacitance were applied, modes appeared between 2.8 and 3 GHz. Further investigation will be required here and care must be taken to shift these modes outside of the operating band if possible. The second would be to design the antenna, using the straight quarter-wave arm length of the dipole to set the lower frequency limit of the antenna and then to optimize the balun to operate at higher frequencies. The findings here indicate that at the lower frequency limit, performance drops off considerably, however the higher frequency measurements were considerably better.

6.7 Summary

The results have demonstrated that, electrical modification of the counter-poise, utilizing a varactor in conjunction with other passive components, the antenna can be made frequency-reconfigurable. The radiation patterns in the XY and XZ planes resemble those of a dipole, though not as closely as for the fixed frequency antennas demonstrated in the previous chapter. The measured gain and bandwidth results were lower than their simulated counter-parts in all cases. This drop in performance is attributed to the operational bandwidth of the balun and the component parasitics now present in the counter-poise. One observes that as an increase in capacitance is applied to reconfigure the antenna frequency, there is a resulting reduction in 2:1 VSWR bandwidth. Usable accessible bandwidth of the antenna extends from 2.3 to 2.8 GHz, result in a reconfigurable percentage bandwidth of 20%. Although there are measured reductions in antenna performance, the measured results still show that the antenna performs adequately for practical use. We have outlined a path in a future work to considerably increase the frequency reconfigurability of the antenna, which shows potential reconfigurable bandwidth to well beyond the 20% experimentally demonstrated here. In an application where there is reduced access to a ground plane, a small physical footprint, and a frequency agility requirement, a design such as the one presented here may bode well.

6.8 Thesis Concluding Remarks

From the outset of this thesis, the overarching aims were to address the physical and electrical criteria of flexibility, robustness, miniaturisation, frequency reconfigurability and low cost implementation. In developing the WOGP transmission line, a technique is demonstrated of creating a low-cost, low-loss, flexible RF line, with the potential of using this technology to develop related transmission line devices. In creating the iron-on fabric stripline transmission line, explored is a novel method of creating a flexible, robust, conductive fabric transmission line for wearable applications. Here stress analysis is performed by delving into the strengths and weaknesses of var-

ious fabrication methods. Addressing the requirement of miniaturisation, research is conducted in exploring antenna asymmetry to reduce antenna size. An exciting outcome is demonstrated through the use of a counter-poise, yielding reasonable electrical performance whilst still allowing for reduction in total size. To further enhance this antenna's robustness and electrical stability, a planar variant was developed on the principle of the asymmetric counter-poise. The final achievement of the thesis is to demonstrate a frequency reconfigurable counter-poised monopole variant, with a 20% reconfigurable bandwidth. Throughout this thesis, designs were aspired to that met the overarching criteria stated at the outset of the thesis. Certainly, it is believed that this thesis has presented ideas, practical designs and outcomes true to addressing this criteria. It is a hope that the designs introduced here are further iterated, advanced upon and newer ideas generated.

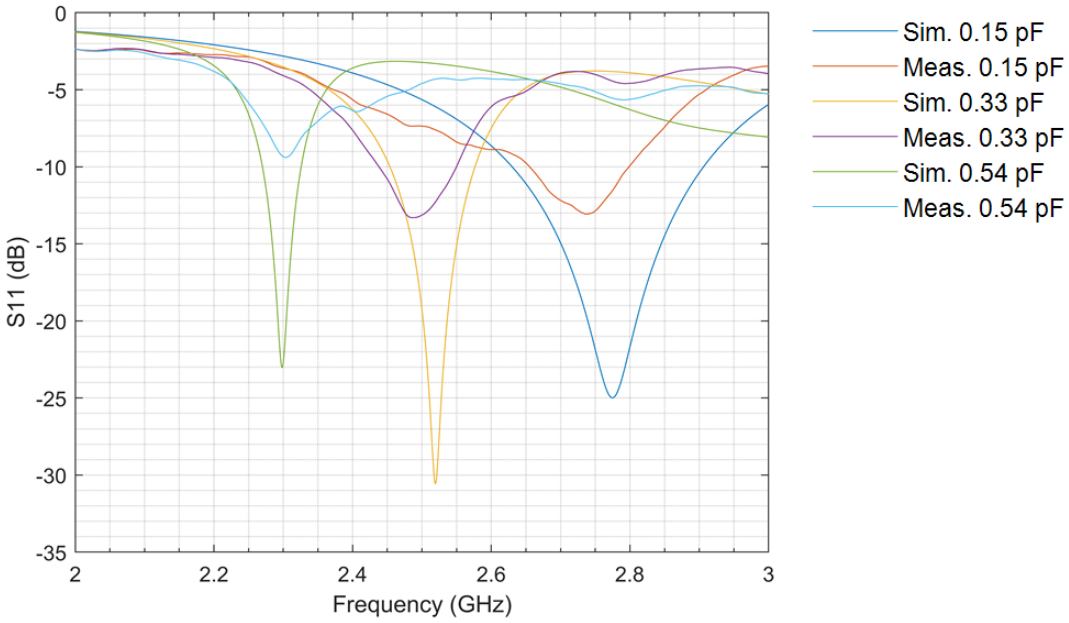

Figure 6.8: Simulated and measured comparisons of the input reflection coefficient, across three varactor settings.

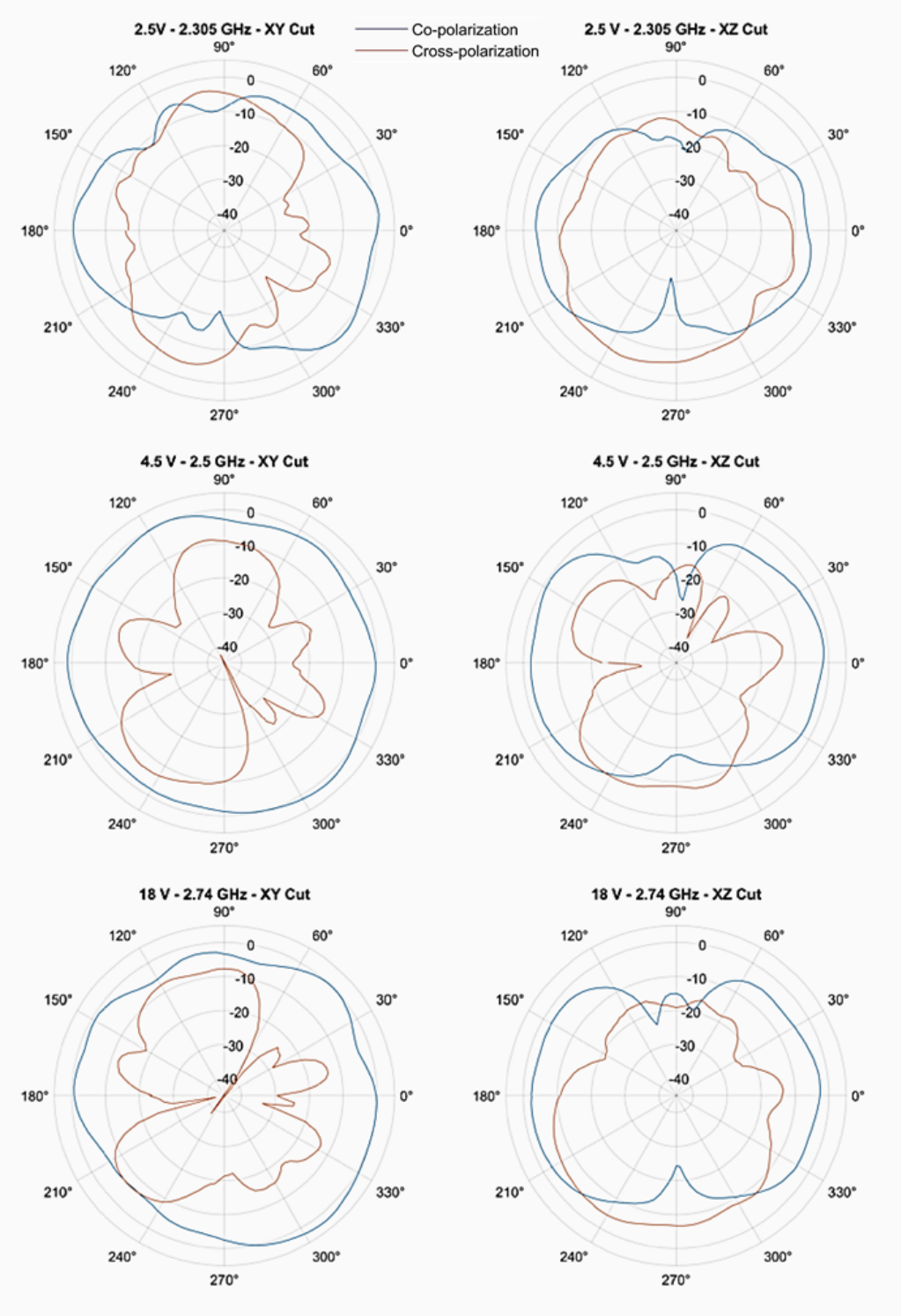

Figure 6.9: Co and cross polarization plots of the variable counter-poised monopole antenna, in the XY and XZ planes.

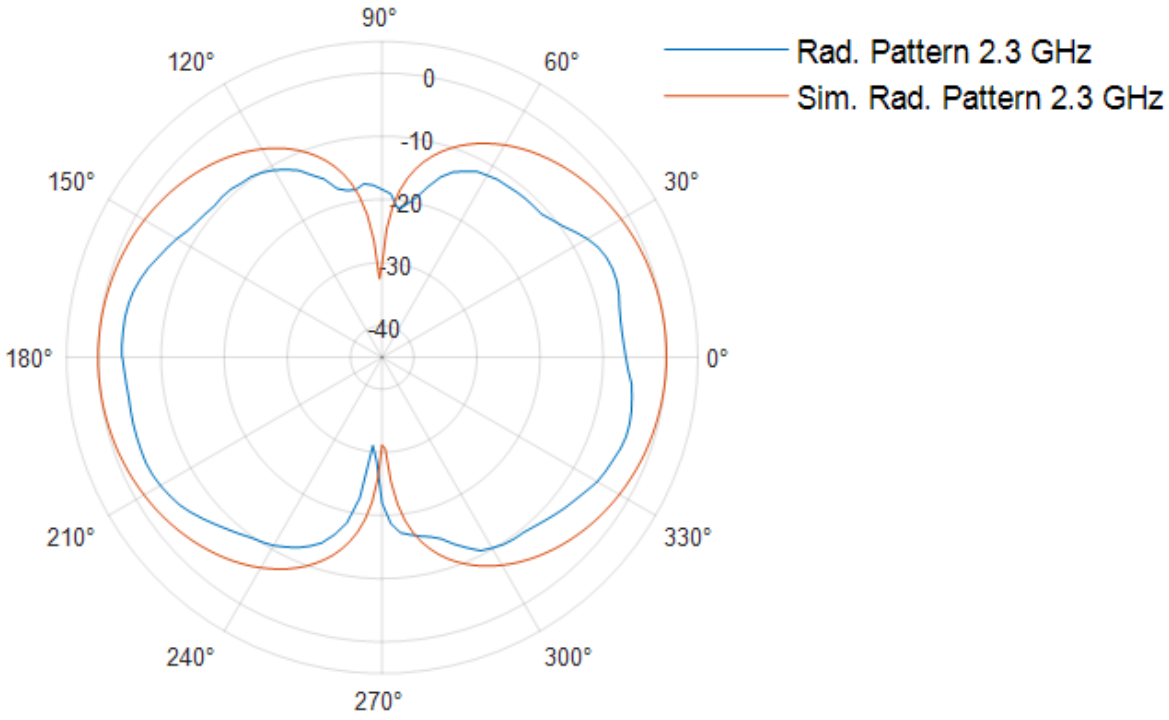

Figure 6.10: Simulated and measured comparison of the antenna radiation pattern in the XZ plane at 2.3 GHz.

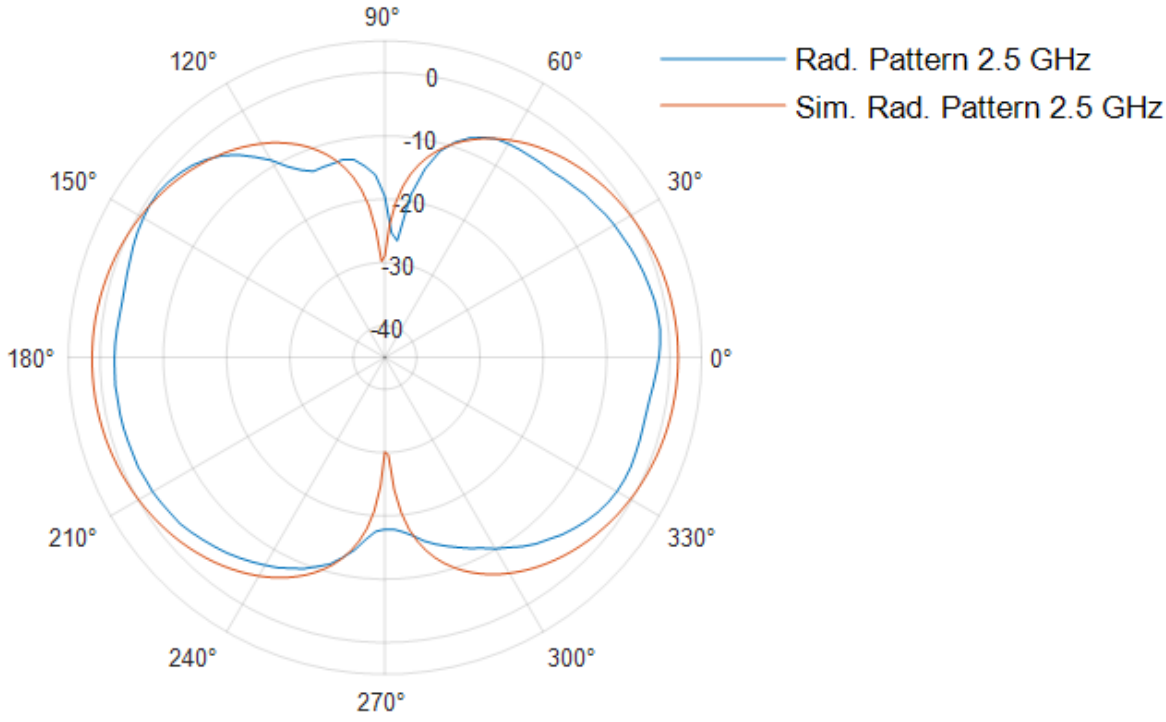

Figure 6.11: Simulated and measured comparison of the antenna radiation pattern in the XZ plane at 2.5 GHz.

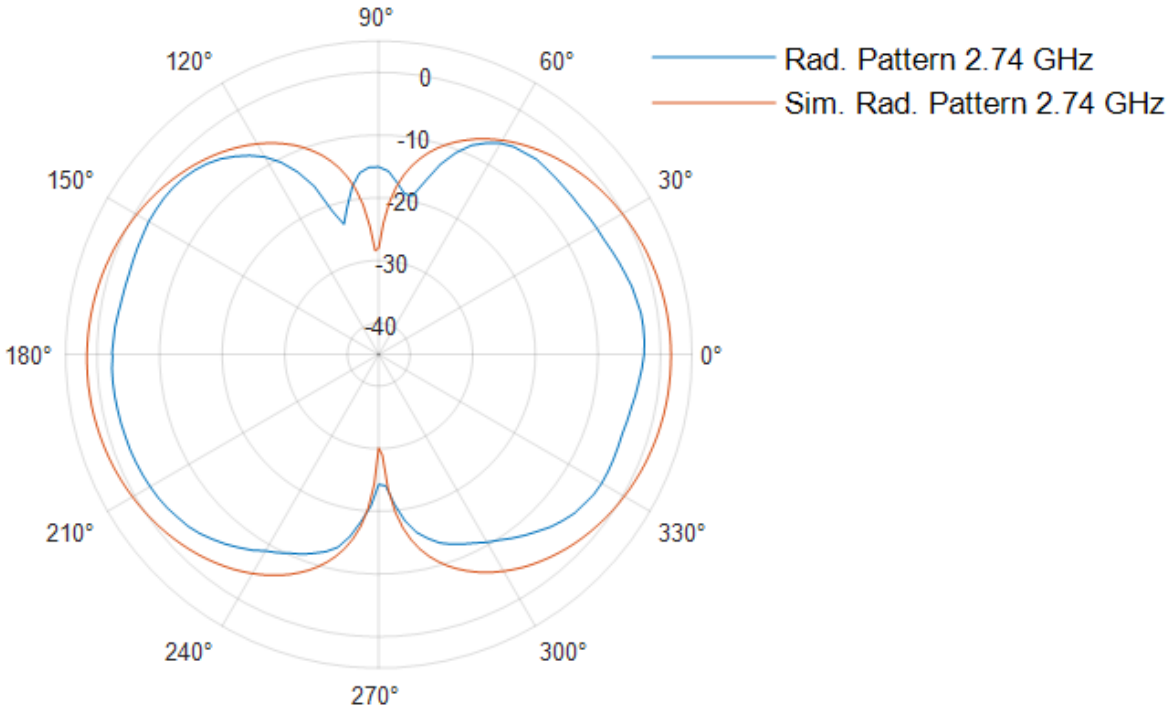

Figure 6.12: Simulated and measured comparison of the antenna radiation pattern in the XZ plane at 2.74 GHz.